HEC-RAS 2D Sediment Technical Reference Manual

HEC-RAS 2D Sediment Technical Reference Manual

Exported on 10/18/2023

Table of Contents

1 Introduction

The Corp's Hydrologic Engineering Center River Analysis System (HEC-RAS) is designed to simulate one-dimensional (1D) steady, unsteady flow and sediment transport. The HEC-RAS release 5.0 and newer also simulates unsteady two-dimensional horizontal (2DH) flow by solving either the diffusion-wave equation or non-conservative shallow water equations using an implicit Finite-Volume and Finite-Difference methods on an unstructured orthogonal mesh. One powerful feature of the 2DH flow solvers is that they implement the subgrid topographic variations directly into the model thus improving the accuracy of the solution and permitting the use of relatively coarse meshes resulting in reduced computational times.

HEC-RAS 6.0 includes a beta release of 2D sediment transport and morphology change. Despite being a beta release, the sediment model includes many features including multiple grain classes, mixed cohesive/ noncohesive transport, and a novel approach to subgrid sediment transport and morphology change. The model is designed for short to mid-term simulations primarily due to limitations in the subgrid bed change calculations. HEC-RAS 2D sediment transport solves a bed-material load transport equation but separates the bed-material load into bedload and suspended-loads with empirical formulas. The transport equation is solved with an implicit Finite-Volume scheme on the same mesh as the hydrodynamics. The bed is can be modeled as a single layer or with a user-defined number of bed layers.

2 Model Description

The objective of this chapter is to describe the theoretical background and mathematical and empirical equations which are utilized in the HEC-RAS 2D sediment transport model. The document assumes the reader is familiar with basic sediment transport concepts and terminology.

2.1 Water and Sediment Properties

2.1.1 Sediment Properties

2.1.1.1 Grain Properties

Particles are generally classified into discrete grain classes which are assumed to have the same grain properties. In HEC-RAS, the grain properties utilized are the grain size, density, shape, and roundness.

2.1.1.1.1 Grain Size

Natural sediments have a distribution of particle sizes, densities, and shapes. For modeling purposes, sediments are grouped into grain classes. Each grain class is characterized by a name, diameter, particle density, and shape factor. The grain classes do not have to have different characteristics may be different only by their name. This allows the modeler to track the movement of sediments within the domain without

having to slightly change their characteristics. Sediment particle size may be characterized by a representative diameter. Since natural sediments are naturally irregular in shape, the particle size is characterized by representative diameter. The nominal diameter is the diameter of a sphere that has the same volume of a particle

1)
$$d = \left(\frac{6V}{\pi} \right)^{1/3}$$

where V is the volume of the particle. A commonly used particle diameter is the smallest square sieve opening through which a particle will just pass. For natural sediment particles over the range of about 0.2 to 20 mm, the sieve diameter is approximately 0.9 times the nominal diameter on average (U.S. Interagency Committee, 1957; Raudkivi, 1990). Sediment particles are classified into by their diameter. The table below shows the sediment grain size classification scheme utilized by HEC-RAS.

Table 2 1. Sediment grain size aggregate names utilized in HEC-RAS.

Size Range (mm)	Aggregate Name
0.00098 – 0.004	Clay
0.004– 0.008	Very Fine Silt
0.008 – 0.016	Fine Silt
0.016 – 0.032	Medium Silt
0.032 – 0.0625	Coarse Silt
0.0625 – 0.125	Very fine sand
0.125 – 0.25	Fine Sand
0.25 – 0.5	Medium Sand
0.5 – 1	Coarse Sand
1 – 2	Very Coarse Sand
2 – 4	Very Fine Gravel
4 – 8	Fine Gravel

8 – 16	Medium Gravel
16 – 32	Coarse Gravel
32 – 64	Very Coarse Gravel
64 – 128	Small Cobbles
128 – 256	Large Cobbles
256 – 512	Small Boulders
512 – 1024	Medium Boulders
1024 – 2048	Large Boulders

2.1.1.1.2 Density

The sediment particle density or grain density, ρ_s , is the mass of sediment per unit volume. For quartz particles it is approximately 2,650 kg/m^3 and does not vary significantly with temperature or pressure. The specific weight or unit weight of particles, γ_s , is the density times the gravitational constant

2) $$\gamma_s = g\rho_s$$

where g is the gravitational constant. The specific gravity, s , is the ratio of the grain density and water density

3) $$s = \frac{\rho_s}{\rho_w}$$

When the specific gravity is utilized to specify the grain density a reference water density is utilized computed with a temperature of 4ºC. The table below shows typical specific gravity ranges for different common minerals and rocks.

Table 2. Specific gravity ranges for different minerals and rocks.

Material	Specific Gravity
Quartz	2.6 – 2.7

Limestone	2.6 – 2.8
Basalt	2.7 – 2.9
Magnetite	3.2 – 3.5
Coal	1.3 – 1.5

However, often when the specific gravity is utilized in sediment transport equations it is more appropriate to utilize the ratio of the grain density and the actual water density.

2.1.1.1.3 Shape Factor

The particle shape factor utilized is attributed to Corey (1949)

4) $$S_F = \frac{c}{\sqrt{ab}}$$

where

a = length of the particle along the long axis perpendicular to the other two axes [L]

b = length along the intermediate axis perpendicular to the other two axes [L]

c = length along the short axis perpendicular to the other two axes [L]

The shape factor is utilized for some of the sediment fall velocity formulas. The shape factor of natural particles is usually about 0.6 to 0.7.

2.1.1.1.4 Roundness

The particle roundness can only be estimated based on the comparison with the images proposed by Powers (1953), shown in the figure below, and the use of Folk's (1955) corresponding scale shown in the table below.

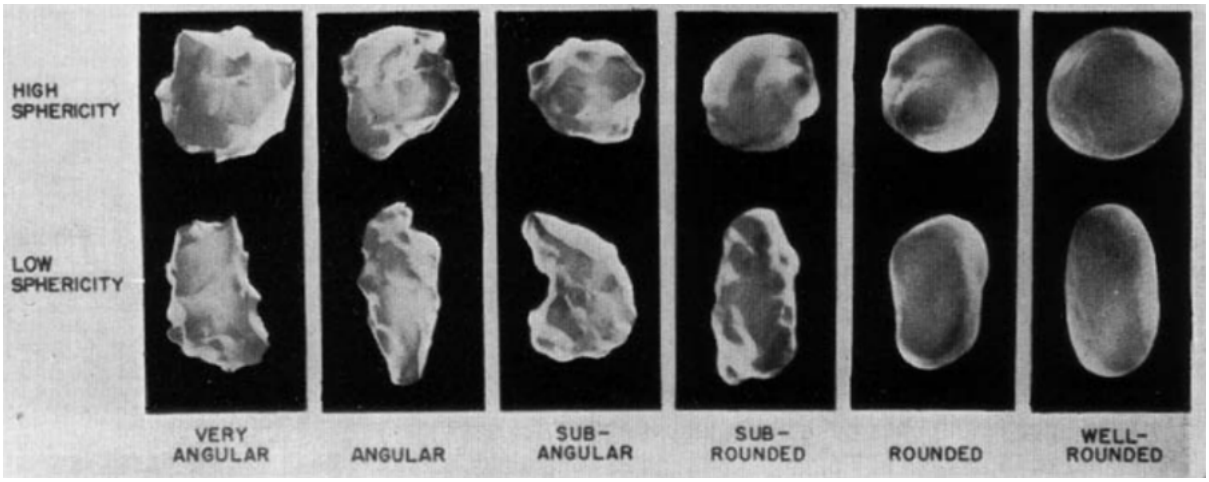

Figure 1. Particle roundness scale proposed by Powers (1953) (from Powers (1953).

Table 3. Folk's (1955) Roundness "rho" Scale.

Powers Verbal Class	Rho Scale Class Intervals
Very angular	0.0 – 1.0
Angular	1.0 – 2.0
Sub-angular	2.0 – 3.0
Sub-rounded	3.0 – 4.0
Rounded	4.0 – 5.0
Well-rounded	5.0 – 6.0

2.1.1.2 Bulk Properties

2.1.1.2.1 Grain-Size Distribution

In general, natural sediments consists of a mixture of sediment sizes, shapes, densities, etc. In the multiple-grain class approach, the sediment mixture is discretized in a fixed number of sediment grain classes, each with own grain properties. The grain properties are generally different from grain classes to grain class, but they may in fact be the same (i.e. same grain size). In fact, allowing grain classes to have the same properties allows tracking (mapping) of sediments without having to artificially change the grain characteristics, namely grain size. Each grain class, numbered *k* is defined by an upper and lower bound

diameters and a representative grain class diameter represented as $d_{k+1/2}$ and $d_{k-1/2}$, respectively. The grain class diameter is defined here as the geometric mean of the bound diameters $d_k = \sqrt{d_{k+1/2} d_{k-1/2}}$. Either the representative diameters or bounding diameters may be specified as model input. The grain class limits are only used to compute the sediment percentile diameters (i.e. the sediment percentile diameters are the diameters corresponding to certain percentile such as the 50th percentile). The algorithm used to compute

The grain class fractions, or percentages are usually measured by weight using a sieving analysis but can be also in units of volume or particle count. The grain class fractions by weight are represented by f_k and fractions by volume by $\hat{f}_k$. If the grain class particle densities, ρ_{sk}, are known the fractions can be converted from by volume to by weight as

5) $$\hat{f}_k = \frac{\rho_{sk}^{-1} f_k}{\sum_i \rho_{si}^{-1} f_i}$$

6) $$f_k = \frac{\rho_{sk} \hat{f}_k}{\sum_i \rho_{si} \hat{f}_i}$$

Most of the grain fractions utilizes in this report represent weight fractions and both the input and output grain fractions are fractions by weight.

The grain-size distribution of a sediment mixture can be represented by a histogram of grain class fractions and a cumulative frequency curve (Krumbein 1934). An example of a grain-size distribution is shown in the figure below.

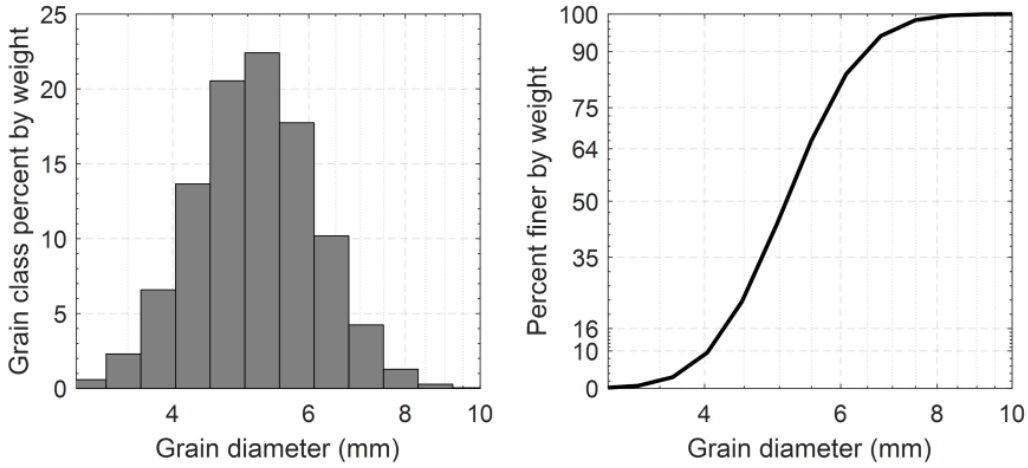

Figure 2. Grain-size distribution histogram (left) and cumulative frequency curve (right).

Many natural sediments have a grain-size distribution which can be approximated by a log-normal distribution. The example grain-size distribution above follows a log-normal distribution. When plotted on a log-scale, the log-normal distribution has an approximate normal (Gaussian) distribution curve.

Characteristic Diameters

The grain size distribution commonly described with by percentile diameters. These diameters correspond to a specific percent by weight finer on the cumulative frequency curve. For example, the 50^{th} percentile (median) diameter, d_{50}, is the particle diameter at which 50% by weight of the same is finer. More generally, the notation d_n represents the diameter at which n percent by weight is finer. Other commonly used percentile diameters are d_{10}, d_{16}, d_{35}, d_{50}, d_{65}, d_{84}, and d_{90}. When interpolating the percentile diameters from the cumulative frequency curve it is usually done in log-space for the grain diameters. Other commonly used representative grain diameters are the arithmetic mean diameter, d_m, and the geometric mean diameter, d_g, defined respectively as

7) $$d_m = \Sigma_k f_k d_k$$

8) $$d_g = exp(\Sigma_k f_k \ln(d_k))$$

2.1.1.2.2 Uniformity

The uniformity of a sediment grain size distribution is a measure of how well sorted the distribution is. The uniformity or sorting is often described can be described by the geometric standard deviation

9) $$\sigma_g = \exp \sqrt{\sum_k f_k (\ln d_k - \ln d_g)^2}$$

where

f_k = grain class fraction by weight [-]

d_k = grain class characteristic diameter [L]

d_g = geometric mean [L]

The following table describes the sorting classifications based on the geometric standard deviation

Table 4. Grain-related roughness height coefficient.

Geometric Standard Deviation (σ_g)	Classification
Very well sorted	<1.27
Well sorted	1.27 – 1.41
Moderately well sorted	1.41 – 1.62

Moderately sorted	1.62 – 2.00
Poorly sorted	2.00 – 4.00
Very poorly sorted	4.00 – 16.00
Extremely poorly sorted	> 16.00

2.1.1.2.3 Porosity

The porosity is a measure of how the volume of voids per unit volume of the deposit

10) $$\phi = \frac{V_v}{V}$$

where

V_v = volume of the voids [L^3]

V = total volume of mixture [L^3]

The porosity of sediments depends on the grain size, shape, roundness, sorting, and the level of compactness. The sediment porosity can vary from 0.82 for freshly deposited clays to 0.25 for extremely poorly sorted sediments.

2.1.1.2.4 Dry Bulk Density

The two most commonly used bulk densities are the wet and dry bulk densities. The dry bulk density or simply dry density is defined as

11) $$\rho_d = \frac{m_s}{V}$$

where

m_s = sediment mass [M]

V = volume water-sediment mixture [L^3]

The dry bulk density can be viewed as a sediment mass concentration. It is a function of the particle densities and the porosity/volume concentration. Dry densities generally vary between

300 to 1,600 kg/m^3. The dry bulk density can be calculated for a grain size distribution with a porosity as

12) $$\rho_d = (1-\phi)\Sigma_k \rho_{sk} \hat{f}_k = (1-\phi)(\Sigma_i \rho_{si}^{-1} f_i)^{-1}$$

where

$\hat{f}_k$ = grain class fraction by volume [-]

f_k = grain class fraction by weight [-]

ρ_{sk} = grain density [M/L^3]

ϕ = porosity [-]

2.1.2 Water Properties

Water has many physical properties. The main physical properties utilized in hydrodynamics and sediment transport are the density and viscosity. These are a function of the water temperature and salinity. However, salinity is currently ignored in HEC-RAS. These correspond to the "clear water" values without sediment. The default water temperature in HEC-RAS is 55.4 F.

2.1.2.1 Density

The water density is a function a water temperature and salinity. There are many formulas in literature for computing the water temperature. The water specific weight or unit weight particles, γ_w, is the density times the gravitational constant

13) $$\gamma_w = g\rho_w$$

The default water unit weight in HEC-RAS is 62.4177 lb/ft^3. If the user specifies a time series of water temperature, the water density is calculated using the UNESCO (1981) equation (at standard atmospheric pressure)

14) $$\rho_w = \rho_0 + B_1 S + C_1 S^{3/2} + d_0 S^2$$

where

ρ = water density [kg/m^3]

$\rho_0 = a_0 + a_1 T + a_2 T^2 + a_3 T^3 + a_4 T^4 + a_5 T^5$ = freshwater density

$$a_0 = +999.842594$$
$$a_1 = +6.793952 \times 10^{-2}$$
$$a_2 = -9.09529 \times 10^{-3}$$
$$a_3 = +1.001685 \times 10^{-4}$$
$$a_4 = -1.120083 \times 10^{-6}$$
$$a_4 = +6.536332 \times 10^{-9}$$
$$B_1 = b_0 + b_1 T + b_2 T^2 + b_3 T^3 + b_4 T^4$$
$$b_0 = 0.824493$$
$$b_1 = -4.0899 \times 10^{-3}$$
$$b_2 = +7.6438 \times 10^{-5}$$
$$b_3 = -8.2467 \times 10^{-7}$$
$$b_4 = +5.3875 \times 10^{-9}$$
$$C_1 = c_0 + c_1 T + c_2 T^2$$
$$c_0 = -5.72466 \times 10^{-3}$$
$$c_1 = +1.0227 \times 10^{-4}$$
$$c_2 = -1.6546 \times 10^{-6}$$
$$d_0 = 4.8314 \times 10^{-4}$$

T = water temperature [ºC]

S = water salinity [PSU]

The above equation is valid for temperatures between 0 and 40˚C and salinities between 0.5 and 43 PSU. The salinity above is assumed to be 0.5 PSU.

2.1.2.2 Viscosity

The dynamic water viscosity of water may be calculated using the curve fit formula presented by Neumeier et al. (2008) based on the data from Riley and Skirrow (1965)

$$\mu_w = 1.802863 \times 10^{-3} - 6.1086 \times 10^{-5} T + 1.31419 \times 10^{-6} T^2 - 1.35576 \times 10^{-8} T^3 + 2.15123 \times 10^{-6} S + 3.59406 \times 10^{-11} S^2 \quad (15)$$

where

μ_w = water dynamic viscosity [kg·s/m]

T = water temperature [ºC]

S = water salinity [PSU]

The error compared to the data of Riley and Skirrow (1965) is less than 0.5% over the range (0 38 PSU and 8 24˚C). The error is less than 1.0% over the range 0 28˚C. Currently, in HEC-RAS the salinity is assumed to be 0.5 PSU.

The water viscosity is a measure of the resistance to deformation at a given rate. When a fluid has zero viscosity it called inviscid. The flows resulting from water with and without viscosity are referred to as

viscous and inviscid flows respectively. In hydrodynamics and sediment transport the kinematic viscosity, μ_w, is often utilized. It is related to the dynamic viscosity by

16) $$\nu_w = \frac{\mu_w}{\rho_w}$$

2.1.3 Water-Sediment Mixture Properties

Bulk properties refer to properties of the sediment-water mixture. Bulk properties usually refer to sediment bed properties such as porosity, bulk densities, and erodibility parameters. The erodibility parameters are discussed in a subsequent section while the porosity and bulk densities are covered below.

2.1.3.1 Density

The wet bulk density is density of the water-sediment mixture and is defined as

17) $$\rho_m = \frac{m}{V} = \frac{m_w + m_s}{V}$$

where

m = mass of water-sediment mixture [M]

m_w = water mass [M]

m_s = sediment mass [M]

V = total volume of sediment mixture [L^3]

The wet bulk density is usually utilized for describing the density of the transported water-sediment mixture. Given a fractional sediment concentration with varying grain densities, the density of the water-sediment mixture can be computed as

18) $$\rho_m = \rho_w(1 - c) + \sum_k \rho_{sk} c_k$$

where

ρ_m = water-sediment mixture density [M/L^3]

ρ_w = water density [M/L^3]

$c = \sum_k c_k$ = sediment volume concentration [-]

ρ_{sk} = grain class particle density [M/L^3]

c_k = grain class (fractional) volume concentration [-]

Wet bulk densities can vary from 1330 kg/m^3 to 2230 kg/m^3.

2.1.3.2 Viscosity

Thomas (1965) proposed the following equation for the water-sediment mixture viscosity

19) $$\frac{\mu_m}{\mu_w} = 1 + 2.5c + 10.05c^2$$

where

μ_m = water-sediment mixture viscosity [M·T/L]

μ_w = water viscosity [M·T/L]

c = sediment volume concentration [-]

The above equation has an accuracy of 97.5% for c < 0.25%.

2.2 Bedform Geometry and Hydraulic Roughness

2.2.1 Bed Roughness Predictors

By default, the total bed roughness is set to the user-specified Manning's roughness coefficient utilized for hydrodynamics. The option is also available to compute the dynamically variable bed roughness based on one of three bed roughness predictors. These are formulations to compute bed roughness based on varying hydrodynamic and surface bed compositions. Here the following formulations are available:

1. Limerinos (1970)
2. Brownlie (1983)
3. van Rijn (1984c)
4. Karim (1995)
5. Wu and Wang (1999)

A comparison of different bed roughness predictors is shown in the figure below. The Karim-van Rijn formulation utilizes the van Rijn (1984c) dune geometry formulas instead of Karim (1995). The Limerinos (1970) formula does not account for bedform roughness and is therefore constant with transport stage. The Wu and Wang (1999) and van Rijn (1984c) formulas produce similar results. The Wu and Wang (1999) formula produces bedform roughness even at transport stages less than one, while the formulations which utilize the van Rijn (1984c) dune geometry only produce bedform roughness for transport stages larger than one. The Brownlie (1983) formula has a sharp discontinuity between the lower and upper flow regimes. This discontinuity may cause stability problems in numerical models and so cautious must be practice when modeling such flows with the Brownlie formula.

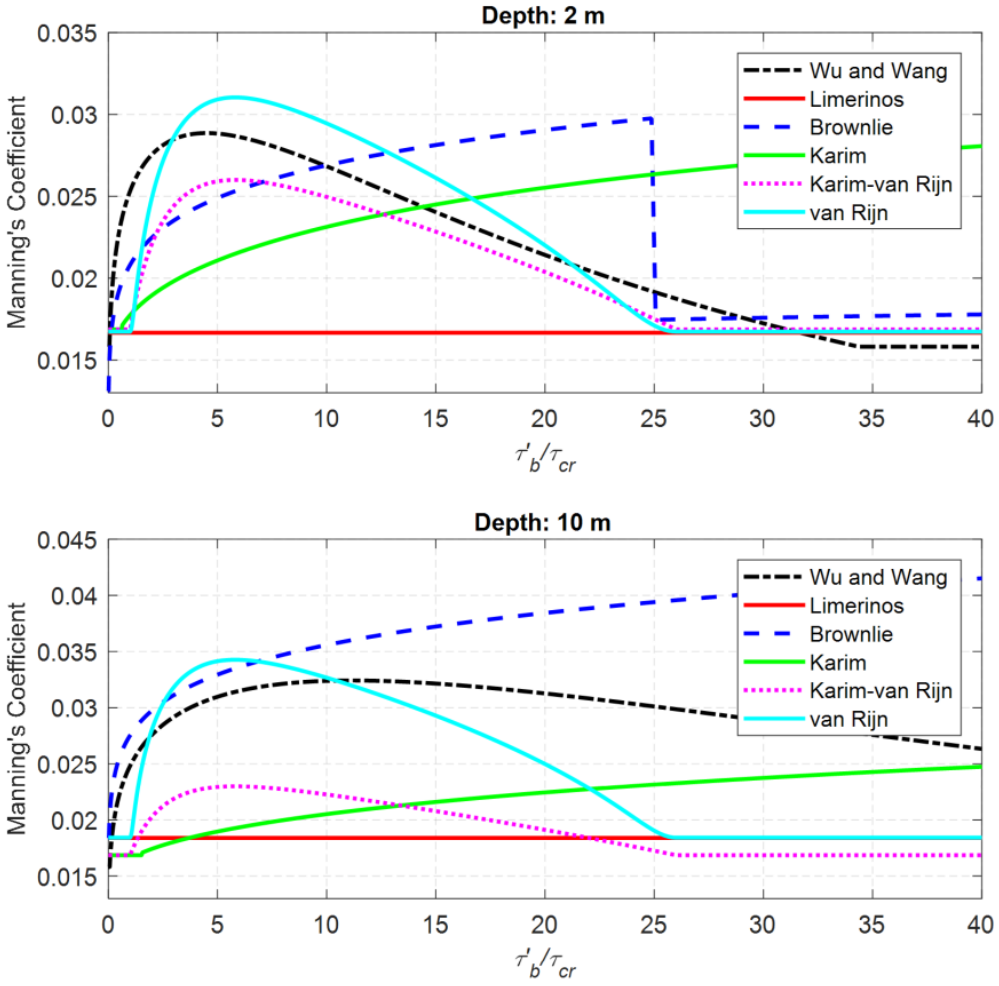

Figure 2 6. Comparison of different bed roughness predictors.

2.2.1.1 Limerinos

Limerinos (1956) developed a bed roughness predictor based on data from 11 gravel-bed streams in California as (see Figure below)

20)
$$n = \frac{0.0926 A R^{1/6}}{1.16 + 2\log_{10}(R/d_{84})}$$

where

$$A = \begin{cases} 1.219 & \text{for SI units} \\ 1 & \text{for English units} \end{cases}$$

n = Manning's roughness coefficient [s/m$^{1/3}$]

R = hydraulic radius [L]

d_{84} = 84th percentile diameter [L]

The equation is applicable to high in-bank flows in straight, gravel-bed channels. All the data used corresponded to Froude numbers less than 1. The Limerinos equation only accounts for the grain roughness in gravel-bed streams and does not include other contributions. Therefore, it may be used as the base value in the Cowan (1956) method. The above formula does not account for the full distribution of sediments and only consider a representative diameter. This is a limitation of the expressions when being applied to poorly sorted bed material.

2.2.1.2 Brownlie

Brownlie (1983) proposed separate resistance relationships for the lower and upper regimes as

21) $$n = \begin{cases} 1.6940\left(\frac{R}{d_{50}}\right)^{0.1374} S^{0.1112}\sigma_g^{0.1605} n' & \text{for } S > 0.006 \text{ or } F_g > 1.25F_g' : \text{ upper regime} \\ 1.0213\left(\frac{R}{d_{50}}\right)^{0.0662} S^{0.0395}\sigma_g^{0.1282} n' & \text{for } F_g < 0.8F_g' : \text{ lower regime} \end{cases}$$

where

n = total manning's roughness coefficient

$q_* = \frac{Uh}{\sqrt{gd_{50}^3}}$ [-]

R = hydraulic radius associated with the bed [L]

S = slope [-]

d_{50} = median grain size [L]

σ_g = geometric standard deviation of bed material [-]

$n = 0.041 d_{50}{}^{1/6}$ = Strickler grain roughness [s/m$^{1/3}$]

$F_g = \frac{U}{\sqrt{\rho g d_{50}(s-1)}}$ = grain Froude number [-]

$F_g' = \frac{1.74}{S^{0.3333}}$ = slope parameter [-]

2.2.1.3 van Rijn

The van Rijn (1984c) alluvial roughness height predictor computed computes the total roughness k_s as the sum of the grain and dune roughness:

22) $$k_s = k_{s,\,g} + k_{s,\,d}$$

where

ks = total roughness height [L]

$k_{s,\,g}$ = grain roughness height [L]

$k_{s,\ d}$ = dune roughness height [L]

The grain roughness is computed as

23) $$k_{s,\ g} = 3d_{90}$$

where d_{90} is the 90th percentile diameter. The dune roughness height is computed as (van Rijn 1984a)

24) $$k_{s,d} = 1.1\gamma_d \Delta_d \left[1 - \exp\left(-25\frac{\Delta_d}{\lambda_d}\right)\right]$$

where

γ_d = dune shape coefficient (~1.0) [-]

Δ_d = dune height [L]

λ_d = dune length [L]

The dune shape coefficient, γ_d, is approximately 1.0 for dzunes with angle-of-repose faces as considered in van Rijn (1984). Dunes with more gently sloping faces have smaller shape coefficients as is common in the field. van Rijn (1993) proposed setting γ_d = 0.7 based on various field measurements of river systems. van Rijn (1984a) provided expressions for calculating the dune height and length and are shown in Equations (2-94) and (2-95). The figure below shows the dune roughness based on van Rijn (1984a) as a function of the sediment transport stage. Here the parameter is set to 1.0 for simplicity.

2.2.1.4 Karim

Karim (1995) developed a formula to predict bedform roughness for ripples, dunes and washed out dunes following a curve fit to flume and field measurements. The proposed formula for the total Manning's roughness coefficient is as follows:

25) $$n = 0.037 d_{50}^{0.126}\left(1.2 + 8.92\frac{\Delta}{h}\right)^{0.465}$$

where

n = Manning's roughness coefficient [s/m$^{1/3}$]

d_{50} = median grain size diameter [m]

h = water depth [m]

Δ = bedform height [m]

Karim (1995) proposed a formula for the bedform height. However, other formulas may also be used. In fact, it has been found that utilizing the van Rijn (1984c) formula for dune height produces results which are more consistent with the Wu and Wang (1999) formula which is described below.

2.2.1.5 Wu and Wang

Wu and Wang (1999) developed a formula to predict bedform roughness for ripples, dunes and washed out dunes following a curve fit to flume and field measurements. The proposed formula for the total Manning's roughness coefficient is as follows:

26) $$n = \max\left(\frac{d_{50}^{1/6}}{A_n}, n_g\right)$$

with

27) $$\frac{A_n}{\sqrt{g}F_r^{1/3}} = \frac{8\left[1 + 0.0235\left(\tau_b'/\tau_{cr50}\right)^{1.25}\right]}{\left(\tau_b'/\tau_{cr50}\right)^{1/3}}$$

where

n = Manning's roughness coefficient [s/m$^{1/3}$]

n_g = Grain-related Manning's roughness coefficient [s/m$^{1/3}$]

$F_r = U/\sqrt{gh}$ = Froude number [-]

U = depth-averaged current velocity [L/T]

h = water depth [m]

g = gravity [L/T^2]

τ'_b = grain shear stress [M/L/T^2]

τ_{cr50} = critical shear stress corresponding to the median grain size [M/L/T^2]

Wu and Wang (1999) computed the grain-related Manning's roughness coefficient with the formula of Li and Liu (1963).

2.2.2 Bedform Geometry

Bedforms are closely related to flow conditions. As the flow strength increases, a stationary flat bed may evolve to form ripples, mega-ripples, dunes, moving planar bed, anti-dunes, and chutes/pools.

2.2.2.1 Ripples

Ripples are relatively triangular bed features formed by current and wave motion over sandy beds with grain sizes between 0.06 mm and about 0.7-1.0 mm. Observations indicate that ripples are independent of the flow depth.
Current-generated ripples are generally asymmetric and travel downstream. They are characteristic of lower flow regimes with Froude numbers less than 1. The ripple slopes on the lee side are generally close the

critical stability slope for sediment. Many formulas are available in literature for calculating current ripples. The formulas included here are:

1. Baas (1993)
2. Raudkivi (1997)

A comparison of the two ripple geometries is provided in the figures below.

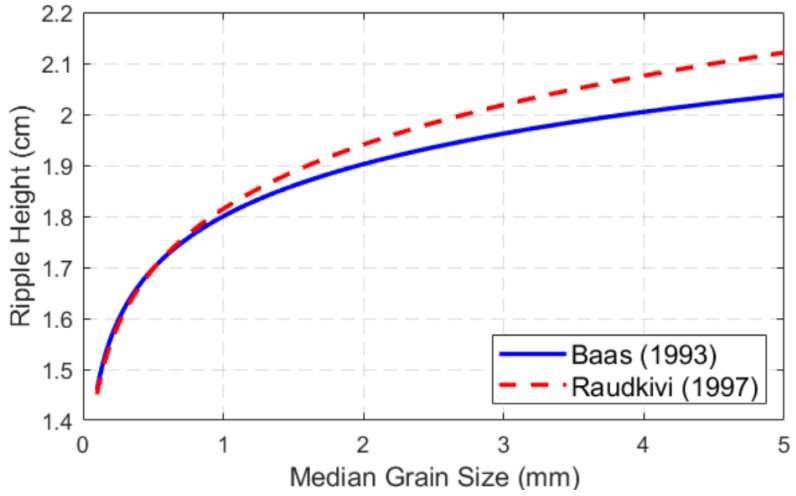

Figure 1. Comparison of ripple height formulas.

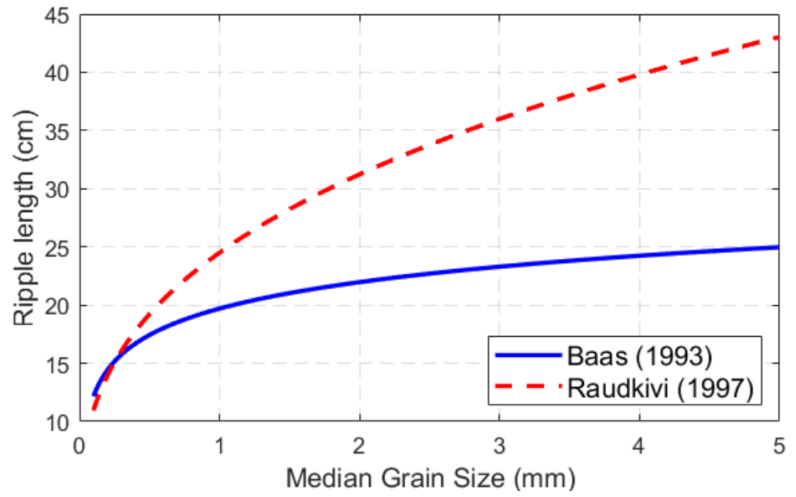

Figure 2. Comparison of ripple length formulas.

Before proceeding, it is useful to define the current-related equilibrium and maximum bedform geometries. The equilibrium bedform geometry corresponds to the geometry under steady conditions considering the bed composition (e.g. d_{50}), flow conditions, and preexisting bedform geometry. Biodegradation is not included in the equilibrium bedform geometry. The maximum bedform geometry corresponds to the maximum ripple height considering only the bed composition and not the flow conditions. Some empirical

formulas only provide an estimate of the maximum ripple geometry without consideration of the flow conditions.

Baas (1993)

The following regression equations for the current-related maximum ripple height and length were proposed by Baas (1993)

28) $$\Delta_{r,\max} = 3.4\log_{10}(d_{50}) + 18$$

29) $$\lambda_{r,\ \max} = 75.4\log_{10}(d_{50}) + 197$$

where $\Delta_{r,\max}$ and $\lambda_{r,\ \max}$ are the maximum ripple height and length respectively, d_{50} is the median grain size, and all variables are in mm. Baas (1993) does not provide a method for estimating the equilibrium ripple dimensions.

Raudkivi (1997)

Raudkivi (1997) proposed the following simple dimensional formulas for the current-related maximum ripple height and length

30) $$\Delta_{r,\max} = 0.074\lambda_{r,c,\max} d_{50}^{-0.253}$$

31) $$\lambda_{r,\ \max} = 245 d_{50}^{0.35}$$

where $\Delta_{r,\max}$ and $\lambda_{r,\ \max}$ are the maximum ripple height and length respectively, d_{50} is the median grain size, and all variables are in mm. Raudkivi (1997) does not differentiate the equilibrium ripple dimensions from the maximum ripple dimensions. It is noted that the Raudkivi (1997) formula is used by the Wu et al. (2000) sediment transport equations.

Dunes

Dunes are current-generated bedforms which are characteristic of lower regime flows with Froude numbers less than one. There are many formulas for predicting dune geometry. Here the following formulas are included:

1. Karim (1995)
2. van Rijn (1984)

Karim (1995)

Karim (1995) proposed the following simple relations for the dune height and length:

32) $$\frac{\Delta_{d,eq}}{h} = \begin{cases} -0.04 + 0.294\frac{u_*}{\omega_{s,50}} + 0.00316\left(\frac{u_*}{\omega_{s,50}}\right)^2 & \text{for } 0.15 < \frac{u_*}{\omega_{s,50}} < 3.64 \text{ and } d_{50} > d_{silt} \\ -0.0319\left(\frac{u_*}{\omega_{s,50}}\right)^3 + 0.00272\left(\frac{u_*}{\omega_{s,50}}\right)^4 & \\ 0 & \text{otherwise} \end{cases}$$

where

u_* = current shear velocity (total) [L/T]

$\omega_{s,\ 50}$ = fall velocity based on the median grain size d_{50} [L/T]

Karim (1995) does not provide a method for estimating the dune length.

van Rijn (1984)

van Rijn (1984c) formulas for the dune height, Δ_d , and length, λ_d , are given by

33) $$\Delta_{d,eq} = \begin{cases} 0.11h\left(\frac{d_{50}}{h}\right)^{0.3}\left[1 - \exp(-0.5T_*)\right](25 - T_*) & \text{for } 0 < T_* < 25 \\ 0 & \text{otherwise} \end{cases}$$

34) $$\lambda_{d,\ eq} = 7.3h$$

where

$T_* = \frac{u_*'^2}{u_{*cr}^2} - 1$ = sediment transport stage parameter [-]

$u_*' = \frac{U\sqrt{g}}{C_h'}$ = bed skin shear velocity [L/T]

$C_h' = 18\log_{10}\left(\frac{12h}{k_{s,g}}\right)$ = Chézy grain roughness coefficient [$L^{1/3}/T$]

$k_{s,\ g} = 3d_{90}$ = grain-related roughness [L]

$u_{*cr}' = g(s-1)d_{50}\theta_{cr}$ = critical shear velocity shear velocity [L/T]

θ_{cr} = critical Shields parameter [-]

The critical Shields parameter is calculated based on van Rijn (1984a)

2.2.3 Bottom Roughness

The total roughness may be computed from the user-specified Manning's roughness coefficient or computed internally from the individual components. The total bottom roughness may be separated into roughness's due to (1) grains, (2) sediment transport, and (3) bedforms. The bedform roughness may be further divided into roughness's due to: (1) ripples, (2) mega-ripples, and (3) dunes. The grain-related roughness is the skin roughness caused by the sediment grains on the bed. It is necessary for many of the

sediment transport formulas. The sediment transport roughness is a friction loss caused by the moving particles near the bed. The transport roughness is usually small compared to the other components. The bedform roughness is the form roughness and can have a large range of values. Bedforms geometry is very difficult to predict and therefore, the bedform roughness has a large uncertainty.

Roughness Specification and Conversion

The total bottom roughness is specified in HEC-RAS with the Manning's roughness coefficient. It is important to note that the bed roughness is assumed constant in time and not changed according to bed composition and bedforms. This is a common engineering approach which can be justified by the lack of data to initialize the bed composition and the large error in estimating the bed composition evolution and bedforms. In addition, using a constant bottom roughness simplifies the model calibration. The bed roughness used for hydrodynamics may not be the same as that which is used for the sediment transport calculations. This is because each sediment transport formula was developed and calibrated using specific methods for estimating bed shear stresses or velocities, and these cannot be easily changed. The choice of what roughness parameter is specified and kept constant over an area has important consequences on the flow and its distribution with respect to the water depth (see figure below). The Nikuradse roughness height k_s is related to the roughness length by (Christoffersen and Jonsson 1985)

35) $$z_0 = \frac{k_s}{30}\left[1 - \exp\left(-\frac{u_* k_s}{27\nu}\right)\right] + \frac{\nu}{9u_*}$$

where

u_* = bed shear velocity [L/T]

k_s = Nikuradse roughness [L]

ν = water kinematic viscosity [L^2/T]

For flat beds consisting of fine sands or mud, the flow is hydraulically smooth or transitional while beds with coarse sands, gravel, or bedforms are hydraulically rough (Soulsby 1997). Most natural river and coastal flows are hydraulically rough for which case the above equation simplifies to

36) $$z_0 = \frac{k_s}{30}$$

The equation is based on a logarithmic velocity profile and covers smooth, transitional, and rough turbulent flows.

Assuming rough turbulent flow, the second part of the equation may be ignored, in which case the Colebrook-White equation may be used to convert the roughness height to a Manning's coefficient as

37) $$n = \frac{AR^{1/6}}{18\log_{10}\left(\frac{12R}{k_s}\right)}$$

where

$$A = \begin{cases} 1 & \text{for SI units} \\ 1.486 & \text{for English units} \end{cases}$$

R = hydraulic radius or water depth [L]

k_s = roughness height [L].

2.2.3.1 Grain-related Roughness

The grain-related roughness may be estimated as (e.g. Meyer-Peter and Muller 1958)

38) $$k_{s,\ g} = \alpha_{g,\ X}\, d_X$$

where

$\alpha_{g,X}$ = Grain-related roughness height coefficient

d_X = Diameter corresponding to the *X* percentile

Examples values of $\alpha_{g,X}$ from literature are shown in the table below.

Table 25. Grain-related roughness height coefficient.

Reference	d_X	$\alpha_{g,X}$
Ackers and White (1973)	d_{35}	1.23
Meyer-Peter and Muller (1948)	d_{50}	1.0
Engelund and Hansen (1972) Nielsen (1992)	d_{50}	2.50
Strickler (1970)	d_{50}	3.3
Engelund and Hansen (1967), Wilcock (2001) and Wilcock and Crowe (2003)	d_{65}	2.0
Limerinos (1970)	d_{84}	2.8
Kamphius (1974)	d_{90}	2.0
van Rijn (1984c)	d_{90}	3.0

In HEC-RAS, the grain roughness height formulations utilized from the above table are van Rijn (1984c)

The grain-related Manning's roughness coefficient may be estimated as

39) $$n_g = \frac{d_X^{1/6}}{A_{n,X}}$$

where

d_X = Xth percentile diameter [m]

$A_{n,X}$ = Grain-related Mannings n corresponding to d_X [1/(s $m^{1/6}$)]

The table below shows some examples of A_n from literature.

Table 26. Grain-related Manning's coefficient.

Reference	d_X	$A_{n,X}$
Strickler (1923)	d_{50}	25.6
Li and Liu (1963)	d_{50}	20
Patel and Ranga Raju (1996)	d_{65}	24
Meyer-Peter and Muller (1948)	d_{90}	26

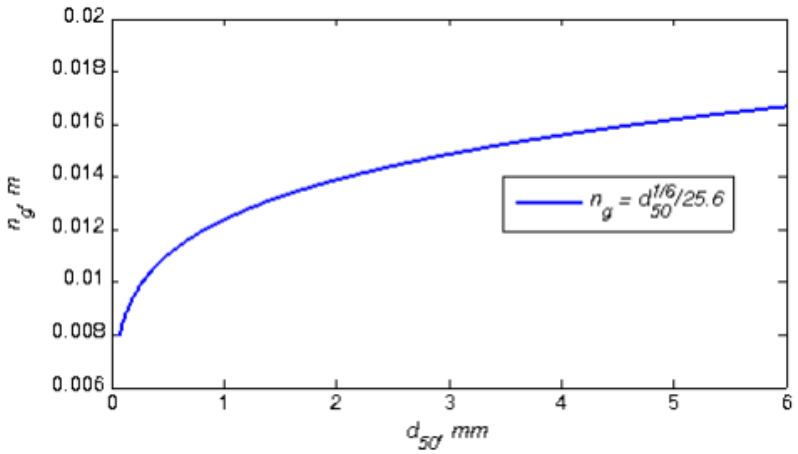

Figure 2 3. Example grain Manning's roughness coefficient following Strickler (1923).

Limerinos

Limerinos (1956) developed a bed roughness predictor based on data from 11 gravel-bed streams in California as (see Figure below)

40)
$$n_g = \frac{0.0926 A R^{1/6}}{1.16 + 2\log_{10}(R/d_{84})}$$

where

$$A = \begin{cases} 1.219 & \text{for SI units} \\ 1 & \text{for English units} \end{cases}$$

n_g = grain-related Manning's roughness coefficient [s/m$^{1/3}$]

R = hydraulic radius [L]

d_{84} = 84th percentile diameter [L]

The equation is applicable to high in-bank flows in straight, gravel-bed channels. All the data used corresponded to Froude numbers less than 1. The Limerinos equation only accounts for the grain roughness in gravel-bed streams and does not include other contributions. Therefore, it may be used as the base value in the Cowan (1956) method.

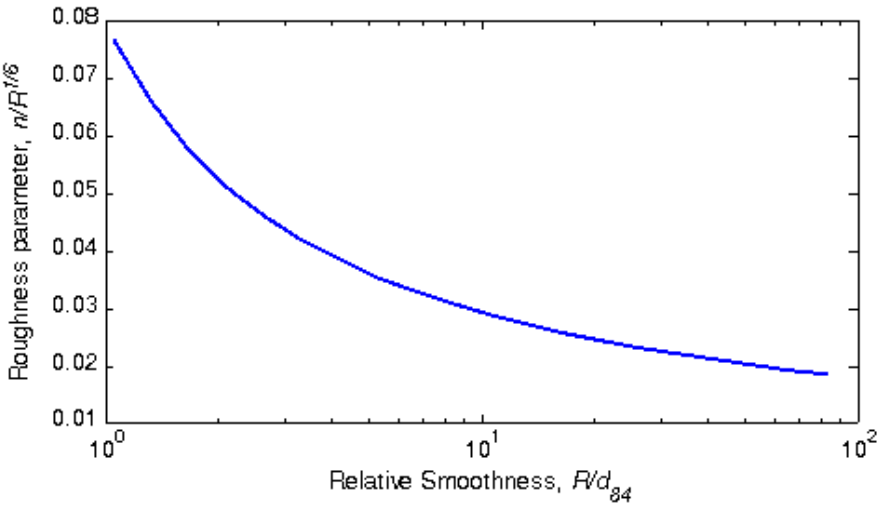

Figure 2 4. Grain roughness using the Limerinos (1956) equation.

It is noted that none of the expression above account for the full distribution of sediments and only consider a representative diameter. This is a limitation of the expressions when being applied to poorly sorted bed material.

2.2.3.2 Sediment Transport Roughness

Moving sediment produces a roughness due to the energy losses in transporting the sediment. This process is poorly understood and relatively few expressions are available in literature to account for this process. Here two simple formulas are available which account for the added roughness of bed-load transport. The formulas included here for sediment transport roughness are:

1. Wilson (1966)

2. Wiberg and Rubin (1989)

Wilson (1966)

A commonly used formula for the sediment transport related roughness is the Wilson formula (Wilson 1966, 1989ab)

41) $$k_{s,\ s} = 5\theta' d$$

where

θ' = $\frac{\tau_b'}{g(\rho_s - \rho)d}$ = grain-related Shields number [-]

d = grain size diameter [L]

The above formula has been used by Camenen and Larson (2007) and others. The above equation must therefore be solved simultaneously with the expressions for the bottom shear stress because the roughness depends on the stress. The exact solution is approximated here using explicit polynomial fits in order to avoid time-consuming iterations in calculating the bed shear stress.

Wiberg and Rubin (1989)

Wiberg and Rubin (1989) proposed the following formula for the sediment transport related roughness

42) $$k_{s,s} = 30\alpha_{WS} d_{50} \frac{a_1 \tau_b'/\tau_{cr}}{1 + a_2 \tau_b'/\tau_{cr}}$$

where

$k_{s,\ s}$ = sediment transport related roughness height [cm]

d_{50} = median grain size [cm]

τ_b' = grain shear stress [M/L/T^2]

τ_{cr} = critical shear stress [M/L/T^2]

α_{WS} = 0.056 [-]

a_1 = 0.68 [-]

a_2 = $0.0204 \ln(100 d_{50})^2 + 0.022 \ln(100 d_{50}) + 0.0709(0.27)$ [-]

The formula is based on the hypothesis that the transport roughness is directly proportional to the thickness of the bed-load layer proposed by Owen (1964). The formula is basically that of Dietrich (1982) with recalibrated coefficients.

2.2.3.3 Bedform Roughness

Ripple Roughness

The ripple roughness may be estimated as (see Grant and Madsen 1982; Nielson 1992; and Soulsby 1997)

43) $$k_{s,r} = \alpha_r \frac{\Delta_r^2}{\lambda_r}$$

where

$k_{s,r}$ = ripple roughness height [L]

α_r = \text{ripple roughness coefficient on the order of 10 [-]}

Δ_r = \text{ripple height }[L]

λ_r = \text{ripple length }[L]

Examples values of α_r from literature presented in the table below.

Table 27. Ripple Roughness Height Coefficient.

Reference	a_r
Grant and Madsen (1982)	27.7
Nielsen (1992)	8
Raudkivi (1997)	21.7
Soulsby (1997)	7.5
van Rijn (1993)	10

Dune Roughness

For dunes van Rijn (1984c) method is given by

44) $$k_{s,d} = 1.1\gamma_d \Delta_d \left[1 - \exp\left(-25\frac{\Delta_d}{\lambda_d}\right)\right]$$

where

γ_d = dune shape coefficient (~1.0) [-]

Δ_d = dune height [L]

λ_d = \text{dune length }[L]

The dune shape coefficient, γ_d, is approximately 1.0 for dunes with angle-of-repose faces as considered in van Rijn (1984c). Dunes with more gently sloping faces have smaller shape coefficients as is common in the field. Van Rijn (1993) proposed setting γ_d = 0.7 based on various field measurements of river systems. van Rijn (1984c) provided expressions for calculating the dune height and length and are shown in Equations

(2-94) and (2-95). The figure below shows the dune roughness based on van Rijn (1984c) as a function of the sediment transport stage.

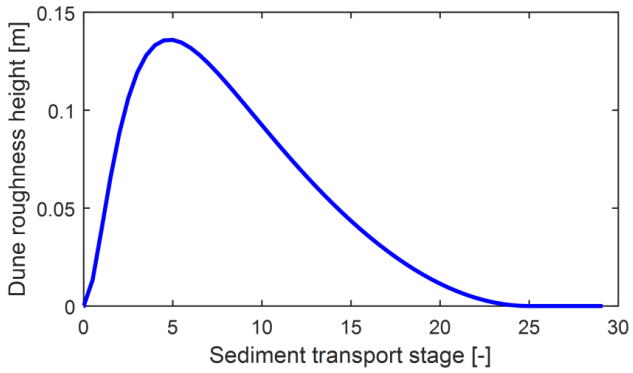

Figure 2 5. Dune roughness height based on van Rijn (1984a).

2.3 Total-load Transport Equation

The total-load sediment transport is the sum of all particles transported. The total-load may be divided into bed and suspended loads as a function of the transport mode. The total-load transport equation may be written as

45) $$\frac{\partial}{\partial t}\left(\frac{hC_{tk}}{\beta_{tk}}\right)+\nabla\cdot(h\boldsymbol{U}C_{tk})=\nabla\cdot(\varepsilon_{tk}h\nabla C_{tk})+E_{tk}^{HF}-D_{tk}^{HF}+S_{tk}$$

where

C_{tk} = total-load sediment concentration of the kth grain class [M/L^3]

β_{tk} = total-load correction factor for the kth grain class

U = depth-averaged current velocity in jth - direction [L/T]

h = water depth [L]

ε_{tk} = total-load diffusion (mixing) coefficient corresponding to the kth grain class}

E_{tk}^{HF} = total-load erosion rate in hydraulic flow [M/L^2/T]

D_{tk}^{HF} = \text{total-load deposition rate in hydraulic flow }[M/L^2/T]

S_{tk} = total-load source/sink term [M/L^2/T]

The main advantage for solving the total-load transport formula instead of separate bed- and suspended-load transport equations is the reduced computational costs since it requires one less transport equation solution and also simplifies the bed change and sorting computations.

It is noted that the velocity-weighted concentration definition is utilized. This definition results in the total-load correction factor appearing in the temporal term whereas the depth-averaged concentration definition results in an advection coefficient in the of the advection terms. Experience has shown that when simulating bedload dominate transport, the advection coefficient can have sharp spatial variations which may not be consistent with the transport capacity leading to unrealistic results. The load correction factor in the

temporal on the other hand is extremely well behaved even when its value varies significantly in space and/or time.

The above formulation is utilized for both cohesive and noncohesive sediments. Erosion is computed differently for cohesive and noncohesive sediment grain classes depending on the grain size and the bed composition. Erosion is also computed differently for the hydraulically wet and dry portions of the domain. The hydraulically wet portion is the region which is submerged by water and erosion is primarily due to bottom shear stresses. The hydraulically dry portion is the region where the erosion is primarily due to precipitation splash and surface runoff in the form of sheet flow. The source/sink term S_{tk} includes boundary conditions including surface runoff S_{tk}^{SR}.

- Bed-load Velocity (see page 35)
- Fraction of Suspended Sediments and Transport Mode Parameter (see page 37)
- Horizontal Diffusion Coefficients (see page 39)
- Load Correction Factor (see page 41)
- Schmidt Number (see page 43)
- Vertical Diffusion Coefficient (see page 43)

2.3.1 Bed-load Velocity

The bed-load velocity is the average particle velocity during transport. It is not the average velocity of the bed-load material, which is what is typically measured in a tracer studies or mobile bed laboratory experiments. The bed-load velocity different formulations available are plotted in the figure below and described in the following sub sections. In general, the formulations produce similar results except for the Julien and Bounvilay (2013) formulation which does not have a critical threshold for bed-load transport.

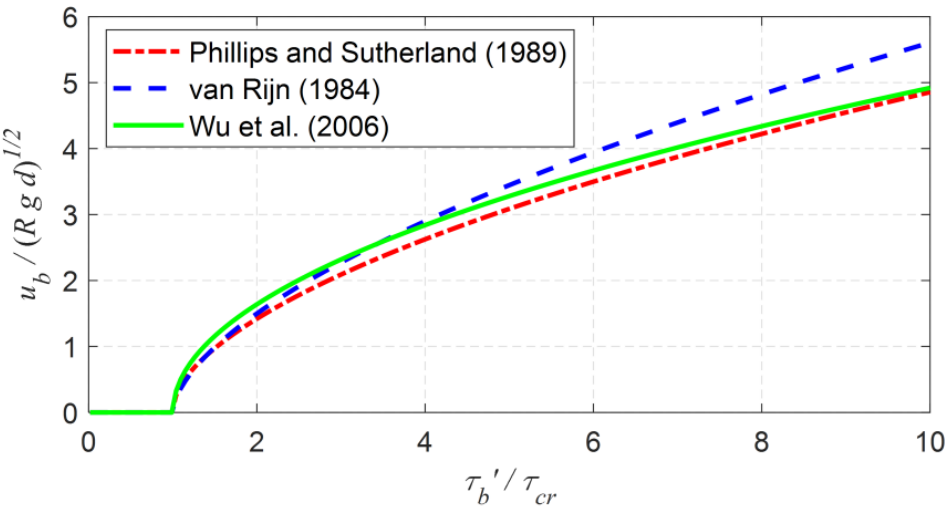

Figure 1. Comparison of bed-load velocity functions.

2.3.1.1 Phillips and Sutherland

Phillips and Sutherland (1989) proposed the following formula for the bed-load velocity

46) $$u_{bk} = 8.5\left\{ \frac{\tau_b'}{\rho_w} \max\left[1 - \left(\frac{\tau_{crk}}{\tau_b'} \right)^{1/2}, 0 \right] \right\}^{1/2}$$

where

τ_b' = grain-related bed shear stress [M/L/T^2]

τ_{crk} = critical bed shear stress for the k^{th} size class [M/L/T^2]

ρ_w = water density [M/L^3]

n' = grain-related Manning's roughness coefficient [T/L$^{1/3}$]

2.3.1.2 van Rijn

The van Rijn (1984a) formula for computing the bed load velocity (u_{bk}) is given by

47) $$\frac{u_{bk}}{\sqrt{R_k g d_k}} = 1.5 \max\left(\frac{\tau_b'}{\tau_{crk}} - 1, 0 \right)^{0.6}$$

where

$R_k = \rho_{sk}/\rho_w - 1$ = submerged specific gravity for the k^{th} grain class [-]

ρ_{sk} = particle density for the k^{th} grain class [M/L^3]

ρ_w = water density [M/L^3]

g = gravitational constant (~9.81 m/s^2) [L/T^2]

d_k = characteristic grain diameter for the k^{th} size class [L]

τ_b' = grain-related bed shear stress [M/L/T^2]

τ_{crk} = critical bed shear stress for the k^{th} size class [M/L/T^2].

The van Rijn (1984a) formula is based on laboratory experiments of Fernandez Luque (1974; 1976).

2.3.1.3 van Rijn-Wu

Wu et al. (2006) recalibrated the coefficients of the van Rijn (1984a) formula as

48) $$\frac{u_{bk}}{\sqrt{R_k g d_k}} = 1.64 \max\left(\frac{\tau_b'}{\tau_{crk}} - 1, 0 \right)^{0.5}$$

where

$R_k = \rho_{sk}/\rho_w - 1$ = submerged specific gravity for the k^{th} grain class [-]

ρ_{sk} = particle density for the k^{th} grain class [M/L^3]

ρ_w = water density [M/L^3]

g = gravitational constant (~9.81 m/s^2) [L/T^2]

d_k = characteristic grain diameter for the k^{th} size class [L]

τ'_b = grain-related bed shear stress [M/L/T^2]

τ_{crk} = critical bed shear stress for the k^{th} size class [M/L/T^2]

The Wu et al. (2006) formula produces similar bed-load velocities as the van Rijn (1984a) formula for low shear stresses but significantly lower bed-load velocities for high shear stresses where the van Rijn (1984a) departs from the other bed-load velocity formulations.

2.3.2 Fraction of Suspended Sediments and Transport Mode Parameter

The fraction of suspended sediments is defined as:

49) $$r_{sk} = \frac{q_{sk}}{q_{tk}}$$

where

r_{sk} : fraction of suspended sediments [-]

q_{sk} : suspended-load transport rate [M/L/T]

q_{tk} : total-load transport rate [M/L/T]

The fraction of suspended sediments is needed in the total-load transport model in order to separate the contributions from bed- and suspend-load to various parameters including the horizontal mixing coefficient and advection coefficients. The parameter is needed in order to close the system of equations. The fraction of suspended sediments is approximated by the transport mode parameter which is the ration of the suspended-load to total-load transport potential rates:

50) $$r_{sk} \approx f_{sk} = \frac{q^*_{sk}}{q^*_{tk}}$$

where

f_{sk} : transport mode parameter [-]

$q_{sk}{}^*$: suspended-load transport potential rate [M/L/T]

$t_k{}^*$: total-load transport potential rate [M/L/T]

There methods available to estimate the transport mode parameter:

1. Transport capacity method (Wu 2007)

2. Rouse parameter method of Greimann et al. (2008)

3. van Rijn (1984)

4. Jones and Lick (2001)

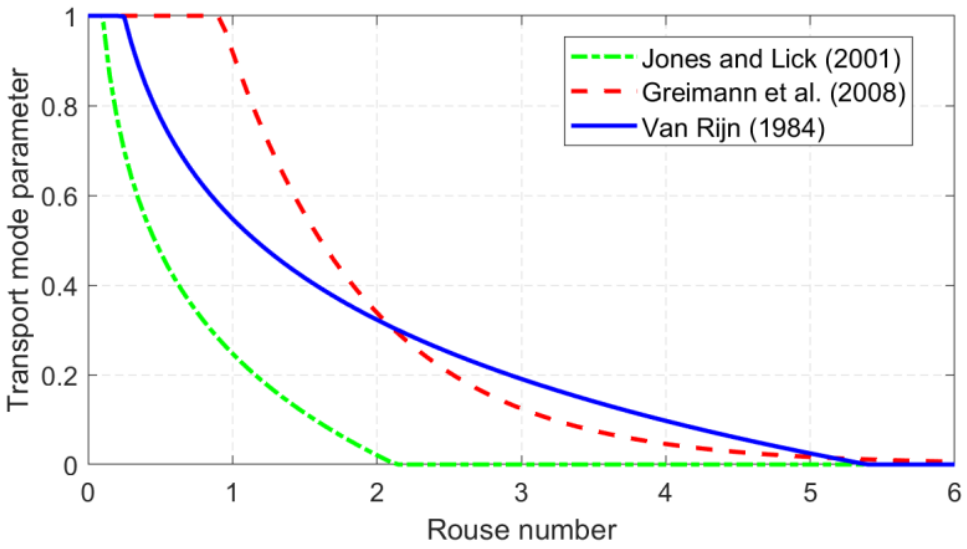

Figure 1. Representative transport mode parameter curves as a function of the Rouse number with d = 1 mm, ρ_w = 1000 kg/m^3, and ρ_s = 2650 kg/m^3.

2.3.2.1 Transport Capacity Method

This is the simplest and preferred method.

51) $$f_{sk} = \frac{q^*_{sk}}{q^*_{tk}}$$

The default option is the transport capacity method. If the total-load transport capacity formula may be written in terms of bed and suspended capacities, the transport capacity method is utilized. This is the most consistent approach with the transport formulas. However, if the transport formula is a bed-material formula such as the Laursen formula, another approach must be used.

2.3.2.2 Greimann et al.

The transport mode parameter proposed by Greimann et al. (2008) is as follows

52) $$f_{sk} = \min[1,\ 2.5\exp(-r_k)]$$

where

r_k = $\omega_{sk}/(\kappa u_*)$: Rouse parameter [-]

ω_{sk} : sediment settling velocity [L/T]

u_* : bed shear velocity [L/T]

2.3.2.3 van Rijn

An alternative formulation for estimating the fraction of suspended sediments was given by van Rijn (1984)

53) $$f_{sk} = 0.25 + 0.325 \ln(u_*/\omega_{sk})$$

where

ω_{sk} : sediment settling velocity [L/T]

u_* : bed shear velocity [L/T]

2.3.2.4 Jones and Lick

Jones and Lick (2001) developed the following formula for the transport mode parameter

54) $$f_{sk} = \begin{cases} 0 & \text{for } \tau_b < \tau_{crk} \\ \dfrac{\ln\left(\frac{u_*}{\omega_{sk}}\right) - \ln\left(\frac{\sqrt{\tau_{cr}/\rho_w}}{\omega_{sk}}\right)}{\ln(4) - \ln\left(\frac{\sqrt{\tau_{cr}/\rho_w}}{\omega_{sk}}\right)} & \text{for } \tau_b > \tau_{crk} \text{ and } u_* < 4\omega_{sk} \\ 1 & \text{otherwise} \end{cases}$$

where

ω_{sk} : sediment settling velocity [L/T]

u_* : bed shear velocity [L/T]

2.3.3 Horizontal Diffusion Coefficients

2.3.3.1 Total-load Horizontal Diffusion Coefficient

The total-load horizontal mixing/diffusion coefficient is determined as

55) $$\varepsilon_{tk} = r_{sk}\varepsilon_{sk} + (1 - r_{sk})\varepsilon_{bk} \quad \text{for} \quad k = 1, \ldots, N$$

where

r_{sk} = fraction of suspended-load [-]

ε_{sk} = suspended-load mixing coefficient [L^2/T]

ε_{bk} = bed-load mixing coefficient [L^2/T]

The calculation of the suspended- and bed-load mixing coefficients is described below.

2.3.3.2 Suspended-load Horizontal Diffusion Coefficient

The suspended-load horizontal mixing coefficient (ε_{sk}) represents the effects of turbulent diffusion. The horizontal sediment mixing coefficient is assumed to be related to the turbulent eddy viscosity as

56) $$\varepsilon_{sk} = \frac{\nu_t}{\sigma_{sk}} \quad \text{for } k = 1, \ldots, N$$

where

σ_{sk} =Schmidt number for k^{th} grain class [-]

ν_t = turbulent eddy viscosity [L^2/T]

If a turbulent eddy viscosity is not available either because the flow model solves a Diffusion Wave equation or simply because it was ignored in the flow model, then it may be calculated as

57) $$\nu_t = c_M u_* h$$

where

c_M = empirical coefficient ($c_M \approx 0.5 - 6$) [-]

u_* = bed shear velocity [L/T]

h = water depth [L]

It is noted that the horizontal and vertical sediment mixing coefficients have similar formulations but generally the horizontal coefficient will be much larger.

2.3.3.3 Bed-load Horizontal Diffusion Coefficient

The bed-load horizontal diffusion coefficient (ε_{bk}) represents the sediment mixing due to spatially and temporally varying bed-load velocities. The following formula is proposed for the bed-load horizontal diffusion coefficient.

58) $$\varepsilon_{bk} = c_B u'_* d_k$$

where

c_B = empirical coefficient ($c_B \approx 5$) [-]

u_* = bed shear velocity [L/T]

d_k = grain size diameter [L]

The bed-load horizontal mixing coefficient is much smaller than the suspended-load mixing coefficient. In addition, the dispersion produced by the mixing in the bed is usually much more significant than horizontal bed-load diffusion. Therefore, the bed-load diffusion coefficient can usually be ignored.

2.3.4 Load Correction Factor

2.3.4.1 Total-load Correction Factor

The total-load correction advection coefficient, β_{tk}, accounts for the vertical distribution of the suspended sediment concentration and velocity profiles, and the generally slower bed-load velocity compared to the depth-averaged current velocity (see figure below) (Wu 2007).

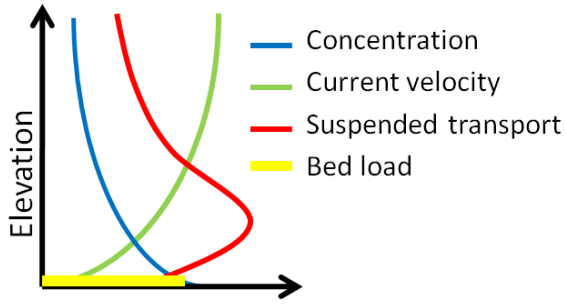

Figure 2.9: Schematic of sediment and current velocity profiles.

The total-load correction factor is given by

59) $$\beta_{tk} = \frac{1}{r_{sk}/\beta_{sk} + (1 - r_{sk})/\beta_{sk}}$$

where

r_{sk}= fraction of suspended-load [-]

β_{sk}= suspended-load correction factor [-]

β_{bk} = bed-load correction factor [-]

It is noted that the sediment transport is assumed to be in the same direction as the flow. Therefore, the influence of the bed-slope on the bedload is not included here. This effect is included separately in the model as an additional term in the bed-change equation. The user is given several options on how to compute the total-load correction factor including specifying a constant or computing it from the bed- and suspended-load correction factors which also may be computed with one of several methods or specified as a constant.

2.3.4.2 Suspended-load Correction Factor

The suspended-load correction factor is defined as the ration between the vertically integrated suspended-load transport and the transport computed as the simple product of the current velocity times the averaged sediment concentration:

60) $$\beta_{sk} = \frac{\int_0^h uc_k \, dz}{UC_k}$$

For fine cohesive sediments, β_{sk} is close to unity while for coarse sediments it is typically between 0.5 and 0.7. There are several options available for computing the suspended-load correction factor. The simplest is a user-specified constant. Two additional options are based on assuming vertical profiles for the current velocity and sediment concentration profiles. By assuming logarithmic current velocity and exponential suspended sediment concentration profiles, an explicit expression for the suspended-load correction factor can be obtained as (Sánchez and Wu 2011b)

61)
$$\beta_{sk} = \frac{\mathrm{E}_1(\phi_k A) - \mathrm{E}_1(\phi_k) + \ln(A/Z)\mathrm{e}^{-\phi_k A} - \ln(1/Z)\mathrm{e}^{-\phi_k}}{\mathrm{e}^{-\phi_k A}\left[\ln(1/Z) - 1\right]\left[1 - \mathrm{e}^{-\phi_k(1-A)}\right]}$$

where

$\phi_k = \omega_{sk} h/\varepsilon_{vk}$ [-]

$A = a/h$ [-]

$Z = z_0/h$ [-]

u = stream-wise current velocity [L/T]

ω_{sk} = sediment settling velocity for size class k L/T]

ε_{vk} = vertical mixing (diffusivity) coefficient [L^2/T]

a = reference height for the suspended load equal to the thickness of bed-load layer [L]

z_a = apparent roughness length [L]

$\mathrm{E}_1(x) = \int_x^\infty \frac{e^{-t}}{t} dt$ = exponential integral

The equation can be further simplified by assuming that the reference height is proportional to the roughness height (e.g. $a = 30 z_0$), so that $\beta_{sk} = \beta_{sk}(Z,\phi_k)$. Figure 3.4 shows a comparison of the suspended-load correction factor based on the logarithmic velocity with exponential and Rouse suspended sediment concentration profiles.

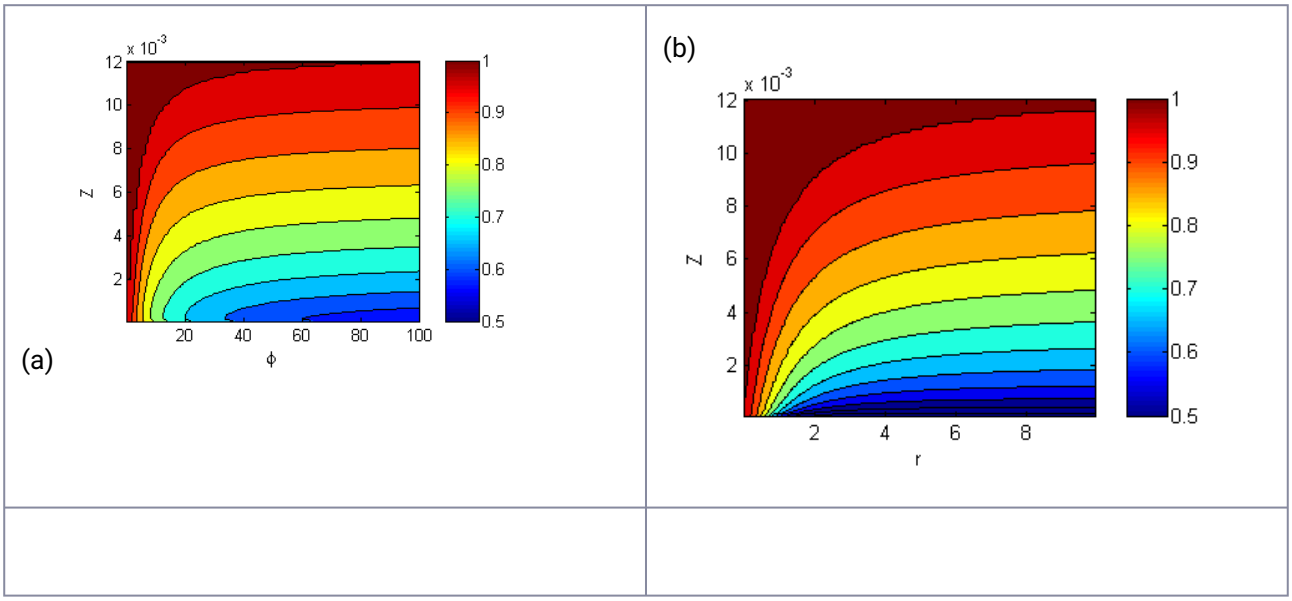

Figure 2 10. Suspended-load correction factors based on the logarithmic velocity profile and (a) exponential and (b) Rouse suspended sediment profiles. The Rouse parameter is $r = \omega_s/(\kappa u_*)$.

2.3.4.3 Bed-load Correction Factor

The bed-load advection coefficient is defined as the ration between the bed-load velocity and the depth-averaged current velocity:

62) $$\beta_{bk} = \frac{u_{bk}}{U}$$

where

u_{bk} = bed-load velocity [L/T]

U = depth-averaged current velocity [L/T]

The bed-load correction factor may be specified as a constant or computed with one of several bed-load velocity formulas (presented in the following section).

2.3.5 Schmidt Number

The Schmidt number is calculated using the van Rijn (1984b) formula which is based on measurements from Coleman (1981)

63) $$\frac{1}{\sigma_{sk}} = 1 + 2\left(\frac{\omega_{sk}}{u_*}\right)^2 \quad \text{for } 0.1 < \frac{\omega_{sk}}{u_*} < 1$$

where

ω_{sk} = sediment settling velocity for k^{th} grain class [L/T]

u_* = total bed shear velocity [L/T]

The applying the above equation the values of ω_{sk}/u_* values are limited to the range indicated above.

2.3.6 Vertical Diffusion Coefficient

The vertical diffusion coefficient is required for determining the suspended-load correction factor. The vertical sediment diffusion coefficient is assumed to be related to the turbulent eddy viscosity as

64) $$\varepsilon_{vk} = \frac{\nu_{tv}}{\sigma_{sk}}$$

where

ν_{tv} = vertical turbulent eddy viscosity [L^2/T]

σ_{sk} = Schmidt number [-]

The vertical turbulent eddy viscosity is computed as

65) $$\nu_{tv} = c_{Mv} u_* h$$

where

c_{Mv} = empirical coefficient [-]

u_* = bed shear velocity [L/T]

h = water depth [L]

2.4 Bed Change Equation

The fractional bed change is calculated as

66) $$\rho_{sk}(1-\phi_b)\left(\frac{\partial z_b}{\partial t}\right)_k = D_{tk} - E_{tk} + \nabla \cdot (\kappa_{bk} |q_{bk}| \nabla z_b)$$

where

z_b = bed elevation with respect to the vertical datum [L]

ρ_{sk} = grain class particle density [M/L^3]

ϕ_b = porosity of the eroded and deposited material [-]

D_{tk} = total-load deposition rate [M/L^2/T]

E_{tk} = total-load erosion rate [M/L^2/T]

$|q_{bk}|$ = bed-load mass transport rate magnitude [M/L/T]

κ_{bk} = empirical bed-slope coefficient for grain class k [-]

The last term on the right-hand side of the above equation accounts for bed-slope effects. The bed-slope term has the effect of moving sediment downslope and thus smoothing the bathymetry. Therefore, it improves stability. Another advantage of the term is that it is independent of the transport formula and therefore can be applied irrespective of the transport formula formulation.

The total bed change is defined as the sum of the fractional bed changes as

67) $$\frac{\partial z_b}{\partial t} = \sum_k \left(\frac{\partial z_b}{\partial t}\right)_k$$

2.4.1 Bed-Slope Coefficient

The bed-slope coefficient is calculated using a following formula (e.g. Koch and Flokstra 1981; Kovacs and Parker 1994; and Parker et al. 2003)

68)
$$\kappa_{bk} = \kappa_{b0}\sqrt{\frac{\tau_{crk0}}{\max(\tau_b', \tau_{crk0})}}$$

in which

κ_{b0} = empirical parameter approximately equal to 0.1 to 0.5 [-]

τ_{crk} = critical shear stress [M/L/T^2]

τ_b' = bed skin shear stress [M/L/T^2]

It is important to include a lower limit for the skin shear stress because not all transport formulas include a critical shear stress (e.g. Engelund-Hansen (1967) formula). A plot of the bed-slope coefficient is shown in the figure below. As the bed skin shear increases with respect to the critical shear stress, the effect of the bed-slope is decreased. Likewise, smaller grain classes will be less affected by the bed-slope compared to coarser grain classes because they will be in less contact with the bed and influenced more by the current than the bed slope.

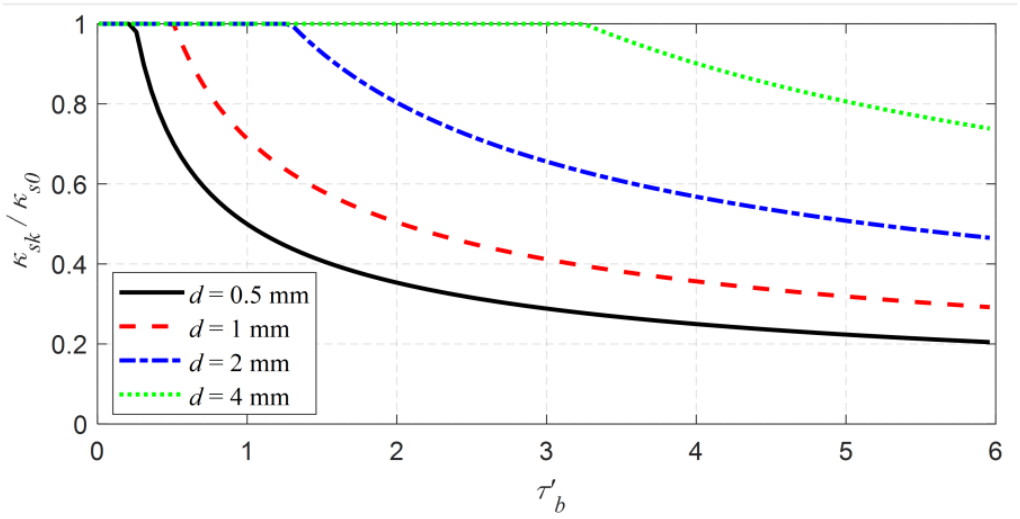

Figure 1. Bed-slope coefficient as a function skin shear stress, T_b', and grain size diameter d. The critical shear stress for each grain size is calculated with the Soulsby and Whitehouse (1997) equation.

2.5 Erosion

The area-averaged sediment erosion rate is computed as a function of the erosion potential

69)
$$E_{tk} = f_{1k} E_{tk}^*$$

where

E_{tk} : erosion rate [M/L^2/T]

f_{1k} : active grain class fractions by weight [-]

E_{tk}^{*} : potential erosion rate [M/L^2/T]

The active layer grain class fractions represent the sediment availability. The erosion potential consists of two components due to (1) hydraulic flow and (2) sheet and splash erosion:

70) $$E_{tk}^{*} = r_A^{HF} E_{tk}^{*HF} + r_A^{SS} E_{tk}^{*SS}$$

where

r_A^{SS} : fraction of horizontal area corresponding to sheet and splash erosion [-]

r_A^{HF} : fraction of horizontal area corresponding to hydraulic flow erosion [-]

E_{tk}^{*SS} : sheet and splash erosion potential [M/T/L^2]

E_{tk}^{*HF} : hydraulic flow erosion rate [M/T/L^2]

The incorporation of r_A^{SS} and r_A^{HF} in the above formulation is important since the present model is designed to support partially hydraulically wet and dry cells. It is noted that $r_A^{SS} + r_A^{HF} + r_A^{NE} = 1$ where r_A^{NE} represents the fraction of surface area which does contribute to erosion and includes structures, vegetation, etc. In the current version of the model, r_A^{NE} is assumed to be zero.

2.5.1 Hydraulic Flow Erosion

2.5.1.1 Cohesive Sediments

At low shear stresses, erosion occurs due to particle and small aggregate detachment, while at high shear stresses, erosion occurs primarily due to detachment of clasts or chunks of material and is referred to as “mass erosion” or “mass wasting”. This behavior may be captured by using different erodibility coefficients and critical shear stresses for surface and mass erosion:

71) $$E_{tc}^{*HF} = \begin{cases} 0 & \text{for } \tau_b \le \tau_{ce} \\ M\,(\tau_b/\tau_{ce} - 1) & \text{for } \tau_{ce} < \tau_b \le \tau_{cM} \\ M\,(\tau_{cM}/\tau_{ce} - 1) + M_M\,(\tau_b - \tau_{cM})/\tau_{ce} & \text{for } \tau_b > \tau_{cM} \end{cases}$$

where

E_{tc}^{*HF} : cohesive erosion potential (same for all cohesive grain classes) [M/L^2/T]

τ_b : bed shear stress [M/L/T^2]

τ_{ce} : critical shear stress for cohesive sediment erosion [M/L/T^2]

τ_{cM} : critical shear stress for mass wasting erosion [M/L/T^2]

M : surface erosion rate coefficient [M/L^2/T]

M_M : erodibility coefficient for mass wasting erosion [M/L^2/T]

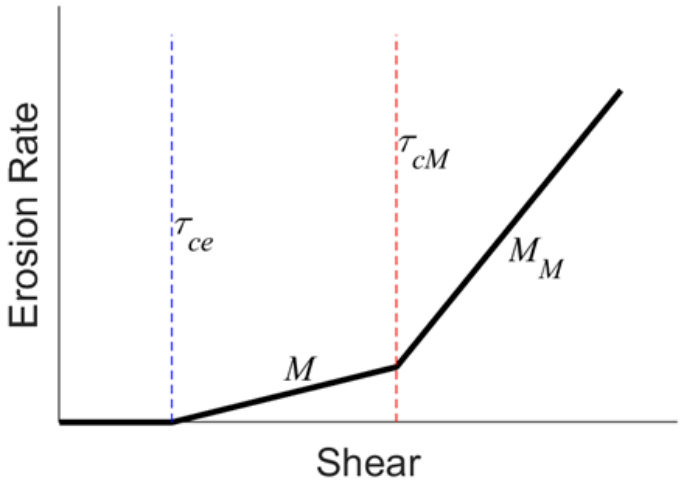

Figure 1. Piece-wise linear erosion potential formulation.

In other words, different values for the erosion coefficient are specified at different ranges of bed shear stress. If the coefficients *M* and M_M are equal then the above formulations reduces to the classic linear formulation by Ariathurai (1974) Ariathurai and Arulanandan (1978) based on the data of the data from Partheniades (1962)

72)
$$E_{tc}^{*HF} = \begin{cases} 0 & \text{for } \tau_b \le \tau_{ce} \\ M\,(\tau_b/\tau_{ce} - 1) & \text{for } \tau_{ce} < \tau_b \end{cases}$$

$$E_{tc}^{*HF} = \begin{cases} 0 & \text{for } \tau_b \le \tau_{ce} \\ M\,(\tau_b/\tau_{ce} - 1) & \text{for } \tau_{ce} < \tau_b \end{cases}$$

where

E_{tc}^{*HF} : cohesive erosion potential [M/L^2/T]

M : surface erosion rate coefficient [M/L^2/T]

2.5.1.2 Noncohesive Sediments

The hydraulic flow erosion is simulated using the adaptation formulation (see Wu et al. 2007 and references therein).

73)
$$E_{tk}^{*HF} = \alpha_{tk}\,\omega_{sk}\,C_{tk}^{*}$$

where

α_{tk} : total-load adaptation coefficient [-]

ω_{sk} : sediment settling velocity [L/T]

$C_{tk}^{*} = q_{tk}^{*}/(hU)$: sediment concentration potential [M/L^3]

q_{tk}^{*} : total-load sediment transport [M//L/T]

It is noted that if the bed consists of both cohesive and noncohesive sediments, then the erosion potential of noncohesive sediments is limited to that of the noncohesive sediments (see also Brown et al. 2014). This is so that the erosion of noncohesive sediment fractions is never larger than that of the cohesive fractions. One advantage of the adaptation coefficient compared to near-bed sediment concentration potential formulations, is that there are many formulations for the sediment transport potential as compared to the near-bed sediment concentration potential. It also makes it easier to compare model results with Exner type models since for uniform equilibrium conditions they should produce the same transport rates. The main disadvantage of the adaptation approach is that it introduces an additional calibration parameter.

When simulating mixed cohesive and noncohesive sediments, the erosion rates for noncohesive sediments are always computed with the transport formulas for noncohesive sediments but with corrections to the critical shear stress or velocity. In addition, the erosion rates for noncohesives grain classes are limited using the cohesive sediment erosion rate.

2.5.2 Splash and Sheet Flow Erosion

Splash and sheet flow erosion occurs in the “hydraulically dry” portion of the domain which is above the water surface elevation but has precipitation and surface runoff. The region is often referred to simply as the inter-rill region. The splash and sheet flow erosion are computed with a modified form of the rangeland erosion formula developed by Wei et al. (2009)

74) $$E_{rk}^{*SS} = r_{E,k} K_{SS} r^{1.052} \upsilon^{0.592}$$

where

K_{SS} = splash and sheet erodibility coefficient (dimensional)

$r_{E,k}$ = grain size function of eroded material (described in a later section) [-]

r = precipitation intensity $[L/T]$

$\upsilon = r - f$ = excess precipitation rate $[L/T]$

f = infiltration rate $[L/T]$

The splash and sheet flow erosion potential formula has been modified for non-uniformly sized sediment by including a grain size function. The function determines the sediment gradation of the eroded material. A simple formulation is proposed as a function of the sediment fall (settling) velocity:

75) $$r_{E,k} = \begin{cases} 0 & \text{for } d_k > d_{sand} \\ \dfrac{\omega_{sk}^{-m}}{\frac{1}{N_{sand}} \sum_{i=1}^{N} \omega_{si}^{-m}} & \text{for } d_k \le d_{sand} \end{cases}$$

where

ω_{sk} = settling velocity for grain class k [L/T]

d_{sand} = grain size threshold equal to 2 mm [L]

N_{sand} = number of grain classes smaller than d_{sand} [-]

m = empirical coefficient between 0 and 0.5 (default = 0.2) [-]

It is assumed that only grains smaller than d_{sand}= 2 mm are eroded by sheet and splash erosion. If the coefficient m is set to 0, then all of the grain classes with diameters less than d_{sand} have equal erosion potential. The figure below shows an example of the sheet and splash erosion grain size function.

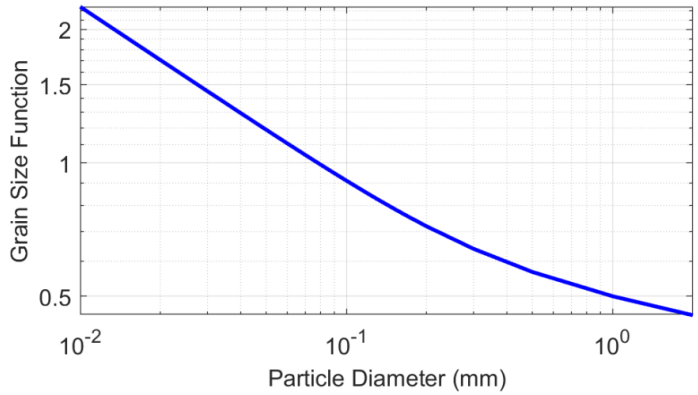

Figure 2 8. Example sheet and splash erosion grain size function with m = 0.2 and the fall velocity computed from Cheng (1997).

The above approximation is a necessary one for non-uniform sediments because without it the sheet and splash erosion formulations can produce extremely unrealistic erosion gradations for sediment beds with coarse material. Additional research is needed to better extend existing sheet and splash erosion formulas to graded sediments.

2.6 Deposition

The deposition is assumed to occur only over the hydraulically wet portion of cells. Hence, the area-averaged deposition rate may be written as

76) $$D_{tk} = r_A^{HF} D_{tk}^{HF}$$

where

r_A^{HF} : fraction of horizontal area corresponding to hydraulic flow [-]

D_{tk}^{HF} : hydraulic flow deposition rate [M/L^2/T]

The formulation for the hydraulic flow deposition rate depends on whether the sediments are cohesive or noncohesive.

2.6.1 Noncohesive Sediments

The concentrated flow erosion and deposition formulation by Wu et al. (2007) and others is given by

77) $$D_{tk}^{HF} = \alpha_{tk}\omega_{sk}C_{tk}$$

where

α_{tk} : adaptation coefficient [-]

ω_{sk} : sediment settling velocity [L/T]

$C_{tk}^{*} = q_{tk}^{*}/(hU)$: sediment concentration potential [M/L^3]

q_{tk}^{*} : sediment transport potential [M/L/T]

h : water depth [L]

U : depth-averaged current velocity [L/T]

2.6.2 Cohesive Sediments

The sediment deposition rate for cohesive sediments is given by (Krone 1962; Partheniades 1962; Mehta and Partheniades 1975)

78) $$D_{tk}^{HF} = P_D\omega_{sf}C_{tk}$$

where

D_{tk}^{HF} : total-load deposition rate [M/L^2/T]

P_D : probability of deposition [-]

ω_{sf} : floc settling velocity [L/T]

C_{tk} : total-load mass concentration [-]

The grain class settling velocity may be equal to the dispersed particle settling velocity or a floc settling velocity depending on the sediment concentration. The probability for deposition by Krone (1962) and Partheniades (1962) is given by

79) $$P_D = \max\left(1 - \frac{\tau_b}{\tau_{crD}}, 0\right)$$

where

τ_b : bed shear stress [M/L/T^2]

τ_{crD} : critical shear stress for deposition [M/L/T^2]

In HEC-RAS 1D sediment the critical shear stress for deposition is set to the critical shear stress for erosion (i.e. mutually exclusive erosion and deposition model). Although the mutually exclusive erosion and deposition model has been successful in many laboratory and field studies (e.g. Dahl et al. 2018) the approach has several issues. Sanford and Halka (1993) found that the mutually exclusive model fails to reproduce field measurements in Chesapeake Bay, USA. Sanford and Halka also presented a summary of field observations with similar behavior. Winterwerp (2003) found that the laboratory experiments of Krone (1962) can be reproduced using a continuous deposition model (i.e. P_D = 1) and a stochastic erosion model. Even if a minimum shear for settling is considered physically reasonable for free settling cohesive particles, it is not reasonable for flocs which can have settling velocities as high as noncohesive particles. In addition,

erosion without deposition represents an equilibrium concentration that is infinite, which is not physically reasonable. The critical shear for deposition could be made a function of the fall velocity, but formulations for this do not exist. Winterwerp and van Kesteren (2004) concluded that the probability of deposition in fact does not exist and that for engineering applications the continuous deposition model should be utilized. In fact, many newer sediment studies have shown that cohesive sediment erosion and deposition occur simultaneously. For these reasons, HEC-RAS 2D the probability of deposition is set to 1 representing a continuous deposition model. This also simplifies the model calibration because there is no need to specify and calibrate a critical shear stress for deposition.

2.7 Adaptation Parameters

2.7.1 Total-Load Adaptation Length

There are several options to calculate the total-load adaptation length. The simplest option is to utilize a constant adaptation length calibrate the parameter using field measurements. Experience has shown that for most field applications, this approach is sufficient. However, several other methods are available with varying degrees of complexity. The total-load adaptation length may also be determined.
The advection coefficient considers several processes which affect the velocity and direction of the sediment transport including the vertically non-uniform distribution of the horizontal current velocity and sediment concentration profiles and bed-slope effects.
There are four methods for calculating the total load adaptation coefficient in HEC-RAS:

1. Constant adaptation length
2. Weighted averaged of bed- and suspended load adaptation lengths

In the case that a constant adaptation length is specified, the total-load adaptation coefficient is computed as

80) $$\alpha_t = \frac{hU}{L_t \omega_s}$$

where

h : water depth [L]

U : Current velocity [L/T]

ω_s : sediment settling velocity [L/T]

L_t : total-load adaptation length [L]

The fall velocity is equal to the transport grain size, for single size sediment transport, or the median grain size, in the case of multiple-sized sediment transport.

A more realistic approach to use a transport weighted average of the bed- and suspended-load adaptation lengths (Wu 2007)

81) $$\alpha_t = r_s \alpha_s + (1 - r_s) \frac{hU}{L_b \omega_s}$$

where

α_s : suspended-load adaptation coefficient [-]

L_b : bed-load adaptation length [L]

r_s : fraction of suspended load of the total load.

The methods for determining and are described in subsequent sections.

2.7.2 Bed-load Adaptation Length

There are two options for the bed-load adaptation length. The first is for the user to specify a constant value. There are two methods for calculating the total load adaptation coefficient in HEC-RAS:

1. Constant bed-load length
2. Depth-dependent method

In the case of the depth-dependent method, the adaptation length is computed as

82) $$L_b = f_{bL} h$$

where

f_{bL} : depth-dependent factor approximately between [-]

h : water depth [L]

2.7.3 Suspended-load Adaptation Coefficient

There are three options for computing the suspended-load adaptation coefficient:

1. Constant coefficient
2. Zhou and Lin (1998)
3. Armanini and Di'Silvio

The figure below shows two examples of the two formulations for the suspended-load adaptation coefficient.

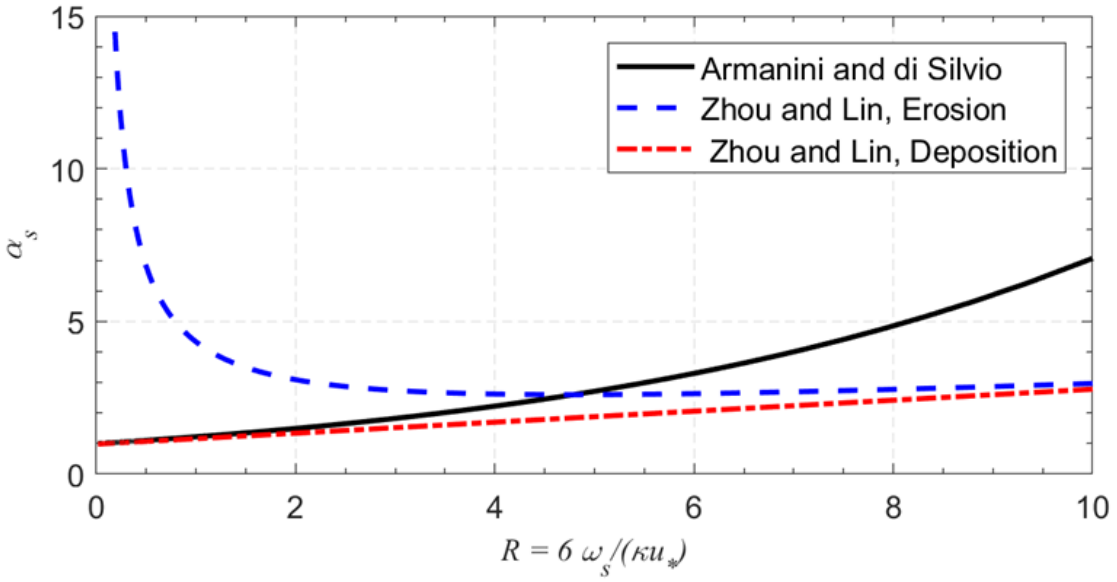

Figure 1. Suspended-load adaptation coefficient.

In the case of the Zhou and Lin (1998) formulation, the adaptation coefficient is computed by solving a 2DV advection-diffusion equation of suspended load with constant diffusivity and uniform flow. A concentration bottom boundary condition is specified for the erosion case, and a gradient boundary condition for the deposition case. The analytical solution is given by

83) $$\alpha_s = \frac{R}{4} + \frac{\sigma_1^2}{R}$$

where

$R = 6\omega_s/(\kappa u_*)$: suspendesion parameter [-]

ω_s : sediment settling velocity [L/T]

u_* : total bed shear velocity [L/T]

σ_1 : first positive root of the following equations:

$\tan\sigma = -\sigma/R$ for erosion

$2\cot\sigma = 2\sigma - R/2$ for deposition

A plot of the suspended-load adaptation coefficient following Zhou and Lin (1998) is shown in the figure below. The adaptation coefficients for erosion and deposition can be very different, especially for low suspension parameter values. In practice, a weighted average of the erosion and deposition values is used in order to avoid stability issues. It is also noted that the adaptation coefficient of Zhou and Lin (1998) is always greater than 1.

Armanini and Di'Silvio (1986) proposed the following formula for the adaptation coefficient

84) $$\frac{1}{\alpha_s} = \frac{a}{h} + \left(1 - \frac{a}{h}\right)\exp\left[-1.5\left(\frac{a}{h}\right)^{1/6}\frac{\omega}{u_*}\right]$$

where

ω_s : sediment particle settling velocity [L/T]

$a = 33z_0$: thickness of the bottom layer [L]

z_0 : roughness length [L]

u_* : total bed shear velocity [L/T]

h : water depth [L]

2.8 Bed Sorting and Layering

Bed sorting is the process in which the bed material changes size composition (fraction of each grain size class). The bed is discretized into multiple layers to consider the heterogeneity of bed material size composition along the bed depth (see figure below). The fraction of each grain class is calculated and stored in each layer. The sorting of sediments is calculated with the active or mixing layer concept (Hirano 1971; Karim and Kennedy 1982; Wu 1991; Wu 2004). The active layer is the top layer of the bed which exchanges directly with the sediment moving in the water column. In other words, only the sediment in the mixing layer exchanges with the moving sediment in the water column; whereas, the sediment in the subsurface layers below the active layer does not directly exchange or contact with the moving sediment.

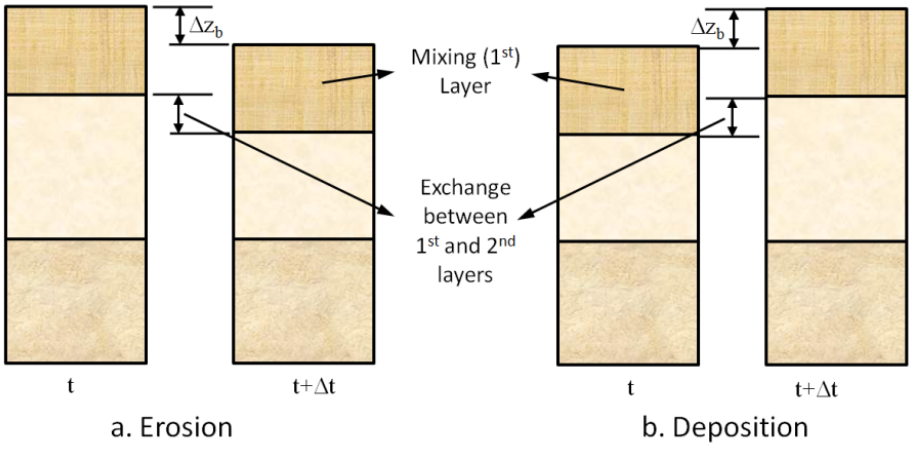

Figure 1. Multiple bed-layer model of bed material sorting (Wu 2007).

There exist several multiple bed layer models in literature (e.g. Spasojevic and Holly 1993; Wu 1991; Lin 2010; Brown 2012; Lai 2020; Wu 2004). Here a new approach is developed based on the work of Wu (1991) and modified for variable bed and grain densities. The bed sorting and layering model solves for fractional sediment mass concentrations in each layer defined as

85) $$m_{jk} = f_{jk}\rho_{dj}$$

where

m_{jk} : fractional mass concentration in layer *j* and grain class *k* [M/L^3]

f_{jk} : grain class fraction by weight in layer *j* and grain class *k* [-]

ρ_{dj} : dry bulk density of layer *j* [M/L^3]

It is straightforward to see that the sum of the fractional mass concentrations is equal to the dry bulk density

86) $$\rho_{dj} = \sum_k m_{jk}$$

The fractional mass concentrations, m_{jk}, are analogous to the total-load fractional mass concentrations, C_{tk}, solved with the transport equation. With the above definitions, the equations describing the bed layer thickness, porosity, and gradation of the first and second layers are given by

87) $$\delta_1 = \max\left(f_{1,90} d_{90}, 0.5\Delta\right)$$

88) $$\frac{\partial \delta_2}{\partial t} = \frac{\partial z_b}{\partial t} - \frac{\partial \delta_1}{\partial t}$$

89) $$\frac{\partial (m_{1k}\delta_1)}{\partial t} + m_{*k}\frac{\partial \delta_2}{\partial t} = \rho_{sk}(1-\phi_b)\left(\frac{\partial z_b}{\partial t}\right)_k$$

90) $$\frac{\partial (m_{2k}\delta_2)}{\partial t} = m_{*k}\frac{\partial \delta_2}{\partial t}$$

where

δ_1 : first layer thickness [L]

δ_2 : second layer thickness [L]

$f_{1,90}$: user-specified active layer scaling factor (typically 1 to 10) [-]

d_{90} : 90th percentile diameter [L]

Δ : bedform height [L]

z_b : bed elevation with respect to the vertical datum [L]

ρ_{sk} : grain density [M/L^3]

ϕ_b : porosity of the eroded and deposited material [-]

$m_{1k} = f_{1k}\rho_{d1}$: fractional mass concentration in the first (active) layer [M/L^3]

$m_{2k} = f_{2k}\rho_{d2}$: fractional mass concentration in the in second layer [M/L^3]

$m_{*k} = \begin{cases} m_{1k} \text{ for } \partial(z_b - \delta_1)/\partial t \geq 0 \\ m_{2k} \text{ for } \partial(z_b - \delta_1)/\partial t < 0 \end{cases}$ [M/L^3]

The approach allows for variable bed density and grain density and is also computationally efficient. For the case when the bed porosity and grain density are constant, the above equations reduce to the equations proposed by Wu (2004). It is noted that there is no material exchanged between the sediment layers below the second layer. Solving for the fractional mass concentrations in each bed layer is more convenient than solving for volumes because the total volume of a bed layer is not conserved while the total mass is conserved. In addition, the sum of the fractional mass concentrations directly produces the dry bulk density which is utilized for computations such as consolidation.

2.9 Porosity

The treatment of the porosity in HEC-RAS 2D sediment is different from that of HEC-RAS 1D. The dry bulk density is treated whenever possible as bulk property of sediment mixtures. There is not a one-to-one relationship between grain fractions and porosity. The temporal variation of the bed density is computed by solving for the fractional mass concentrations in each bed layer (analogous to sediment concentrations in the water column). The dry bulk density is the sum of the fractional mass concentrations. During this computation it is necessary to calculate the porosity of newly deposited sediments. Newly deposited sediments are mixed in the active layer with existing sediments to calculate the evolution of the active layer dry bulk density. The dry bulk density calculation is different for cohesive, noncohesive, and mixed cohesive/ noncohesive sediments as outlined in the sections below. In addition, if the dry bulk density of the initial bed is not specified the same methods are applied to compute the initial bed. Therefore, the methods described below apply to both the initial bed and freshly deposited sediments.

2.9.1 Noncohesive Sediments

There are two methods in for estimating the dry bulk density of graded noncohesive sediments (i.e. sands and larger):

1. Colby: User-defined noncohesive grain-class dry densities and the Colby (1963) formula
2. Wooster: User-defined particle density, the empirical porosity formula of Wooster et al. (2008) and the Colby (1963) formula

The Colby (1963) formula is utilized when the user-specifies grain-class porosities, dry bulk densities, or dry unit weights, while the Wooster et al. (2008) formula is applied when these are left empty.

2.9.1.1 Colby

The simplest option to compute the noncohesive porosity the Colby (1963) formula

91) $$\frac{\hat{f}_n}{1-\phi_n} = \sum_k \frac{\hat{f}_k}{1-\phi_k} \quad \text{for } k \in \text{noncohesive}$$

where

ϕ_n : porosity of noncohesive deposited sediments [-]

$\hat{f}_n = \sum_k \hat{f}_k \quad \text{for} \quad k \in$ noncohesive : noncohesive fraction by volume [-]

$\hat{f}_k$: grain class fraction (by volume) of deposited sediments [-]

ϕ_k : user-specified porosity of grain class *k* [-]

It is noted that the grain class fractions above are represent the fractions by volume. This is necessary for simulating sediments with variable grain densities.

2.9.1.2 Wooster

There several formulas in literature for estimating the bed porosity of natural sands and gravels (e.g. Carling and Reader 1982; Wu and Wang 2006; Wooster et al. 2008). Rogers and Head (1961) who found that the bed porosity is mainly controlled by the sediment sorting and particle shape and presented several graphical curves. Frings et al. (2011) compared several formulas from literature to fluvial sand-gravel deposits and found that the best predictors for the sediment porosity were those methods which utilized the information on the entire grain size distribution such as the Wooster et al. (2008) formula given by

92) $$\phi_n = 0.621\sigma_{gn}^{-0.659}$$

where ϕ_n and σ_{gn} are the porosity and geometric standard deviation of the deposited material, respectively. Although Wooster et al. (2008) developed their formula based on 32 laboratory samples with unimodal sediments packed by hand, they recommend the applicability of the formula to naturally packed sediment deposits or deposits with bimodal distributions.

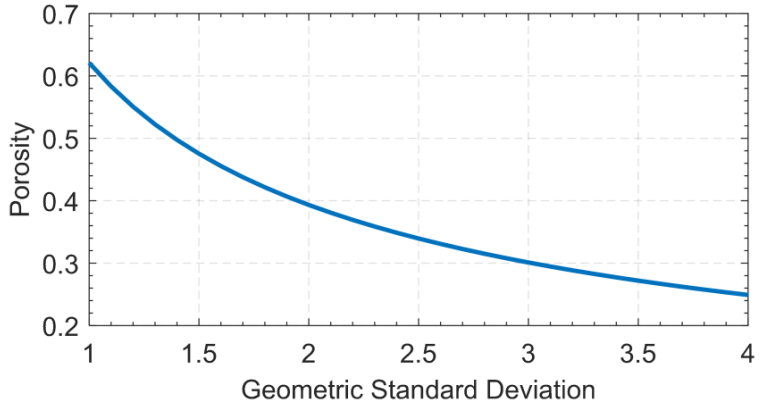

Figure 1. Porosity as a function of geometric standard deviation from Wooster et al. (2008).

The geometric standard deviation of the noncohesive transported material is

93) $$\sigma_{gn} = \exp\sqrt{\frac{1}{f_n}\sum_k f_k(\ln d_k - \ln d_{gn})^2} \quad \text{for } k \in \text{noncohesive}$$

where

f_k : grain class fractions by weight [-]

d_k : characteristic grain diameter for grain class *k* [L]

$f_n = \sum_k \hat{f}_k$ for $k \in$ noncohesive

d_{gn} : geometric mean of the noncohesive material [L]

The geometric mean of the transported material is

94) $$d_{gn} = \exp\left(\frac{1}{f_n} \sum_k f_k \ln d_k \right) \quad \text{for } k \in \text{noncohesive}$$

2.9.2 Cohesive Sediments

For fine sediments, the filling may be assumed to be negligible and following formula is used by Colby (1963)

95) $$\frac{\hat{f}_c}{1-\phi_c} = \sum_k \frac{\hat{f}_k}{1-\phi_k} \quad \text{for } k \in \text{cohesive}$$

where

ϕ_c : porosity of cohesive sediments [-]

f_k : grain class fraction by volume [-]

ϕ_k : user-specified porosity corresponding to each grain class [-]

2.9.3 Mixed Cohesive and Noncohesive Sediments

For mixed cohesive and noncohesive sediments the porosity of deposited sediments may be calculated assuming a bimodal mixture consisting of a cohesive and non-cohesive sediments with fractions $\hat{f}_c$ and $\hat{f}_n$ respectively. By definition $\hat{f}_n + \hat{f}_c = 1$. The porosity for the deposited mixture is calculated as (Han et al. 1981; Wu and Li 2017)

96) $$\frac{1}{1-\phi} = \frac{\hat{f}_n}{1-\phi_n}(1-B) + \hat{f}_n B + \frac{\hat{f}_c}{1-\phi_c}$$

where

B : filling or packing parameter [-]

$\hat{f}_n = \sum_k \hat{f}_k \quad \text{for} \quad k \in$ noncohesive : fraction by volume of noncohesive sediments [-]

$\hat{f}_c = \sum_k \hat{f}_k \quad \text{for} \quad k \in$ cohesive : fraction by volume of cohesive sediments [-]

ϕ_n : porosity of non-cohesive sediments [M/L^3]

ϕ_c : porosity of cohesive sediments [M/L^3]

The packing parameter is calculated following Wu et al. (2017) as

97) $$B = \min\left(\frac{PR_N}{nN_c}, B_{\max} \right)$$

where

$P = \frac{\hat{f}_c/d_c}{\hat{f}_n/d_n+\hat{f}_c/d_c}$: probability of a coarse sediment particle contacting a fine sediment particle [-]

$R_N = \frac{\hat{f}_c d_n^3}{\hat{f}_n d_c^3}$: ratio of numbers of fine and coarse particles in the sediment mixture [-]

$n = 0.1124\frac{d_n}{d_c}$: number of layers of fine particles to fill the void corresponding to each coarse particle [-]

$N_c = \frac{4\pi}{\beta^2 cos30}$: number of fine particles needed to cover the surface of a coarse particle [-]

$\beta = 2\sin^{-1}\left(\frac{d_n}{d_n+d_c}\right)$

$d_c = \hat{f}_c^{-1}\sum_k \hat{f}_k \quad \text{for} \quad k \in$ cohesive:= characteristic grain size for cohesive transported sediments [L]

$d_n = \hat{f}_n^{-1}\sum_k \hat{f}_k \quad \text{for} \quad k \in$ noncohesive : characteristic grain size for noncohesive transported sediments [L]

$\hat{f}_c$: fraction by volume of cohesive sediments [-]

$\hat{f}_n$: fraction by volume of noncohesive sediments [-]

B_{max} : maximum filling parameter (approximately 0.9) [-]

As an example of the Wu and Li (2017) method, the figure below shows the dry bulk density and porosity of a bimodal sediment mixture. The porosity of fines and noncohesives are 0.61 and 0.4, respectively. The grain density is 2650 kg/m^3. The plots show how the porosity first decreases as the fraction of fines increases to a minimum value at around 30% fines, and then increases afterwards.

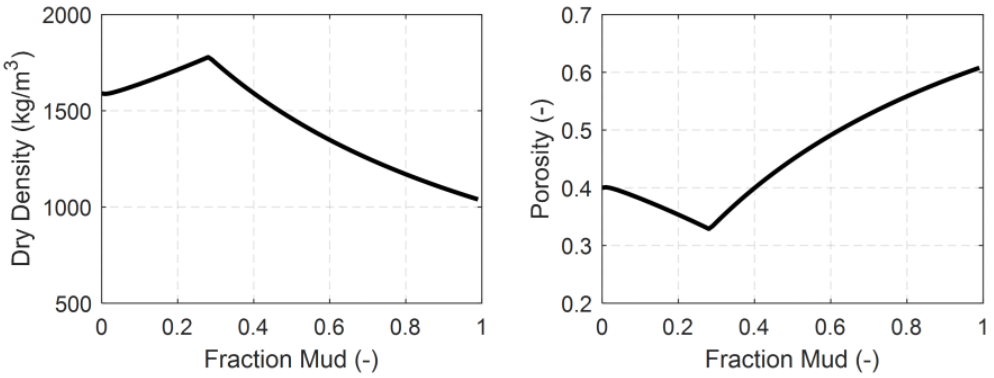

Figure 2. Example variation of dry bulk density (left) and porosity (right) for a bimodal sediment mixture of fines and sand.

2.10 Subsidence

Subsidence is the lowering of the Earth's surface due to aquifer-system compaction, drainage of organic soils, underground mining, primary and secondary compaction, hydrocompaction, etc., which occur below the upper sediments. It is therefore assumed that subsidence does not affect the dry bulk density of the upper sediments and only modifies the elevation of the bed surface and layers. The change in elevation due to subsidence is specified as user-defined subsidence rate (i.e. velocity).

2.11 Consolidation

Consolidation is the process of the compaction through the expulsion or pore water resulting in an increase in bed dry bulk density and bed material strength. The consolidation process in the upper sediment layer is modelled in order to calculate the compaction, increase in dry bulk density, and shallow subsidence. The mass continuity equation for the surface sediment layer is given by

98) $$\frac{\partial}{\partial t}\int_{z_0}^{z_b}\rho_d\,dz = 0$$

where

t : time [T]

ρ_d : dry bulk density [M/L^3]

z_0 : bottom of surface sediment layer [L]

z_b : bed surface elevation [L]

z : vertical coordinate [L]

Consolidation is computed utilizing a user-specified curve of dry bulk density as a function of time

99) $$\rho_d = f(t)$$

where

ρ_d : dry bulk density [M/L^3]

f : consolidation function

t : time [T]

The approach therefore ignores variables such as self-weight, bed composition, water temperature, etc. Although simplistic, the approach captures the general behavior of consolidation and is easy to specify. During the model simulation, the bed dry bulk density is used to estimate a corresponding time, then the time is advanced by a computational time step, and the curve is again used to compute a new dry bulk density. If the bed dry bulk density is higher than the largest value on the curve, then no consolidation occurs.

2.12 Fall Velocity and Settling

2.12.1 Fall Velocity of Cohesives

Cohesive particles may settle in the form of particles, flocs and/or aggregates. Generally, flocculation is negligible for sediment particles larger than 0.03 mm (see Migniot 1968). The flocculation of particles is

affected by the sediment size and concentration, water salinity, temperature, and turbulence intensity, and among others. The settling velocity of flocs can be several orders of magnitude larger than that of the dispersed sediment particles it is important to consider the sediment velocity of flocs. However, the flocculation process is very complicated as it is a function of the sediment concentration, particle sizes, turbulence, water temperature, salinity, pH, etc. At present, the Hwang (1989) floc settling velocity formulation is implemented as well as a user-specified concentration versus settling curve. These two methods compute the floc settling velocity as a function of concentration. It is also important to mention that there are a wide range of settling velocities for a given concentration, and the settling velocity utilized represents an average settling velocity of all the particles and flocs for a given concentration. The floc settling velocity is corrected for water temperature by assuming the fall velocities are inversely proportional to the dynamic viscosity (see Wu 2007). Other factors such as salinity and turbulence are presently not accounted for the floc settling velocities. Currently, the settling velocity of aggregates is not considered. The only way aggregates can be modeled currently is by assuming they are conservative particles which are not created or destroyed and computing their settling velocity utilizing one of the particle settling velocity formulas described above.

2.12.1.1 Hwang

The Hwang (1989) floc settling formula is based on Wolanski et al. (1989) may be written as

100)
$$\omega_{sf} = \begin{cases} l\omega_{sk} & \text{for } C \le C_1 \\ a\frac{C^n}{(C^2+b^2)^m} & \text{for } C_1 < C \le C_3 \\ \omega_{s3} & \text{for } C > C_3 \end{cases}$$

where

ω_{sf} = median floc settling velocity [m/s]

ω_{sk} = dispersed particle settling velocity [m/s]

ω_{s3} = settling velocity corresponding to C_3 [m/s]

C = suspended sediment concentration [kg/m^3]

C_1 = free settling upper concentration limit (~0.1 0.3) [kg/m^3]

C_2= flocculation settling upper concentration limit (~4 kg/m^3) [kg/m^3]

C_3= hindered settling upper concentration limit (~75 kg/m^3) [kg/m^3]

a = empirical coefficient between 0.01 and 0.23 [m/s]

b = empirical coefficient between 1.3 and 25.0 [kg/m^3]

m = empirical exponent between 1.0 and 2.8

n = empirical exponent between 0.4 and 2.8

A representative settling velocity curve for a silt particle as a function of total sediment concentration is shown in the figure below. The settling velocity has four distinct zones. At low concentrations, flocculation is negligible, and particles settle freely. At a certain concentration, C_1, flocculation settling occurs and the settling velocity increases with sediment concentration as more and more flocs are formed. At a certain

concentration, C_2, the setting velocity reaches a maximum value and begins to decrease as the concentration decreases due to hindered settling.

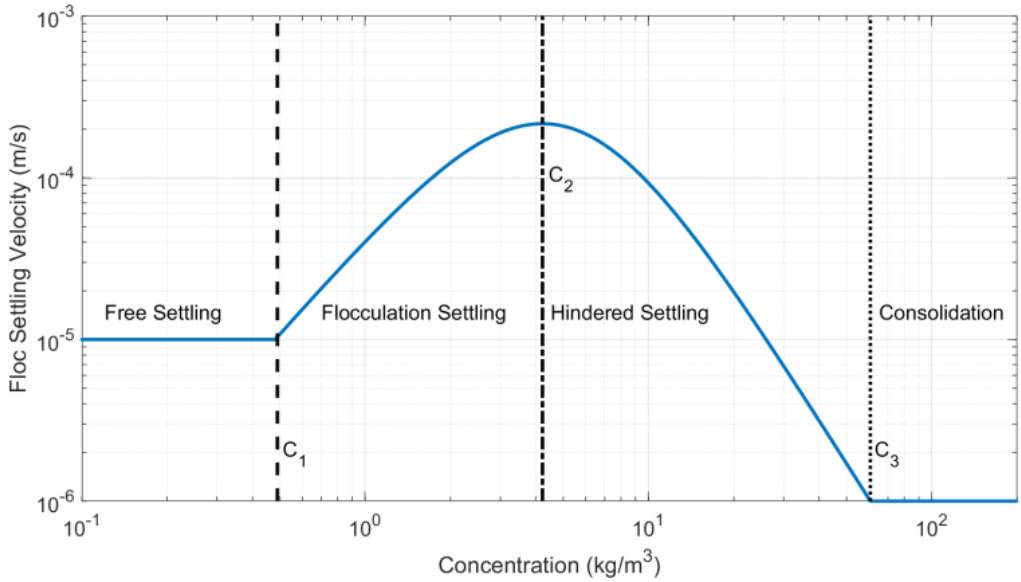

Figure 2 18. Flow settling velocity following Hwang (1989).

2.12.1.2 User-Defined Table

The simplest option for specifying the settling velocity of cohesives is a user-defined curve. Below is an example of the fall velocity for cohesives as a function of the sediment concentration. If the concentration goes beyond the curve, then the nearest point is utilized. The settling velocity is interpolated in log-space.

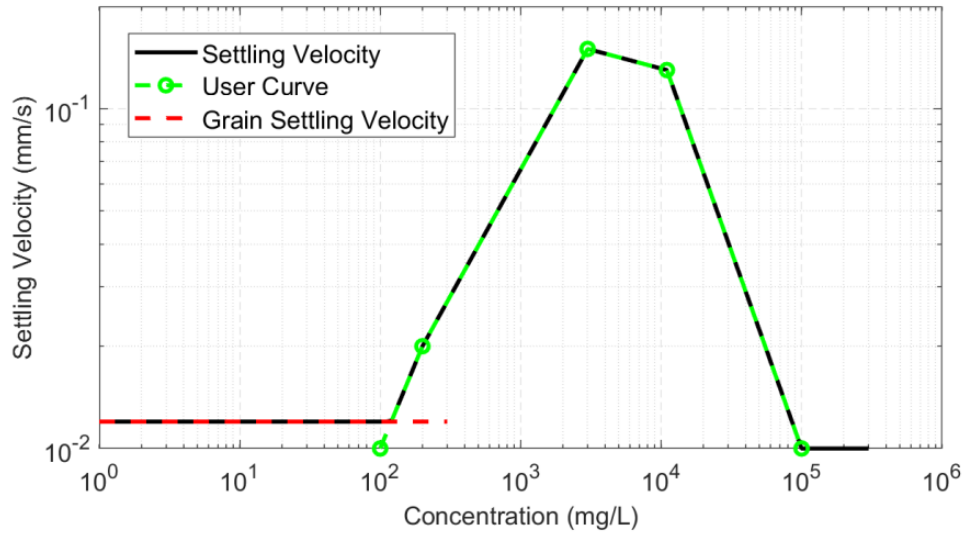

Figure 2 19. Example user-specified floc settling velocity curve (green dashed line with circle markers), grain-settling velocity (dashed red line) computed settling velocity as a function of concentration (black solid line).

When the settling velocities are less than the particle velocities and the concentration is less that the

concentration corresponding to the maximum settling velocity, the settling velocity is set to the particle velocity.

2.12.1.3 Temperature Correction

The floc settling velocity obtained from the Hwang or user-defined curve are assumed to be at a water temperature 55.4˚F. If the water temperature is changes, the floc settling velocity from the Hwang and user-defined curves is corrected as the ratio (Wu 2007)

101)
$$\frac{\omega_{sf,T}}{\omega_{sf,R}} = \frac{\mu_{w,R}}{\mu_{w,T}}$$

where $\mu_{w,R}$ and $\mu_{w,T}$ are the dynamic viscosities at the reference and actual water temperatures respectively. Similarly $\omega_{sf,R}$ and $\omega_{sf,T}$ are the floc settling velocities at the reference and actual water temperatures, respectively.

2.12.2 Hindered Settling

When the sediment concentration is high (approximately larger than 3,000 mg/l), the settling of particles is reduced due to return flow, particle collisions, increased mixture viscosity, increased buoyancy, and wake formation. This process is referred to as hindered settling. Of the sediment particle settling velocities presented above, only the Soulsby (1997) formula considers this process. When using other particle settling velocities hindered settling is considered using a modified form of Richardson and Zaki (1952)

102)
$$\frac{\omega_{sd}}{\omega_{sd0}} = (1 - C_{tV})^n$$

where

ω_{sd} = sediment particle settling velocity for turbid water [L/T]

ω_{sd0} = sediment particle settling velocity for clear water [L/T]

C_{tV} = total sediment concentration by volume [-]

n = empirical exponent [-]

The empirical coefficient n ranges between 3.75 to 4.45 for medium to fine sands (approximately 4.0 for normal flow conditions and particles in the range of 0.05 to 0.5mm). The above formulation differs from Richardson and Zaki (1952) in the inclusion of the maximum suspended sediment concentration which may be set to the bed dry bulk density. This is physically correct since the particle velocity should become zero when the concentration is equal to the bed dry bulk density. The empirical exponent that varies from is a function of the particle Reynolds number but is set to user-defined constant here for simplicity.

2.12.3 Particle Settling Velocity

For non-cohesive sediments, the sediment particles settle as individual particles and the sediment fall velocity may be determined utilizing the grain size particle. The settling velocity formulas which consider the particle shape are the Dietrich (1982) and Wu and Wang (2006). The Dietrich (1982) formula is the only one

which considers the particle roundness. Of the particle settling velocity formulas available in HEC-RAS, the Rubey (1933) and Toffaleti (1968) produce the slowest and fastest velocities for particle sizes larger than 0.5 mm, respectively. The van Rijn (1993) formula has a discontinuity at a particle size of 1 mm.

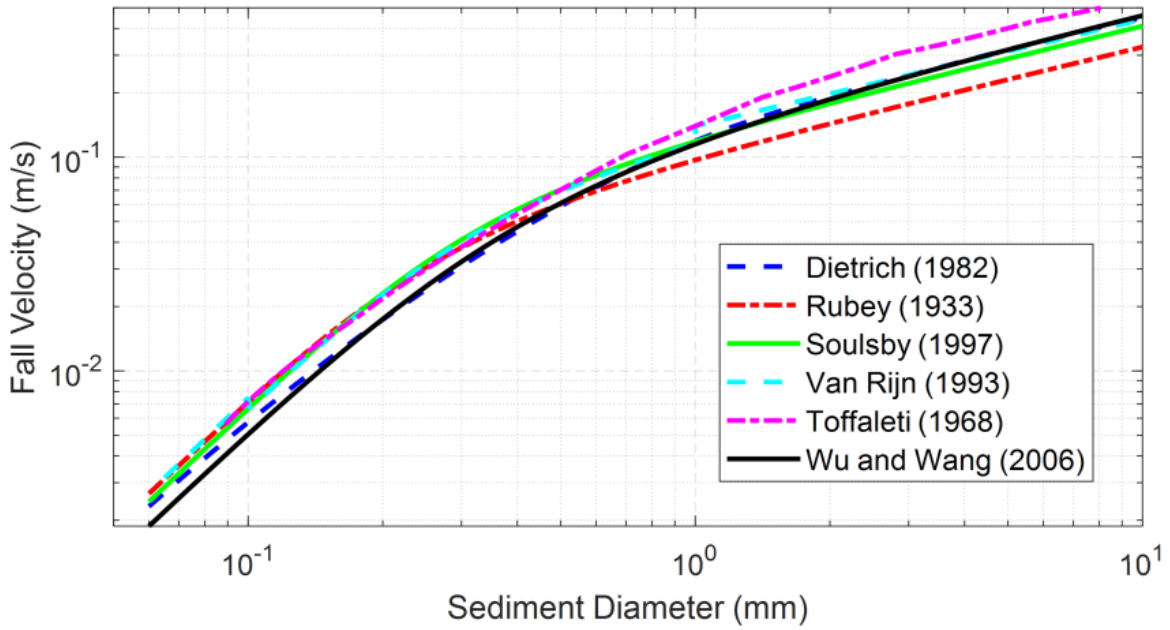

Figure 2 17. Sediment particle fall velocity formulas (assuming a water temperature is 13°C, Corey shape factor of 0.7, specific gravity of 2.65, and a Power's roundness index of 3.5).

2.12.3.1 Dietrich

Dietrich (1982) proposed the following formula to estimate the sediment settling velocity of noncohesive particles

103)
$$\frac{\omega_{sd}^3}{Rg\nu} = W_* = R_3 10^{R_1+R_2}$$

where

$R = \rho_s/\rho_w - 1$ = Submerged specific gravity [-]

ρ_s = particle density [M/L^3]

ρ_w = pater density [M/L^3]

g = gravitational constant (~9.81 m/s^2) [L/T^2]

$$R_1 = -3.76715 + 1.92944\log_{10} D_* - 0.09815(\log_{10} D_*)^2 - 0.00575(\log_{10} D_*)^3 + 0.00056(\log_{10} D_*)^4$$

$$R_2 = \left[\log_{10}\left(1 - \frac{S_F}{0.85}\right)\right] - (1 - S_F)^{2.3}\tanh(\log_{10} D_* - 4.6) + 0.3(0.5 - S_F)(1 - S_F)^2(\log_{10} D_* - 4.6)$$

$$R_3 = \left\{0.65 - \left[\frac{S_F}{2.83}\tanh\left(\log_{10} D_* - 4.6\right)\right]\right\}^{1+(3.5-P)/2.5}$$

$$D_* = \frac{Rgd_n^3}{\nu^2}$$

ν = kinematic viscosity [L^2/T]

S_F = Corey (1949) shape factor (typically 0.6 - 0.7) [-]

P = Powers (1953) roundness index (typically 3.5) [-] (see also Folk 1955)

It is noted that in the Dietrich formula, the non-dimensional grain size is defined slightly differently from the other formulas. Of all the formulas available in HEC-RAS, the Dietrich formula is the only formula to consider the particle roundness by means of the Powers roundness index. The formula also considers the particle shape through the Corey shape factor.

2.12.3.2 Rubey

Rubey (1933) developed an analytical formula for the sediment fall velocity based on the sediment and fluid properties utilizing Stoke's law for fine particles and an impact formula for large particles. The formula is given by

104) $$\omega_{sd} = F_1\sqrt{Rgd}$$

in which

105) $$F_1 = \sqrt{\frac{2}{3} + \frac{36\nu^2}{Rgd^3}} - \sqrt{\frac{36\nu^2}{Rgd^3}}$$

and

ν = kinematic viscosity [L^2/T]

g = gravitational constant (~9.81 m/s^2) [L/T^2]

d = grain size diameter [L]

$R = \rho_s/\rho_w - 1$ = submerged specific gravity [-]

ρ_s = particle density [M/L^3]

ρ_w = water density [M/L^3]

The parameter F_1 has an upper limit of 0.79 which corresponds to particles larger than 1 mm settling in water with temperatures between 10 and 25˚C. The Rubey formula is one of the earliest sediment fall velocity formulas developed. However, it tends to significant under-predict the fall velocity for sediments courser than fine sand.

2.12.3.3 Soulsby

Soulsby (1997) proposed a sediment settling velocity formula for non-cohesive sediments which includes the effects of grain size and density, water viscosity, and sediment concentration

106)
$$\omega_{sd} = \frac{\nu}{d}\left[\left(10.36^2 + 1.049 d_*^3\right)^{1/2} - 10.36\right]$$

where

ν = kinematic viscosity [L^2/T]

d = grain size diameter [L]

d_* = $d(Rg)^{1/3}\nu^{-2/3}$ = nondimensional grain size [-]

R = $\rho_s/\rho_w - 1$ = submerged specific gravity [-]

ρ_s = particle density [M/L^3]

ρ_w = water density [M/L^3]

g = gravitational constant (~9.81 m/s^2) [L/T^2]

2.12.3.4 Toffaleti

Toffaleti (1968) presented a table of fall velocities with a shape factor of 0.9 and a specific gravity of 2.65. Different fall velocities are given for a range of temperatures and grain sizes. These are presented in the table below. Sediment fall velocities are linearly interpolated from the values in the table below.

Table 28. Sediment fall velocities from Toffaleti (1968).

Sand Grain Settling Velocity Versus Temperature, SP.G. 2.65, Shape Factor 0.9

TEMP °F	SETTLING VELOCITY IN FT/SEC							
	VFS	FS	MS	CS	VCS	VFG	FG	MG
35	.013	.045	.130	.305	.590	1.00	1.41	1.95
36	.013	.045	.131	.307	.592	1.00	1.41	1.95
37	.013	.046	.132	.310	.594	1.00	1.41	1.95
38	.014	.047	.133	.312	.596	1.00	1.41	1.95
39	.014	.047	.135	.314	.598	1.00	1.41	1.95
40	.014	.048	.136	.316	.600	1.00	1.41	1.95
41	.015	.049	.137	.318	.602	1.00	1.41	1.95
42	.015	.050	.138	.320	.604	1.00	1.41	1.95
43	.015	.051	.140	.321	.606	1.00	1.41	1.95
44	.016	.051	.141	.322	.608	1.00	1.41	1.95
45	.016	.052	.142	.323	.609	1.00	1.41	1.95
46	.016	.053	.143	.325	.610	1.00	1.41	1.95
47	.016	.053	.144	.326	.612	1.00	1.41	1.95
48	.017	.054	.145	.328	.614	1.00	1.41	1.95
49	.017	.055	.146	.330	.616	1.00	1.41	1.95
50	.017	.055	.147	.331	.618	1.00	1.41	1.95
51	.018	.056	.148	.333	.620	1.00	1.41	1.95
52	.018	.057	.150	.334	.621	1.00	1.41	1.95
53	.018	.057	.151	.336	.623	1.00	1.41	1.95
54	.018	.058	.152	.338	.624	1.00	1.41	1.95
55	.018	.059	.153	.340	.626	1.00	1.41	1.95
56	.019	.059	.154	.341	.627	1.00	1.41	1.95
57	.019	.060	.155	.343	.629	1.00	1.41	1.95
58	.019	.061	.156	.344	.630	1.00	1.41	1.95
59	.019	.061	.157	.346	.632	1.00	1.41	1.95
60	.020	.062	.158	.347	.633	1.00	1.41	1.95
61	.020	.063	.160	.349	.635	1.00	1.41	1.95
62	.020	.063	.161	.350	.636	1.00	1.41	1.95
63	.020	.064	.162	.351	.638	1.00	1.41	1.95
64	.021	.065	.163	.353	.639	1.00	1.41	1.95

TEMP °F	SETTLING VELOCITY IN FT/SEC							
	VFS	FS	MS	CS	VCS	VFG	FG	MG
65	.021	.065	.165	.354	.640	1.00	1.41	1.95
66	.021	.066	.166	.356	.641	1.00	1.41	1.95
67	.021	.067	.167	.357	.643	1.00	1.41	1.95
68	.022	.067	.168	.359	.644	1.00	1.41	1.95
69	.022	.068	.170	.360	.646	1.00	1.41	1.95
70	.022	.069	.171	.361	.647	1.00	1.41	1.95
71	.022	.070	.172	.362	.649	1.00	1.41	1.95
72	.023	.071	.173	.363	.650	1.00	1.41	1.95
73	.023	.071	.175	.364	.652	1.00	1.41	1.95
74	.023	.072	.176	.365	.653	1.00	1.41	1.95
75	.024	.072	.177	.366	.655	1.00	1.41	1.95
76	.024	.073	.178	.367	.656	1.00	1.41	1.95
77	.024	.073	.180	.368	.657	1.00	1.41	1.95
78	.024	.074	.181	.370	.658	1.00	1.41	1.95
79	.025	.074	.182	.371	.659	1.00	1.41	1.95
80	.025	.075	.183	.373	.660	1.00	1.41	1.95
81	.025	.075	.184	.375	.661	1.00	1.41	1.95
82	.025	.076	.185	.376	.662	1.00	1.41	1.95
83	.025	.077	.186	.378	.663	1.00	1.41	1.95
84	.026	.077	.187	.380	.664	1.00	1.41	1.95
85	.026	.078	.188	.381	.665	1.00	1.41	1.95
86	.026	.078	.190	.383	.666	1.00	1.41	1.95
87	.026	.079	.192	.385	.667	1.00	1.41	1.95
88	.027	.079	.194	.386	.668	1.00	1.41	1.95
89	.027	.080	.195	.388	.669	1.00	1.41	1.95
90	.027	.080	.196	.390	.670	1.00	1.41	1.95
91	.028	.081	.197	.391	.671	1.00	1.41	1.95
92	.028	.081	.198	.392	.672	1.00	1.41	1.95
93	.028	.082	.199	.393	.673	1.00	1.41	1.95
94	.028	.082	.200	.394	.674	1.00	1.41	1.95

2.12.3.5 Van Rijn

Van Rijn (1993) proposed the following sediment fall velocity

107)
$$\omega_{sd} = \begin{cases} l\frac{Rgd^2}{18\nu} & \text{for } 0.065\,\text{mm} < d \le 0.1\,\text{mm} \\ \frac{10\nu}{d}\left(\sqrt{1+0.01\frac{Rgd^3}{\nu^2}}-1\right) & \text{for } 0.1\,\text{mm} < d \le 1\,\text{mm} \\ 1.1\sqrt{Rgd} & \text{for } 1\,\text{mm} \ge d \end{cases}$$

where

ν = kinematic viscosity [L^2/T]

d = grain size [L]

$d_* = d(Rg)^{1/3}\nu^{-2/3}$ = dimensionless grain size [-]

$R = \rho_s/\rho_w - 1$ = submerged specific gravity [-]

ρ_s = particle density [M/L^3]

ρ_w = water density [M/L^3]

g = gravitational constant (~9.81 m/s^2) [L/T^2]

2.12.3.6 Wu and Wang

Wu and Wang (2006) proposed a formula for the sediment fall velocity which includes the particle shape:

108)
$$\omega_{sd} = \frac{M\nu}{Nd}\left[\sqrt{\frac{1}{4}+\left(\frac{4N}{3M^2}d_*^3\right)^{1/n}}-\frac{1}{2}\right]^n$$

where

ν = kinematic viscosity [L^2/T]

d = grain size [L]

$d_* = d\left(\frac{Rg}{\nu^2}\right)^{1/3}$ = nondimensional grain size [-]

$R = \rho_s/\rho_w - 1$ = submerged specific gravity [-]

ρ_s = particle density [M/L^3]

ρ_w = water density [M/L^3]

g = gravitational constant (~9.81 m/s^2) [L/T^2]

$M = 53.5\exp(-0.65S_F)$

$$N = 5.65\exp(-2.5S_F)$$

$$n = 0.7 + 0.9S_F$$

S_F = Corey shape factor [-] (Corey 1949)

Wu and Wang (2006) calibrated the coefficients to the natural sediment settling data from various authors with shape factors varying from 0.3 to 1.0 and a wide range of Reynolds numbers. The Wu and Wang (2006) fall velocity may be seen as a general form of the Rubey (1933), Zhang (1961), and Cheng (1997) with different values for the coefficients *M*, *N*, and *n*

2.13 Transport Potential Formulas

In order to close the system of equations describing the sediment transport, bed change, and bed sorting equations, the fractional depth-averaged total-load concentration potential (C_{tk}^*) must be estimated from an empirical formula. The depth-averaged concentration potential is defined as

109) $$C_{tk}^* = \frac{q_{tk}^*}{Uh}$$

where q_{tk}^* is the total-load transport potential for the k^{th} sediment size class.

HEC-RAS 2D Sediment supports the following Transport Potential Formulas:

- Ackers and White (see page 68)
- Engelund-Hansen (see page 70)
- Laursen-Copeland (see page 71)
- Meyer-Peter and Müller (see page 72)
- Soulsby-van Rijn (see page 72)
- Toffaleti (see page 73)
- Van Rijn (see page 74)
- Wilcock and Crowe (see page 74)
- Wu et al. (see page 75)
- Yang (see page 76)

2.13.1 Ackers and White

The original Ackers and White (1973) (see page 115)was developed for to estimate the total load of uniform material. Ackers (1993) subsequently provided an update to the formula empirical coefficients. Day (1980) and Proffitt and Sutherland (1983) extended the original Ackers and White (1973) by multiplying it by a hiding and exposure correction factor. The fractional total-load transport potential is given by

110) $$q_{tk}^* = \rho_w g h U X_{tk}^*$$

where

q_{tk}^* = sediment transport potential [M/L/T]

ρ_w = water density [M/L^3]

g = gravity acceleration [L/T^2]

h = water depth [L]

U = depth-averaged current velocity [L/T]

$X_{tk}{}^*$ = sediment concentration potential by weight

The sediment concentration potential is determined from

111) $$\frac{X_{tk}^* h \rho_w}{d_k \rho_{sk}} \left(\frac{u_*}{U} \right)^n = \Lambda \left(\frac{F_{grk}}{A_c} - 1 \right)^m$$

where

F_{grk} = sediment mobility factor [-]

$u_* = \sqrt{\tau_b / \rho_w}$ = bed shear velocity [M/T]

ρ_{sk} = sediment density [M/L^3]

$\Lambda = \Lambda(d_{*k})$ = empirical coefficient [-]

$A_c = A_c(d_{*k})$ = empirical coefficient [-]

$n = n(d_{*\ k})$ = empirical exponent [-]

$m = m(d_{*\ k})$ = empirical exponent [-]

The sediment mobility factor is given by

112) $$F_{grk} = \eta_k \frac{u_*^n}{\sqrt{R_k g d_k}} \left[\frac{U}{\sqrt{32} \log_{10}(10h/d_k)} \right]^{1-n}$$

where

$R_k = \rho_{sk}/\rho_w - 1$ = submerged specific gravity of a particle [-]

ρ_{sk} = sediment density [M/L^3]

ρ_w = water density [M/L^3]

ρ_w = water density [M/L^3]

η_k = hiding and exposure correction factor [-]

τ_b = bed shear stress [M/L/T^2]

d_k = sediment diameter [L]

The firs term in the above equation corresponds to the bed-load transport while the second the suspended-load transport. The formula is based on the understanding that bed load is attributed to the grain shear stress while the suspended load is related to the turbulence intensity. The empirical coefficients were revised by Ackers (1993) as

113) $$n = \begin{cases} 1 & \text{for } d_{*k} \le 1 \\ 1 - 0.56\log_{10}(d_{*k}) & \text{for } 1 < d_{*k} \le 60 \\ 0 & \text{for } d_{*k} > 60 \end{cases}$$

114) $$A_c = \begin{cases} 0.23 d_{*k}^{-1/2} + 0.14 & \text{for } d_{*k} \le 60 \\ 0.17 & \text{otherwise} \end{cases}$$

115) $$m = \begin{cases} 6.83 d_{*k}^{-1} + 1.67 & \text{for } d_{*k} \le 60 \\ 1.78 & \text{otherwise} \end{cases}$$

116) $$\Lambda = \begin{cases} \exp\left\{2.791\log_{10}(d_{*k}) - 0.98\left[\log_{10}(d_{*k})\right]^2 - 3.46\right\} & \text{for } d_{*k} \le 60 \\ 0.0025 & \text{otherwise} \end{cases}$$

Wu (2007) tested and compared the Ackers-White (AW) formula for graded sediments and found that it tends to over predict the transport significantly for fine sediments less than 0.2 mm. However, the Ackers-White formula performs very well for uniform sediments. Day (1980) and Proffitt and Sutherland (1983) developed hiding and exposure correction factors for the Ackers-White formula and are available here to the user. It is noted that in AW, hiding and exposure is considered through a transport multiplication factor rather than through the sediment mobility.

2.13.2 Engelund-Hansen

The Engelund-Hansen (1967) (see page 115) formula is a total-load transport potential formula based on stream power. The formula is most appropriate for environments with uniform sediments and dominated by suspended load. The formula has been modified here for multiple grain classes and to include a critical shear stress for sediment transport as

117) $$q_{tk}^{*} = \begin{cases} 0.05\eta_k \rho_{sk} U^2 \sqrt{\frac{d_k}{gR_k}} \left(\frac{\tau_b}{g(\rho_{sk} - \rho_w) d_k} \right)^{3/2} & \text{for } \tau_b > \tau_{crk} \\ 0 & \text{otherwise} \end{cases}$$

where

q_{tk}^{*} = sediment transport capacity [M/L/T]

τ_b = bed shear stress [M/L/T^2]

τ_{crk} = critical shear stress [M/L/T^2]

U = current velocity magnitude [L/T]

R_k = $\rho_{sk}/\rho_w - 1$ = submerged specific gravity of a particle [-]

ρ_{sk} = sediment density [M/L^3]

ρ_w = water density [M/L^3]

d_k = grain class diameter [L]

The suggested applicability of the Engelund-Hansen formula is for $\sqrt{d_{75}/d_{25}}$<1.6 and d_{50}<0.15 mm. It is noted that the Engelund-Hansen formula does not include a critical threshold for transport. England Hansen is the simplest transport equations. Application should be restricted to sand systems.

2.13.3 Laursen-Copeland

Laursen (1968) developed a total-load sediment transport formula based on flume experiments initially and later expanded it to included data from Arkansas River. Copeland and Thomas. (1989) then generalized the equation for gravel transport. One important aspect of the Laursen-Copeland formula is that it is valid from silts to gravel.

118) $$q_{tk}^{*} = a\rho_w U h \left(\frac{d_k}{h}\right)^{7/6} \left(\frac{\theta'_b}{\theta_{crk}} - 1\right)^{n} f_{tk}^{LC}\left(\frac{u'_*}{\omega_{sk}}\right)$$

where

$q_{tk}{}^{*}$ = sediment transport capacity [M//L/T]

a = 0.01

θ'_b = grain-related Shields number [-]

θ_{crk} = critical Shields number [-]

U = current velocity magnitude [L/T]

h = water depth [L]

n = empirical coefficient (default is 1.0) [-]

ρ_w = water density [M/L^3]

ω_{sk} = sediment particle fall velocity [L/T]

d_k = grain class diameter [L]

The transport function $f_{tk}{}^{LC}(u*/\omega_{sk})$ is approximated by the following regression equation:

119) $$f_{tk}^{LC}\left(\frac{u_*}{\omega_{sk}}\right) = \begin{cases} 7.04 \times 10^{15}\left(\frac{u_*}{\omega_{sk}}\right)^{22.99} & \text{for } \frac{u_*}{\omega_{sk}} \le 0.225 \\ 40\frac{u_*}{\omega_{sk}} & \text{for } 0.225 < \frac{u_*}{\omega_{sk}} \le 1.0 \\ 40\left(\frac{u_*}{\omega_{sk}}\right)^{1.843} & \text{for } 1.0 < \frac{u_*}{\omega_{sk}} \end{cases}$$

Larson (1968) and Copeland (1989) used a critical Shields number of 0.039. In HEC-RAS 2D sediment the Shields number may be calculated with another method or be user-specified. In addition the coefficient *a* and exponent *n* may be modified by the user. However, it is recommended to calibrate the transport formulas using the transport scaling and mobility factors.

2.13.4 Meyer-Peter and Müller

The Meyer-Peter and Müller (MPM) formula (1948) is a bed-load formula developed from flume experiments of sand and gravel under plane bed conditions. It was originally developed for uniform sediment beds. HEC-RAS uses the version of MPM from Vanoni (1975), ASCE Manual 54, the version used in HEC 6. This version includes a form drag correction (the RKR parameter, based on the roughness element ratio, $(k_b/k_r)^{3/2}$, computed from the Darcy-Weisbach bed fiction factor). The form drag correction isolates grain shear, computing transport based on the bed shear component acting only on the particles. The form drag correction should be unnecessary in plane-bed conditions, so some versions of MPM exclude it. Wong and Parker (2006) demonstrate that using MPM without the form drag correction over-predicts bed load transport.

120)
$$\frac{q_{bk}^{*}}{\sqrt{R_k g d_k^3}} = A_M \rho_{sk} \left(\theta_b' - \theta_{crk}\right)^{E_M}$$

where

$\theta_b' = \frac{\tau_b'}{(\rho_{sk}-\rho_w)gd_k}$ = grain-related Shields parameter [-]

ρ_{sk} = sediment density [M/L^3]

ρ_w = water density [M/L^3]

θ_{crk} = critical Shields parameter [-]

A_M = empirical coefficient [-]

Meyer-Peter Müller (1948) estimated A_M = 8, E_M = 3/2, and θ_{crk} = 0.047. However, Wong and Parker (2006) recalibrated the equation and found A_M = 3.97, E_M = 1.6, and θ_{crk}=0.0495. The MPM formula is most applicable to uniform gravel bed and tends to under-predict transport for fine sands and silts.

2.13.5 Soulsby-van Rijn

Soulsby (1997) proposed the following equation for the total load sediment transport rate

121)
$$q_{bk}^{*} = \begin{cases} 0.005Uh\left(\frac{U-U_{crk}}{\sqrt{R_k g d_k}}\right)^{2.4}\left(\frac{d_k}{h}\right)^{1.2} & \text{for } U > U_{crk} \\ 0 \quad \text{otherwise} \end{cases}$$

122)
$$q_{sk}^{*} = \begin{cases} 0.012Uh\left(\frac{U-U_{crk}}{\sqrt{R_k g d_k}}\right)^{2.4}\left(\frac{d_k}{h}\right) d_{*k}^{-0.6} & \text{for } U > U_{crk} \\ 0 \quad \text{otherwise} \end{cases}$$

where

$q_{bk}{}^{*}$ = fractional bed-load sediment transport potential [L^2/T]

q_{sk}^* = fractional suspended-load sediment transport potential [L^2/T]

R_k = $\rho_{sk}/\rho_w - 1$ = submerged specific gravity of a particle [-]

ρ_{sk} = sediment density [M/L^3]

ρ_w = water density [M/L^3]

U = effective depth-averaged current velocity [m/s]

U_{crk} = critical depth-averaged velocity for incipient motion [m/s]

The Soulsby-van Rijn formula was developed by calibrating the above equations to the van Rijn (1993) sediment transport model. The formulas were originally proposed for well-sorted sediments. The formulas have been modified here for nonuniform sediments by replacing the median grain size with the grain class diameter and multiplying the critical depth-averaged current velocity with a hiding and exposure correction factor. Here the Wu et al. (2000) hiding and exposure correction factor is utilized but in principle others may also be used. van Rijn (1984a,b; 2007a,b) computed the critical depth-averaged current velocity using the van Rijn formula.

2.13.6 Toffaleti

Toffaleti (1968) developed a total-load transport formula primarily for sand particles. The method splits the water column into three vertical zones as shown in the figure below.

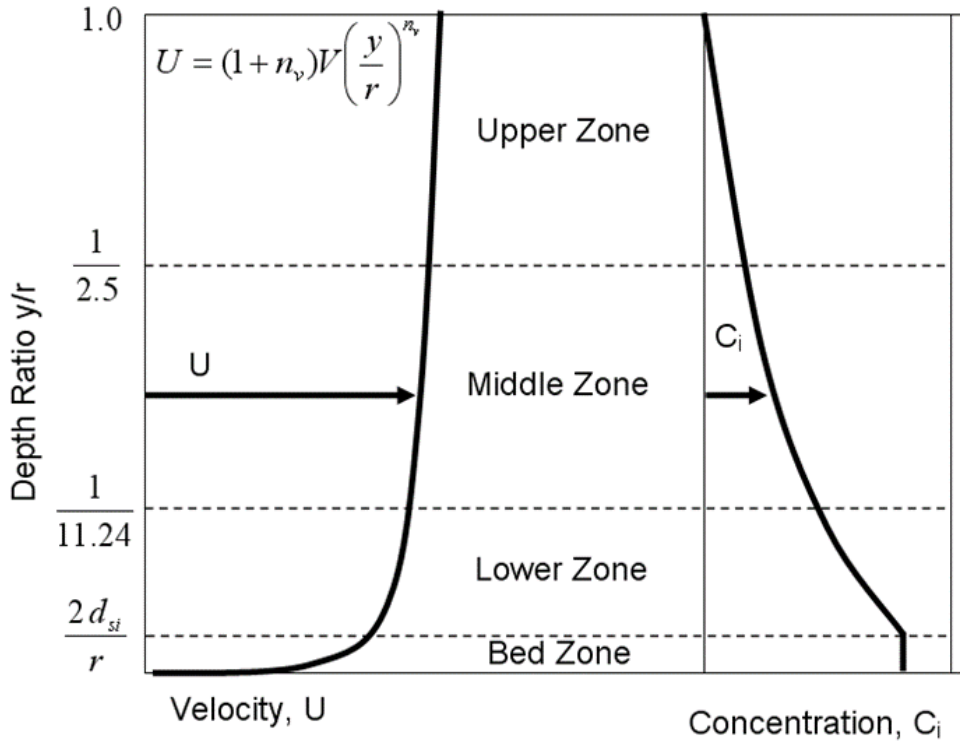

Figure 2 20. Toffaleti total-load transport zones.

The formula computes the concentration in each of the three zones using a Rouse concentration profile. The

suspended-load transport potential for each zone is computed analytically assuming a current velocity profile. The total-load transport potential is computed as the sum of the three suspended-load zones and the bed-load zone. The sediment transport potential formulas are not based on excess shear but rather are regression equations based on sediment and water properties, and hydraulic variables. The Toffalti formula was originally developed for bulk transport but here it is applied to individual grain classes. The Toffaleti formula is usually applied at "large" rivers since most of the data used to develop it were from large suspended-load dominant rivers. The Toffaleti bed-load transport potential does not perform for gravel size or coarse particles. For this reason, the option is available to replace the bed-load transport potential in the Toffaleti formula with an estimate from the Meyer-Peter and Muller formula. This formula is referred to as the Toffaleti-MPM formula.

2.13.7 Van Rijn

The van Rijn sediment transport formula are given by (1984a,b; 2007a,b)

123) $$q_{bk}^{*} = 0.015Uh\left(\frac{U - U_{crk}}{\sqrt{R_k g d_k}}\right)^{1.5}\left(\frac{d_k}{h}\right)^{1.2}$$

124) $$q_{sk}^{*} = 0.012Uh\left(\frac{U - U_{crk}}{\sqrt{R_k g d_k}}\right)^{2.4}\left(\frac{d_k}{h}\right)d_{*k}^{-0.6}$$

where

$q_{bk}{}^{*}$ = fractional bed-load sediment transport potential [L^2/T]

$q_{sk}{}^{*}$ = fractional suspended-load sediment transport potential [L^2/T]

$R_k = \rho_{sk}/\rho_w - 1$ = submerged specific gravity of a particle [-]

ρ_{sk} = sediment density [M/L^3]

ρ_w = water density [M/L^3]

U = effective depth-averaged current velocity [m/s]

U_{crk} = critical depth-averaged velocity for incipient motion [m/s]

The van Rijn formulas were originally proposed for well-sorted sediments. The formulas have been modified here for nonuniform sediments by replacing the median grain size with the grain class diameter and multiplying the critical depth-averaged current velocity with a hiding and exposure correction factor.

2.13.8 Wilcock and Crowe

Wilcock (2001) and Wilcock and Crowe (2003) developed a surface-based bed-load transport equation for graded beds with sand and gravel. The transport potential of the Wilcock and Crowe (WC) formula is given by

125) $$q_{bk}^{*} = \frac{u_{*}^{3} W_{k}^{*}}{R_k g}$$

where

$q_{bk}{}^*$ = fractional bed-load sediment transport potential [L^2/T]

u_* = bed shear velocity [L/T]

W_k* = transport function [-]

$R_k = \rho_{sk}/\rho_w - 1$ = submerged specific gravity of grain class [-]

ρ_{sk} = sediment grain density [M/L^3]

ρ_w = water density [M/L^3]

g = gravitational constant [L/T^2]

The transport function is given by

126) $$W_k^* = \begin{cases} 0.002\phi^{7.5} & \text{for } \phi < 1.35 \\ 14\left(1 - \frac{0.894}{\phi^{0.5}}\right)^{4.5} & \text{for } \phi \geq 1.35 \end{cases}$$

where

$\phi = \tau_b/\tau_{r,\ k}$ = sediment mobility [-]

τ_b = bed shear stress [-]

$\tau_{r,\ k}$ = reference shear stress

2.13.9 Wu et al.

The bed- and suspended-load transport formula of Wu et al. (2000) are given by

127) $$q_{bk}^* = \begin{cases} 0.0053\sqrt{R_k g d_k^3}\left(\frac{\tau_b'}{\tau_{crk}} - 1\right)^{2.2} & \text{for } \tau_b' > \tau_{ck} \\ 0 \quad \text{otherwise} \end{cases}$$

128) $$q_{sk}^* = \begin{cases} 2.62 \times 10^{-5}\sqrt{R_k g d_k^3}\left[\left(\frac{\tau_b}{\tau_{crk}} - 1\right)\frac{U}{\omega_{sk}}\right]^{1.74} & \text{for } \tau_b > \tau_{ck} \text{ and } \tau_b' > \tau_{ck} \\ 0 \quad \text{otherwise} \end{cases}$$

where

$q_{bk}{}^*$ = fractional bed-load sediment transport potential [L^2/T]

$q_{sk}{}^*$ = fractional suspended-load sediment transport potential [L^2/T]

$R_k = \rho_{sk}/\rho_w - 1$ = submerged specific gravity of a particle [-]

ρ_{sk} = sediment density [M/L^3]

ρ_w = water density [M/L^3]

τ_b = bed shear stress [$M/L/T^2$]

τ'_b = skin bed shear stress [M/L/T^2]

τ_{crk} = critical shear stress [M/L/T^2]

d_k = Sediment diameter [L]

Since the total bed shear stress is equal or larger than the skin bed shear stress, it is possible for the original formulation to produce suspended load without bed load. This situation is considered unrealistic and is avoided here by adding the additional condition in the above equation.

2.13.10 Yang

Yang (1979; 1984) developed a total sediment transport method based on the regression of potential energy dissipation per unit weight of water and the total sediment concentration:

129) $$\log_{10}\left(C_{tk}^{*}\right) = \begin{cases} M + N\log_{10}\left[\frac{S_f}{\omega_{sk}}(U - U_{crk})\right] & \text{for } U > U_{crk} \\ 0 & \text{otherwise} \end{cases}$$

130) $$M = \begin{cases} 5.435 - 0.286\log_{10}\left(\frac{\omega_{sk} d_k}{\nu}\right) - 0.457\log_{10}\left(\frac{u_*}{\omega_{sk}}\right) & \text{for } d_k < 2\,\text{mm} \\ 6.681 - 0.681\log_{10}\left(\frac{\omega_{sk} d_k}{\nu}\right) - 4.816\log_{10}\left(\frac{u_*}{\omega_{sk}}\right) & \text{for } 2\,\text{mm} < d_k < 10\,\text{mm} \end{cases}$$

131) $$N = \begin{cases} 1.799 - 0.409\log_{10}\left(\frac{\omega_{sk} d_k}{\nu}\right) - 0.314\log_{10}\left(\frac{u_*}{\omega_{sk}}\right) & \text{for } d_k < 2\,\text{mm} \\ 2.784 - 0.305\log_{10}\left(\frac{\omega_k d_k}{\nu}\right) - 0.282\log_{10}\left(\frac{u_*}{\omega_{sk}}\right) & \text{for } 2\,\text{mm} < d_k < 10\,\text{mm} \end{cases}$$

where

$C_{tk}{}^{*}$ = sediment concentration in parts per million (ppm) by weight

u_* = bed shear velocity [L/T]

ω_{sk} = sediment fall velocity [L/T]

ν = kinematic water viscosity [L^2/T]

U = depth-averaged current velocity [L/T]

U_{crk} = critical depth-averaged current velocity [L/T]

S_f = friction slope [-]

The Yang (1973) transport equations tend to overestimate transport for very coarse sands and there is also a sharp discontinuity between sand and gravel at d_s = 2 mm.

2.14 Critical Thresholds for Transport and Erosion

2.14.1 Noncohesive Sediments

The critical and reference shear stresses are related to the critical and reference Shields numbers by

132) $$\frac{\tau_{cr}}{(\rho_s - \rho_w)gd} = \theta_{cr}$$

133) $$\frac{\tau_r}{(\rho_s - \rho_w)gd} = \theta_r$$

where

τ_{cr} = critical shear stress for noncohesives [M/L/T^2]

τ_r = reference shear stress for noncohesives [M/L/T^2]

θ_{cr} = critical Shields parameter for noncohesives [-]

θ_r = reference Shields parameter for noncohesives [-]

ρ_s = sediment grain density [M/L^3]

ρ_w = water density [M/L^3]

g = gravitational constant [L/T^2]

d = grain diameter [L]

The formula for computing the critical Shields or reference Shields number is automatically selected by the program depending on the transport potential formula selected. However, the formula may be overwritten. Some of the transport formula utilize constant Shields parameters while others utilize a Shields parameter as function of the non-dimensional grain diameter.

Below is a comparison of the three methods to compute the Shields parameter which are not constant.

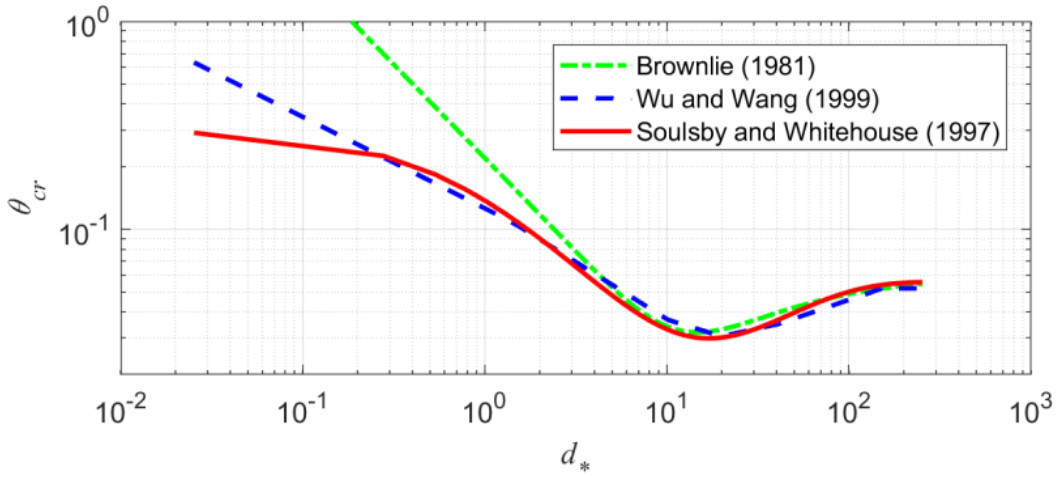

Figure 2-21. Example Shields parameter formulations.

2.14.1.1 Soulsby and Whitehouse

Soulsby and Whitehouse (1997) proposed the following formula for the critical Shields Parameter

134) $$\theta_{cr} = \frac{0.3}{1 + 1.2d_*} + 0.055\left[1 - \exp(-0.02d_*)\right]$$

2.14.1.2 Laursen and Laursen-Copeland

The Laursen (1968) and Laursen and Copeland (Copeland 1989) transport potential formula utilize the following critical Shields number for incipient motion

135) $$\theta_{cr} = 0.039$$

This equation should only be used in combination with Laursen and Copeland transport potential formula.

2.14.1.3 Meyer-Peter and Muller

Meyer-Peter and Müller (1948) utilized a constant Shields number of

136) $$\theta_c r = 0.047$$

This equation should only be used in combination with the Meyer-Peter and Muller transport potential formula.

2.14.1.4 Wilcock and Crowe

In the Wilcock transport potential formula, a reference Shields number is computed for the substrate which is a function of the sand content of the bed surface

137) $$\theta_r = 0.021 + 0.015\exp(-2000 f_S)$$

where θ_r is the reference Shields number for the noncohesive sediment mixture and f_S is the fraction of sand on the surface.

2.14.1.5 Wu et al.

The sediment transport equations of Wu et al. (2000) utilize a simple approximation of the critical Shields number as a constant value.

138) $$\theta_{cr} = 0.03$$

This equation is used in combination with the bed load and total load equations from Wu et al. (2000).

2.14.1.6 van Rijn

The critical depth-averaged velocity (U_{cr}) is calculated using the formula proposed by van Rijn (1984c)

139) $$U_{cr} = \begin{cases} l0.19 d_{50}^{0.1} \log_{10}\left(\frac{4h}{d_{90}}\right) \text{for} 0.1 \le d_{50} \le 0.5\,\text{mm} \\ 8.5 d_{50}^{0.6} \log_{10}\left(\frac{4h}{d_{90}}\right) \quad \text{for } 0.5 \le d_{50} \le 2.0\,\text{mm} \end{cases}$$

where d_{50} and d_{90} are the sediment grain size in meters of 50^{th} and 90^{th} percentiles, respectively. The above criteria are used in the van Rijn (2007a,b) and Soulsby-van Rijn (Soulsby 1997) transport formulas. For use in the multiple-sized sediment transport model, the particle diameters d_{50} and d_{90} are replaced with d_k for simplicity.

2.14.1.7 Yang

Yang (1973) proposed the following formula for the critical depth-averaged velocity:

140) $$\frac{U_{cr}}{\omega_{sd}} = \begin{cases} \frac{2.5}{\log_{10}\left(\frac{u_* d}{\nu}\right) - 0.06} + 0.66 & \text{for } 1.2 < \frac{u_* d}{\nu} < 70 \\ 2.05 & \text{for } \frac{u_* d}{\nu} \ge 70 \end{cases}$$

where

u_* = bed shear velocity [L/T]

ω_{sd} = particle free settling velocity [L/T]

d = particle diameter [L]

ν = water kinematic viscosity [L^2/T]

The Yang (1973) formula is the default formula utilized with the Yang (1973) transport potential formula.

2.14.2 Cohesive Sediments

For cohesive sediments, the critical shear stress for erosion is significantly affected by consolidation (i.e. varying dry bulk density). Several authors have proposed formulations for the critical shear stress as a function of the dry bulk density. Here the formulation by Owen (1975) is utilized because of its simplicity and the reduced number of input parameters required. In Owen's formulation the critical shear stress for erosion is computed as a function of the dry bulk density as

141) $$\tau_{ce} = a\rho_d^{\,b}$$

where

τ_{ce} = critical shear stress [$M/L/T^2$]

ρ_d = dry bulk density [M/L^3]

a = empirical coefficient

b = empirical coefficient

Generally, the value of *a* decreases as *b* increases. When a single bed layer is specified the coefficient, *b* is set to one and *a* is estimated from the initial erosion critical shear. If more than one bed layer is specified, than the empirical coefficients are estimated with a weighted least-squared method with the weight being the inverse of the dry bulk densities.

Owen (1975) reported of $a = 6.85\times10^{-6}$ and $b = 2.44$. Zheng and An (2017) present different values of *a* and *b* as a function of the solid content by weight of silts and clays. Liu et al. (2002) reported calibration fits of $a = 6.30\times10^{-4}$, $b = 1.44$, and $a = 5.77\times10^{-5}$, $b = 1.41$, at two stations in the Tanshui River, Taiwan. Perera and Wu (2016) compiled a large set of measurements from various sources and fit the coefficients $a = 7.46\times10^{-7}$, $b = 2.27$.

In addition to the critical shear stress for erosion, the power-law formula is used to fit all of the other cohesive parameters; namely the critical shear stress for mass wasting, τ_{cM}, the erosion rate coefficient, *M*, and, mass wasting coefficient, M_w.

2.14.3 Mixed Cohesive/Noncohesive Sediments

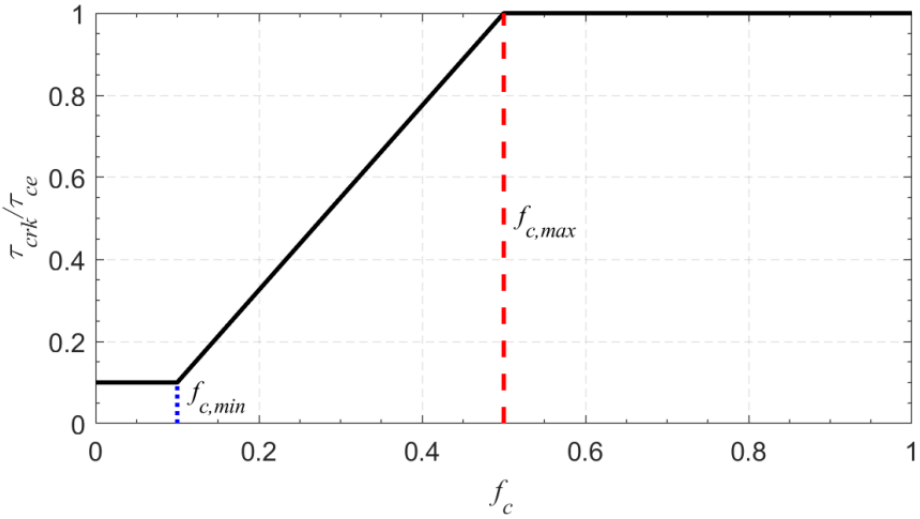

Figure 2 22. Example Shields parameter formulations.

In the case that the transport formula utilizes a critical Shields parameter or critical current velocity, the above formulation may still be applied by converting the critical Shields or critical current velocity into a critical shear stress, applying the above formulation, and then converting back to a critical Shields parameter or critical current velocity.

2.15 Hiding and Exposure Corrections

When the bed material is composed of multiple grain sizes, larger grains have a greater probability of being exposed to the flow while smaller particles have a greater probability of being hidden from the flow. The figure below shows an example of a sediment grain d_j being hidden by d_k.

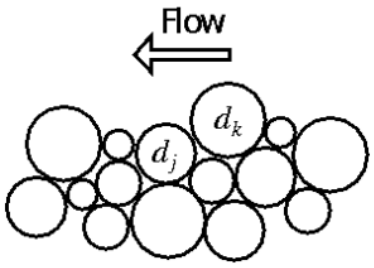

Figure 2 23. Schematic of the exposure height of bed sediment grains.

Depending on the form of the sediment transport formula, the hiding and exposure effect may be included in different ways. In many cases, the correction is done by adjusting the incipient motion in which case the hiding and exposure correction is defined as

142)
$$\xi_k = \frac{\theta_{crk}}{\theta_{cr}} = \frac{\tau_{crk}}{\tau_{cr}} = \frac{U_{crk}^2}{U_{cr}^2}$$

in which

τ_{cr} = uncorrected critical shear stress [M/L/T^2]

τ_{crk} = corrected critical shear stress [M/L/T^2]

$\theta_{cr} = \frac{\tau_{cr}}{(\rho_{sk}-\rho)gd_k}$ = uncorrected critical Shields parameter [-]

$\theta_{crk} = \frac{\tau_{crk}}{(\rho_{sk}-\rho)gd_k}$ = corrected critical Shields parameter [-]

U_{cr} = uncorrected critical depth-averaged current velocity [L/T]

U_{crk} = corrected critical depth-averaged current velocity [L/T]

Examples of hiding and exposure correction factors for incipient motion are Egiazaroff (1965), Ashida and Michiue (1971), and Wu et al. (2000). Some transport formulas such as (e.g. Ackers-White and Engelund-Hansen) do not have a threshold for transport. In these cases, a different form of a hiding and exposure correction is utilized as

143) $$\eta_k = \frac{q_k^*}{q^*}$$

where

q_k^* = corrected sediment transport potential for hiding and exposure

q^* = uncorrected or original sediment transport potential

Examples of the above formulation are Day (1980) and Proffitt and Sutherland (1983).

It is possible to utilize hiding and exposure correction factors for both the incipient motion and transport potential utilizing the following relationship

144) $$\eta_k \approx \frac{1}{\xi_k^a}$$

where *a* is an empirical coefficient (close to one) which depends on the hiding and exposure function. For example, Wu and Lin (2011) extended the Lund-CIRP (Camenen and Larson 2007) sediment transport formula to multiple grain sizes in this way and found $a \approx 0.6$ when applying the Wu et al. (2000) hiding and exposure correction formula developed for the Shields parameter.

2.15.1 Ashida and Michiue

The Ashida and Michiue (1971) formula is given by

145) $$\xi_k = \begin{cases} \left[\frac{\log_{10}(19)}{\log_{10}(19 d_k/d_m)}\right]^2 & \text{for } d_k/d_m \geq 0.4 \\ d_m/d_k & \text{for } d_k/d_m < 0.4 \end{cases}$$

where d_m is mean particle diameter. The Ashida and Michiue (1971) formula is basically a slightly modified version of the Egiazaroff (1965) formula described below for ratios $d_k/d_m < 0.4$.

2.15.2 Day

The hiding and exposure correction factor of Day (1980) is given by

146) $$\eta_k = \frac{1}{0.4(d_k/d_A)^{-0.5} + 0.6}$$

where d_A is a reference diameter determined by

147) $$d_A = 1.6 d_{50} \left(\frac{d_{84}}{d_{16}} \right)^{-0.28}$$

in which d_{16} and d_{84} are the 16^{th} and 84^{th} percentile diameters. The Day (1980) formula was developed specifically for the Ackers and White (1973) transport potential formula.

2.15.3 Egiazaroff

The Egiazaroff (1965) formula is given by

148) $$\xi_k = \left[\frac{\log_{10}(19)}{\log_{10}(19 d_k/d_m)} \right]^2$$

where d_m is the arithmetic mean particle diameter. Egiazaroff (1965) also assumed a critical Shields parameter of θ_{cr} = 0.06, which is relatively high for most sediments.

2.15.4 Hayashi et al.

The Hayashi et al. (1980) formula is given by

149) $$\xi_k = \begin{cases} \left[\frac{\log_{10}(8)}{\log_{10}(8 d_k/d_m)} \right]^2 & \text{for } d_k/d_m \geq 1 \\ d_m/d_k & \text{for } d_k/d_m < 1 \end{cases}$$

where d_m is the arithmetic mean particle diameter. The Hayashi et al. (1980) formula is a recalibrated version of the Ashida and Michiue (1971) which itself is based on the Egiazaroff (1965) formula.

2.15.5 Parker et al.

The hiding and exposure formula by Parker et al. (1982) and others has the form

150) $$\xi_k = \left(\frac{d_k}{d_{50}} \right)^{-m}$$

where *m* is an empirical coefficient between 0.5 to 1.0.

2.15.6 Proffitt and Sutherland

The hiding and exposure correction factor of Proffitt and Sutherland (1983) is given by

151) $$\eta_k = \begin{cases} 0.4 & \text{for } d_k/d_u \leq 0.075 \\ 0.53 \log_{10}(d_k/d_u) + 1 & \text{for } 0.075 < d_k/d_u \leq 3.7 \\ 1.3 & \text{for } d_k/d_u > 3.7 \end{cases}$$

where the reference diameter d_u is given in graphical form by Proffitt and Sutherland and may be approximated by the curves (HEC 2008)

152) $$\frac{d_u}{d_k} = \begin{cases} 1.1 & \text{for } \theta \leq 0.04 \\ 2.3 - 30\theta & \text{for } 0.04 < \theta \leq 0.045 \\ 1.4 - 10\theta & \text{for } 0.045 < \theta \leq 0.095 \\ 0.45 & \text{otherwise} \end{cases}$$

The Proffitt and Sutherland (1983) formula was developed specifically for the Ackers and White (1973) transport potential formula.

2.15.7 Wilcock and Crowe

Wilcock (2001) and Wilcock and Crowe (2003) developed a surface-based bed-load transport equation for graded beds with sand and gravel. In their formulation the hiding and exposure correction is calculated as

153) $$\xi_k = \frac{\tau_{r,k}}{\tau_{r,sm}} = \left(\frac{d_k}{d_{sm}} \right)^{b_k}$$

where

$\tau_{r,\ k}$ = reference shear stress corresponding to d_k

$\tau_{r,m}$ = reference shear stress corresponding to d_m

d_k = grain size diameter [L]

d_{sm} = surface mean grain size diameter [L]

The empirical exponent b_k is given by

154) $$b_k = \frac{0.67}{1 + \exp\left(1.5 + \frac{d_k}{d_{sm}}\right)}$$

2.15.8 Wu et al.

The hiding and exposure correction for each sediment size class is based on Wu et al. (2000):

155) $$\xi_k = \left(\frac{P_{ek}}{P_{hk}} \right)^{-m}$$

where

m = empirical coefficient that varies for each transport formula (approximately between 0.6-1.0) [-]

P_{hk} = hiding probability [-]

P_{ek} = exposure probability [-]

The total hiding and exposure probabilities (P_{hk} and P_{ek}, respectively) are calculated as

156) $$P_{hk} = \sum_{j=1} \hat{f}_{1j} \frac{d_j}{d_k + d_j}$$

157) $$P_{ek} = \sum_{j=1} \hat{f}_{1j} \frac{d_k}{d_k + d_j}$$

where $\hat{f}_{1j}$ are the active layer fractions by volume. Therefore, the formulation takes into account the size composition of the bed material by using the probabilities of each grain class of being exposed or hidden by other grain classes in the bed. The Wu et al. (2000) was developed in conjuction with the bed- and suspended-load transport potential formulas developed in the same reference.

2.16 Avalanching

When the slope of a bed, φ_b, is larger than the angle of repose, φ_R, the bed material will slide (avalanche) to form a new slope approximately equal to the angle of repose. The process of avalanching is simulated by enforcing $|\varphi_b| \leq \varphi_R$ while maintaining mass conservation between adjacent cells (Sánchez and Wu 2011a). Avalanching may occur between computational cells as well as within cells. The details of the avalanching algorithm in the following chapter.

3 Numerical Methods

The objective of this chapter is to present the numerical methods utilized in solving the 2D sediment transport equations, subgrid erosion and deposition, and bed sorting equations. Sediments are grouped into representative grain classes. A total-load transport equation is solved for each grain class with the HEC-RAS 2D Transport Module (Sánchez et al. 2020). The transport module solves for the cell-averaged fractional sediment concentration. Fractional and total bed change equations are solved. The bed composition is evolved with bed sorting equations. The transport equations are coupled to each other and the bed change and bed sorting equations utilizing Picard iterations. A full description of the sediment computation algorithm is provided in Section 3.19.

3.1 Transport Equation

A brief description of the Finite-Volume discretization of the total-load transport equation is provided here without any derivation or details. For addditional information including advection schemes, gradient operators, etc., the reader is referred to the HEC-RAS 2D Transport Module Technical Reference document (Sánchez et al. 2020). The 2D Transport Module solves generic Advection-Diffusion equations using explicit and implicit Finite-Volume methods. The final form of the discretized total-load advection-diffusion equation is given by

158) $$\frac{\Omega_P^{n+1} C_{tk,P}^{n+1}}{\Delta t \beta_{tk,P}^{n+1}} = \frac{\Omega_P^{n} C_{tk,P}^{n}}{\Delta t \beta_{tk,P}^{n}} + \sum_f \left[\frac{A_f \varepsilon_{tk,f}}{\delta_{PN}} \left(C_{tk,N}^{n+\theta} - C_{tk,P}^{n+\theta} \right) - F_f C_{tk,f}^{n+\theta} \right] + \left(E_{tk,P} - D_{tk,P} \right) A_P$$

where

Ω = cell volume

P = subscript indicating cell

f = subscript indicating face between cells *P* and *N*

N = subscript indicating neighboring cell to *P* and sharing face *f*

n = superscript indicating time step

C_{tk} = total-load sediment concentration of the k^{th} grain class [M/L^3]

β_{tk} = total-load correction factor for the k^{th} grain class

ε_{tk} = total-load diffusion coefficient corresponding to the k^{th} grain class

A_f = face vertical area [L^2/T]

F_f = face-normal water flow [L^3/T]

E_{tk} = total-load erosion rate [M/T/L^2]

D_{tk} = total-load deposition rate [M/T/L^2]

A_P = cell wetted horizontal area [L^2]

δ_{PN} = distance between cell points *N* and *P* [L]

θ = implicit weighting factor [-]

$n + \theta$ = superscript representing the temporal weighting $X^{n+\theta} = \theta X^{n+1} + (1-\theta)X^n$ (Generalized Euler scheme)

When the implicit weighting factor θ is equal to 1, the scheme reduces to the first-order fully implicit Backward Euler scheme. When the implicit weighting factor is equal to 0.5, the scheme is the second-order Crank-Nicholson scheme. An implicit discretization is utilized for robustness. However, future versions will have the option to use an explicit scheme.

3.2 Source and Sink Term

The source and sink term contains the sum of internal sediment sources and sinks due to internal boundary conditions S_{tk}^{IB} and surface runoff S_{tk}^{SR}. These include structures such as culverts and gates as well as surface runoff.

159) $$S_{tk} = S_{tk}^{IB} + S_{tk}^{SR}$$

where

S_{tk}^{IB} = source/sink due to internal boundary conditions such as structures [M/L^2/T]

S_{tk}^{SR} = source due to surface runoff [M/L^2/T]

The surface runoff contributes water and sediment to the hydraulically wet portion of wet cells. Currently, the model assumes that the eroded sediment from the hydraulically dry portion of cells is transported instantly to the wet portion of cell without any storage effects.

160) $$S_{tk}^{SR} A_P^W = E_{tk}^{SS} A_P^D$$

where

$A_P{}^W$ = cell wet area [L^2]

$A_P{}^D$ = cell dry area [L^2]

E_{tk}^{SS} = sheet and splash erosion [$M/L^2/T$]

3.3 Subgrid Concept

The bed change, sorting and layering are simulated in HEC-RAS using a subgrid approach. In this approach each computational cell has two sets of curves for the horizontal wetted area and water volume as a function of elevation. In addition, each face also has two sets of curves for the wetted horizontal length and vertical wetted area as a function of elevation. These curves are referred to as the subgrid curves. One of these sets of curves is relatively high-resolution and is utilized by the flow model in order to capture to effects of the subgrid bathymetry on the water storage and conveyance. The high-resolution (hydraulic) curves are obtained from a detailed terrain model, while the coarse (sediment) curves are derived from the flow curves. In theory it is possible to utilize the same high-resolution curves for both hydraulic and sediment, but this would make the computational time and memory requirements for the sediment transport calculations prohibitively expensive. This is the reason why a second set of relatively coarse curves are utilized by the sediment transport model to compute the subgrid bed change, sorting and bed layering.

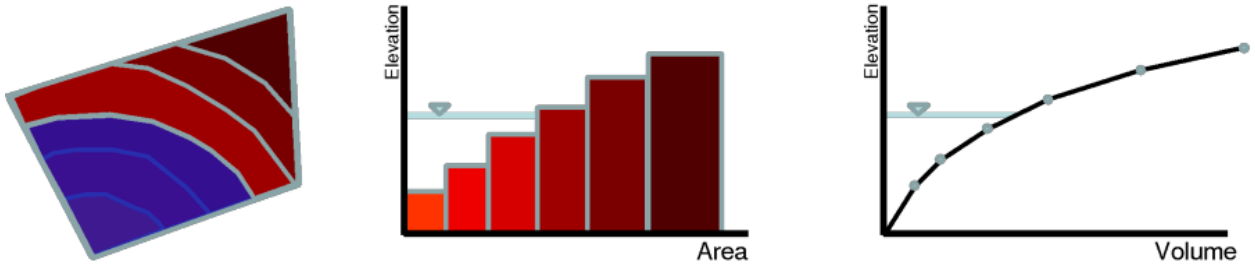

Figure 3 24. Schematic illustrating the subgrid concept utilized in HEC-RAS.

The computational cell and faces have piece-wise constant elevations as a function of area and length. Therefore, the subgrid topography is schematized as having "subareas" or "sublengths" for cells and faces respectively with discrete elevations. These subareas and sublengths are referred to collectively as subregions. The location of the discrete elevations is not known. Only the amount of area at cells and length at faces which corresponds to each discrete elevation is known.

3.3.1 Subgrid Sediment Transport

As discussed above, the sediment transport calculations for bed change, sorting, and layering may be computed on a coarser subgrid resolution than the hydraulics grid due to computational and memory restrictions. Since the flow and sediment transport utilize different subgrid curves it is necessary to transfer information from one set to another without losing information or causing numerical artifacts. In order to

simplify the computations, the sediment transport subareas (for cells) and sublengths (for faces) are defined by grouping hydraulic subareas and sublengths. The approach followed here is to simply group the high-resolution subregions based on a target number of grouped subregions and also similar bed elevations (i.e. inflections in the area-elevation and length-elevation curves). The figure below shows an example where high-resolution subareas are grouped for two different cases.

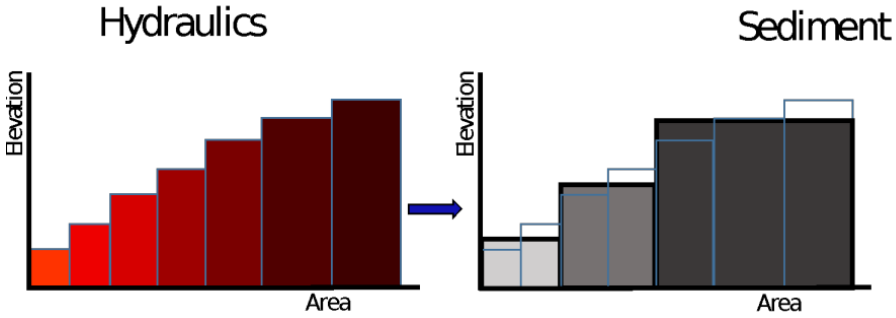

Figure 3 25. Schematic showing the grouping of high-resolution subareas for use in sediment transport.

The algorithm begins by computing a grouping number n_G = round(M_h/M_s) in whichround(X) is the rounding function, M_h is the number of hydraulics subareas, and M_s is the number of sediment subareas. In both cases the input hydraulics curve has 6 subareas and the desired sediment curve is set to have 3 subareas. A first attempt at grouping the hydraulics subareas is done using the grouping number starting from the lowest elevation. Since the grouping number is calculated using a rounding function, the last group of subareas may contain fewer or more than the rest in order to maintain the number of sediment subareas). This is illustrated in Figure 8a. In some situations the first grouping may lead to a poor description of the elevation-area curve inflections. An improvement of the sediment curves is done further grouping subregions on the high-resolution curve based on similar elevations. This process is illustrated in Figure 8b. Grouping the hydraulics subgrid regions into sediment subregions greatly simplifies the computations since each subregion may be treated separately.

3.3.2 Subcell Bed Elevations and Bed Change

The computation of the subgrid bed change, sorting, and layering is done on the sediment subgrid but using the wetted area computed from the hydraulics subgrid. It is possible to develop an algorithm in which the sediment subgrid regions are dynamically adjusted to match the wet/dry interface in a way similar to how the vertical bed layers are treated. However, this approach would require mass transfer (mixing) between adjacent areas as well as merging and splitting of areas. This added complexity and computational costs is not considered worth the benefits and a simpler, faster, albeit slightly less accurate is proposed here. The process of computing the subgrid bed change is illustrated in the schematic below.

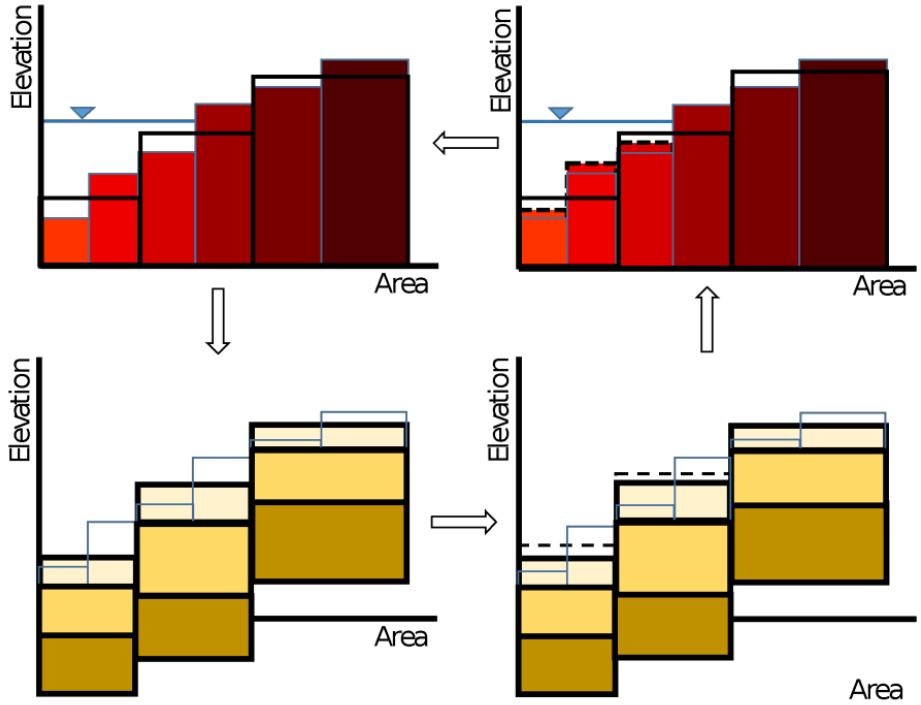

Figure 3 26. Schematic representing computation of bed change.

3.3.2.1 Subcell Bed Change

The total bed change is computed

161) $$\Delta z_{bi} = \frac{1}{1-\phi_{bi}} \sum_{k} \frac{\Delta M_{bki}}{\rho_{sk}}$$

where

Δz_{bi} : bed change for sediment subarea *i* [L]

ΔM_{bki} : fractional mass exchange with the bed in subarea *i* [M/L^2]

ϕ_{bi} : porosity of the eroded and deposited material [M/L^3]

ρ_{sk} : grain class particle density [M/L^3]

The fraction a mass exchange is computed as the sum of the mass rates times the scaled time step as

162) $$\Delta M_{bki} = f_M \Delta t \left(D_{tki} - E_{tki} + S_{bki}\right)$$

where

ΔM_{bki} : fractional mass exchange with the bed in subarea *i* [M/L^2]

D_{tki} : fractional deposition rate for sediment subarea *i* [M/L^2/T]

E_{tki} : fractional erosion rate for sediment subarea *i* [M/L^2/T]

S_{bki} : fractional bed-slope term for sediment subarea *i* [M/L^2/T]

f_M : morphologic acceleration factor [-]

Δt : time step [T]

3.3.2.2 Subcell Erosion Potential

The subcell erosion may be computed with one of five methods. The table below summarizes how each method treats the bed and hydrodynamic variables and if the erosion is scaled with the local depth.

Table 3 1. Summary of subcell erosion potential approaches.

Method	**Depth-Weighting**	**Bed Properties**	**Hydraulics**
Constant	None	Cell Wet-Average	Cell Wet-Average
Variable Bed	None	Subcell	Cell Wet-Average
Full Subgrid	None	Subcell	Subcell

In all of the methods the actual local erosion erosion rates are computed using the local grain fractions as

163) $$E_{tki} = f_{1ki} E^*_{tki}$$

3.3.2.2.1 Constant

This is the simplest and most computationally efficient approach. Constant erosion rate potentials are computed for the hydraulically wet and dry portions of a cell using representative (i.e. area-average) bed fractions and properties, hydraulic variables, etc. The local subarea erosion rate potential are then computed as a weighted average of those two rates depending on how much of the sediment subarea is wet. This may be expressed as

164) $$E^*_{tki} = \phi_i^W E^{*HF}_{tk}(f^W_{1k}) + \phi_i^D E^{*SS}_{tk}(f^D_{1k})$$

where

E^*_{tk} : cell fractional erosion rate potential [M/L^2/T]

ϕ_i^W : fraction of subarea which is hydraulically wet area [-]

ϕ_i^D : fraction of subarea which is hydraulically dry area $\left(\phi_i^W + \phi_i^D = 1\right)$ [-]

f_{1k}^W : cell wet area average grain fractions by weight [-]

f_{1k}^D : cell dry area average grain fractions by weight [-]

The advantage of the above approach is that the erosion potentials only need to be estimated once per cell and not for each cell subarea. However, the approach does not take into account the bed gradation of each subregion.

3.3.2.2.2 Variable Bed

In this method, the subarea erosion rates are computed using the local bed gradations and wet-averaged hydrodynamics as

165) $$E_{tki}^* = \phi_i^W E_{tki}^{*\,HF}(f_{1ki}) + \phi_i^D E_{tki}^{*SS}(f_{1ki})$$

where

E_{tki}^* : subcell fractional potential erosion rate [M/L^2/T]

$E_{tki}^{*HF}(f_{1ki})$: subcell fractional potential erosion rate corresponding to hydraulic flow erosion [M/L^2/T]

$E_{tki}^{*SS}(f_{1ki})$: subcell fractional potential erosion rate corresponding to sheet and splash erosion [M/L^2/T]

f_{1ki} : subcell active layer grain class fractions [-]

ϕ_i^W : fraction of subarea which is hydraulically wet [-]

ϕ_i^D = fraction of subarea which is hydraulically dry $\left(\phi_i^W + \phi_i^D = 1\right)$ [-]

In this approach, the sediment erosion potentials are computed for each subarea using cell-averaged hydrodynamic variables along witht the bed gradation for each subarea. Therefore it is significantly more computationaly expensive than assuming constant subcell erosion potentials. However, the erosion potentials are more realistic because they take into account the bed gradation of each subregion.

3.3.2.2.3 Full Subgrid

The full subgrid approach computes subcell erosion rates using subcell bed gradations and hydrodynamics:

166) $$E_{tki}^* = E_{tki}{}^*(f_{1ki}{}^*, \quad h_i, \quad u_{*i}, \quad U_i, \quad \ldots)$$

where

E_{tki} : subcell fractional erosion rate [M/L^2/T]

f_{1ki} : subcell area active layer grain class fractions [-]

E_{tki}^* : subcell fractional potential erosion rate [M/L^2/T]

h_i : subcell water depth [L]

u_{*i} : subcell total shear velocity [L/T]

U_i : subcell current velocity [L/T]

This approach is the most computationally expensive of all the methods because it requires reconstructing the subcell hydrodynamic variables and utilizing the subcell bed composition to compute subcell erosion potentials. However, the erosion potentials are more realistic because they take into account the bed gradation of each subregion.

3.3.2.3 Subcell Deposition

Sediment deposition is a function of the sediment fall velocity and the sediment concentration. In order to efficiently solve the transport equation implicitly, the sediment deposition is formulated as

167) $$\varpi_{tk} = \begin{cases} \alpha_{tk}\omega_{sk} & \text{for noncohesives} \\ P_D\omega_{sf} & \text{for cohesives} \end{cases}$$

where

$\overline{\omega}_{tk}$: fractional deposition rate coefficient [L/T]

α_{tk} : total-load adaptation coefficient [-]

ω_{sk} : sediment particle settling velocity [L/T]

P_D : probability of deposition for cohesive sediments [-]

ω_{sf} : sediment floc settling velocity [L/T]

There are two approaches for calculating the cell subgrid deposition rate.

Table 32. Summary of deposition approaches.

Method	**Depth-Weighting**	**Capacity-Weighting**
Veneer (Constant)	None	None
Depth-Weighted	Yes	None
Capacity-Weighted	None	Yes

3.3.2.3.1 Veneer Method

The simplest approach for computing the subgrid deposition rate is to simply assume that the deposition rate is constant within the wet portion of a cell:

168) $$D_{tki} = \phi_i^W \varpi_{th} C_{th}$$

where

D_{tki} : fractional deposition coefficient for sediment subarea *i* [L/T]

D_{tk}^{HF} : fractional deposition rate for sediment subarea *i* [M/L^2/T]

ϕ_i^W = wet fraction of subarea *i* (between 0 and 1) [-]

Since it is assumed deposition only occurs in wet portion of cells, the above equation only has one term on the right-hand-side representing the “wet” deposition. The veneer method is the default method because of its simplicity. The method basically assumes that the subgrid sediment concentration is the same as the cell-averaged concentration.

3.3.2.3.2 Depth-Weighted Method

Chang (1998) proposed a method for computing the lateral bed change in 1D cross-sections which distributes the total area change as a function of the local excess shear stress. A simpler version of the formula is applied here to the deposition rate by setting the critical shear to zero and assuming a constant friction slope within the cell. This leads to the depth-dependent formulation

169)
$$D_{tki} = \begin{cases} \frac{h_i^m A^W}{\sum_j h_i^m a_j^W} \varpi_{tk} C_{tk} & \text{for } h_i > 0 \\ 0 & \text{for } h_i = 0 \end{cases}$$

where

ϕ_i^W : wet fraction of subarea *i* (between 0 and 1) [-]

h_i : subarea water depth [L]

m : empirical coefficient generally between 0 and 1 (set to 0.6 here) [-]

$a_i^W = \phi_i^W a_i$: wet area of subarea *i* [L^2]

a_i : area of subregion *i* [L^2]

ϕ_i^W : fraction of subregion which is wet [-]

C_{tk} : cell-average total-load concentration [M/L^3]

The above option is similar to the “Reservoir Option” in the HEC-RAS 1D sediment transport model.

3.3.2.3.3 Capacity-Weighted Method

Volp (2017) proposed a subgrid deposition method which utilizes the concentration capacity (i.e. equilibrium concentration) to compute subgrid sediment deposition rates. The method assumes that the subgrid sediment concentration tend toward equilibrium. A similar formulation is utilized here as

170)
$$D_{tki} = \begin{cases} \frac{C_{tki*} A^W}{\sum_j C_{tkj*} a_j^W} \varpi_{tk} C_{tk} & \text{for } h_i > 0 \\ 0 & \text{for } h_i = 0 \end{cases}$$

where

$C_{tki*} = f_{1ki} C^*_{tki}$: subgrid equilibrium sediment concentration [M/L^3]

f_{1ki} : grain class fraction in active layer [-]

$a_i^W = \phi_i^W a_i$: wet area of subarea *i* [L^2]

a_i = area of subarea *i* [L^2]

ϕ_i^W = fraction of subarea which is wet [-]

C_{tk} = cell-average total-load concentration [M/L^3]

3.3.2.4 Subcell Wet and Dry Bed Change

Using the total wetted area from the hydraulics area-elevation curve ($\Updelta A^{W}$), the fraction of wetted area on each sediment subarea is calculated as

171)
$$\phi_i^W = \begin{cases} \min\left(\frac{A^W}{a_i}, 1\right) & \text{for } i = 1 \\ \min\left[\frac{1}{a_i}\left(A^W - \sum_j^{i-1} a_j\right), 1\right] & \text{for } i > 1 \end{cases}$$

where

$\phi_i^W = 1 - \phi_i^D$: wetted fraction of subarea *i* (between 0 and 1) [-]

ϕ_i^D : dry fraction of subarea of subarea *i* (between 0 and 1) [-]

A^W : total wetted area determined from high-resolution elevation-area curve [L^2]

a_i : area corresponding to subarea *i* [L^2]

It is noted that it is assumed to be no deposition in the dry areas. Once the above fractional erosion and deposition rates are calculated for each subarea, the one-dimensional (1DV) bed-sorting and layering model may be applied. The result from the 1DV model is the fractional and total bed change Δz_{bi} , dry bulk density ρ_{dji}, and gradation f_{jki} for each subarea.

The bed change corresponding to the wet and dry portions of a subarea are determined as

172)
$$\Delta z_{bi}^W = \frac{f_M \Delta t}{1 - \phi_{bi}} \sum_k \rho_{sk}^{-1} \left(D_{tki}^{HF} - E_{tki}^{HF} + S_{bki}\right)$$

173)
$$\Delta z_{bi}^D = -\frac{f_M \Delta t}{1 - \phi_{bi}} \sum_k \rho_{sk}^{-1} E_{tki}^{SS}$$

in which

Δt : time step [T]

f_M : morphologic acceleration factor [-]

D_{tk}^{HF} : hydraulic flow total-load deposition rate [M/T/L^2]

E_{tk}^{HF} : hydraulic flow total-load erosion rate [M/T/L^2]

E_{tk}^{SS} : sheet and splash total-load erosion rate [M/T/L^2]

ρ_{dbi} : dry bulk density of exchange material [M/L^3]

The subarea-averaged bed change is therefore

174) $$\Delta z_{bi} = \phi_i^W \Delta z_{bi}^W + \phi_i^D \Delta z_{bi}^D$$

The next step is to apply the bed change to the high-resolution hydraulics curve. The bed change could directly be applied without consideration of the wet/dry status of the hydraulics curve, but this would lead to artificial artifacts where the dry land is eroded by concentrated flow and vice versa. A simple approach is devised here which avoids this problem.

By applying a simple mass conservation between the two subgrid curves, the bed elevations on the hydraulics elevation-area χ is then updated as

175) $$\Delta z_{b\chi} = \phi_\chi^W \Delta z_{bi}^W + \phi_\chi^D \Delta z_{bi}^D \quad \text{for } \chi \in i$$

where

χ = subscript indicating hydraulic elevation-area

i = subscript indicating sediment subregion

$$\phi_\chi^W = \begin{cases} 1 & \text{for } \eta > z_{b\chi} \\ 0 & \text{otherwise} \end{cases}$$

A^W = wetted area determined from high-resolution elevation-area curve [L^2]

a_i = area corresponding to subarea *i* [L^2]

The approach avoids “bleeding” of the bed change across the wet/dry interface.

3.3.3 Subface Bed Elevations and Bed Change

The hydraulic curves must also be modified at the cell faces for deposition and erosion. Since bed elevations at faces may have very different characteristics from the neighboring cells, it is not possible to simply interpolate the bed elevations at faces. Instead, the bed change as a function of elevation is interpolated from neighboring cells and applied on the face bed elevations. The first step is to interpolate the neighboring cell bed changes to the same elevation points as the face:

176) $$\Delta z_{b,L}(z_L) \Rightarrow \Delta z_{b,L}(z_f)$$

177) $$\Delta z_{b,R}(z_R) \Rightarrow \Delta z_{b,R}(z_f)$$

where z_f is the face bed elevations above the face invert, and z_L and z_R are the elevations above the inverts for the left and right cells respectively. The face bed elevations are then computed as a simple weighted average of the neirghboring cell bed changes:

178) $$\Delta z_{b,f}(z_f) = w_L \Delta z_{b,L}(z_f) + w_R \Delta z_{b,R}(z_f)$$

where w_L and w_R are interpolation weights. Many interpolation schemes are possible including inverse area weighting, however here for simplicity a simple arithmetic average is utilized. Further testing with other interpolation schemes will be done in the future.

It is noted that the face property tables are the same resolution for both hydrodynamics and sediment transport. This means that they can be very high resolution with more than 30 or 40 elevations per face. This is one of the reasons for utilizing a simple scheme for updating the face bed elevations. An alternative scheme could be invisioned in which the bed elevations are updated by computing face erosion and deposition rates similar to how the cell bed elevations are computed. However, it would also be very computationally expensive since it would require storing, interpolating, and computing many additional variables at faces. It is expected that different approaches will perform better than others in different situations and more testing will be done on this in the future.

3.3.4 Subcell Hydrodynamic Variables

Some of the erosion and deposition methods depend on the subgrid hydrodynamics. Depending on the transport potential formula applied, there may be one or more subgrid hydrodynamic variables which need to be estimated. These variables include subgrid current velocities, water depths, various types of shear stresses, and shear velocities:

179) $$h_i = \frac{\Omega_i}{a_i}$$

where

h_i = subarea hydraulic depth [L]

$\Omega_i = \sum_{j \cap i} h_j a_j$ = subarea water volume [L^3]

The subcell current velocities are computed following Volp (2017) assuming a uniform over the cell friction slope is uniform within the cell. With this assumption and with the approximation of the hydraulic depth as the hydraulic radius for the friction coefficient, the following equation can be obtained

180) $$U_i = \frac{\Omega}{\sum_{j \in h>0} \frac{h_j^{5/3}}{n_j} a_j^W} \frac{h_i^{2/3}}{n_i} U$$

The cell-averaged current velocity is defined as the volume average of the cell as

181) $$U = \frac{1}{\Omega} \sum_i h_i a_i^W U_i$$

where

Ω = cell volume [L^3]

h_i = subcell water depths [L]

a_i^W = subcell wetted areas [L]

The constant friction slope assumption also leads to the following subarea shear stress formulation

182) $$S_f = \frac{\tau_{bi}}{\rho g h_i} = \frac{\tau_b}{\rho g h} \Rightarrow \tau_{bi} = \frac{h_i}{h}\tau_b$$

The hydraulic radius is computed as

183) $$R_{h,i} = \begin{cases} h_i \frac{a_i}{s_i + (h_{i+1} - h_\ell)\sqrt{a_i}} & \text{for } i = 1, 2, n-1 \\ h_i \frac{a_i}{s_i} & \text{for } i = n \end{cases}$$

where

h_i = subregion water depth [L]

η = water surface elevation [L]

z_{bi} = subregion bed elevation [L]

$A^W = \phi^W A$ = cell wetted area [L^2]

$a_i{}^W = \phi_i{}^W a_i$ = subregion wetted area [L^2]

$R_{h,\ i}$ = subarea hydraulic radius [L]

n_i = subarea Manning's roughness coefficient [L]

All other hydrodynamic variables are computed from the above variables.

3.4 Cell Averaged Bed Elevations and Bed Change

The average bed elevation and bed change over the wet and dry portions of the cell are

184) $$z_b = \frac{1}{A}\sum_i^M a_i z_{bi}$$

185) $$\Delta z_b = \frac{1}{A}\sum_i^M a_i \Delta z_{bi}$$

in which

i : subscript indicating sediment subregion

A : total cell horizontal area [L^2]

$\phi_i^W = 1 - \phi_i^D$: wetted fraction of subarea *i* (between 0 and 1) [-]

ϕ_i^D = dry fraction of subarea of subarea *i* (between 0 and 1) [-]

a_i = area corresponding to subarea *i* [L^2]

The average wet bed change Δz_b^W is used for the bed change correction to sediment concentrations. Δz_b^W is also used to compute an average bed change rate for the bed slope term. The average dry bed change Δz_b^D is not used in any calculations except the average bed change rate which is a model output.

The cell averaged bed elevation and bed change are given by

186) $$z_b^W = \frac{1}{A^W} \sum_i a_i^W z_{bi}^W$$

187) $$z_b^D = \frac{1}{A^D} \sum_i a_i^D z_{bi}^D$$

188) $$\Delta z_b^W = \frac{1}{A^W} \sum_i a_i^W \Delta z_{bi}^W$$

189) $$\Delta z_b^D = \frac{1}{A^D} \sum_i a_i^D \Delta z_{bi}^D$$

in which

i : subscript indicating sediment subregion

$A = \sum_i^M a_i$ = cell area [L^2]

$a_i^W = \phi_i^W a_i$

$a_i^D = \phi_i^D a_i$

a_i : subregion *i* area [L^2]

A^W : wetted area determined from high-resolution elevate

$A^D = A - A^W$: dry area of a cell [L^2]

$\phi_i^W = 1 - \phi_i^D$: wetted fraction of subarea *i* (between 0 and 1) [-]

ϕ_i^D : dry fraction of subarea of subarea *i* (between 0 and 1) [-]

3.5 Cell Hydraulic Properties

The hydrodynamic model requires two hydraulic property tables at cells:

1. Cumulative or total horizontal wetted cell area A_i
2. Cumulative or total cell volume Ω_i

The curve A_i is piece-wise constant while Ω_i is piece-wise linear. The cell volume $\Omega_i(\eta_i)$ are obtained by simple integration of A_i

190) $$\Omega_i = \begin{cases} 0 \quad \text{for } i = 1 \\ \Omega_{i-1} + (\eta_i - \eta_{i-1}) A_{i-1} \quad \text{for } i > 1 \end{cases}$$

Similarly the area may be obtained from the cell volumes as

191) $$A_i = \begin{cases} \frac{\Omega_{i+1} - \Omega_i}{\eta_{i+1} - \eta_i} \quad \text{for } i < n \\ A_c \quad \text{for } i = n \end{cases}$$

It is noted that the A_1 is the minimum cell area even when the cell is completely dry.

3.6 Face Hydraulic Properties

The hydrodynamic model requires three hydraulic property tables at faces:

1. Vertical wetted face area
2. Hydraulic radius
3. Manning's roughness coefficient

The vertical face area A_k is simply the integration of the cumulative horizontal wetted width W_k as:

192) $$A_k = \begin{cases} l0 \quad \text{for } k = 1 \\ A_{k-1} + (\eta_k - \eta_{k-1}) W_{k-1} \quad \text{for } k > 1 \end{cases}$$

In which η_k is the face water surface elevation, and W_k is the face width. The curve A_k is piece-wise linear and W_k is piece-wise constant. Similarly the face widths may be obtained from the cell areas as

193) $$W_k = \begin{cases} \frac{A_{k+1} - A_k}{\eta_{k+1} - \eta_k} \quad \text{for } k < M \\ W_f \quad \text{for } k = M \end{cases}$$

where W_f is the maximum face width which is the same as the face length and M is the number of faces. It is noted that the W_1 is the minimum face width even when the face is completely dry.

The face conveyance is updated using the Single Channel Method and the Manning's roughness coefficient as

194) $$K = \frac{A R^{2/3}}{n} = \frac{A^{5/3}}{n P^{2/3}}$$

where

n : Manning's roughness coefficient [T/L$^{1/3}$]

A : wetted area [L^2]

R : hydraulic radius [L]

P : wetted perimeter [L]

The subface shape factor is utilized to compute the wetted perimeter and during the simulation as the face bed elevations are updated. Initially, the wetted perimeter P_i is computed from a high-resolution terrain model. This allows the model to take into account all of the details of the terrain. As the subface bed elevations are updated, new estimates of the wetted perimeter are necessary. This is done by assuming that the wetted perimeter is of the form:

195)
$$P_k = \begin{cases} l0 \quad \text{for } k = 1 \\ P_{k-1} + K_k \sqrt{W_{k-1}^2 + (\eta_k - \eta_{k-1})^2} \quad \text{for } k > 1 \end{cases}$$

where

P_k : cumulative wetted perimeter corresponding to η_k [L]

K_k : shape factor for subsegment k [-]

W_k : effective top width corresponding to η_k [L]

η_k : elevation of subsegment k [L]

The shape factor K_k is computed with the above equation and the initial given wetted perimeter and is assumed to remain constant throughout the simulation.

Once an estimate of the wetted perimeter is obtained, the hydraulic radius is simply

196)
$$R_{h,k} = \frac{A_k}{P_k}$$

where

$R_{h,k}$: face hydraulic radius corresponding to η_k [L]

A_k : vertical face area corresponding to η_k [L^2]

P_k : face wetted perimeter corresponding to η_k [L]

3.7 Sediment Transport Potential Limiters

Some of the sediment transport potential formulas such as the Engelund-Hansen (1967), Kilinc and Richardson (1973), and others do not include thresholds for transport. This leads to unrealistic transport conditions such as transport of boulders in low flows. In order to avoid this issue, the transport potential formulas are multiplied by a reduction factor when the bed shear stress is below the critical shear stress for transport. The reduction factor is given by

197)
$$f_T = \max[\min(2\tau_b/\tau_{crk} - 1, 1), 0]$$

where

τ_b = bed shear stress [$M/L/T^2$]

τ_{crk} = critical shear stress [$M/L/T^2$]

A plot of the transport stage correction function is shown in the figure below. The function limits the transport when $\tau_b < \tau_{crk}$, but has no effect for $\tau_b > \tau_{crk}$.

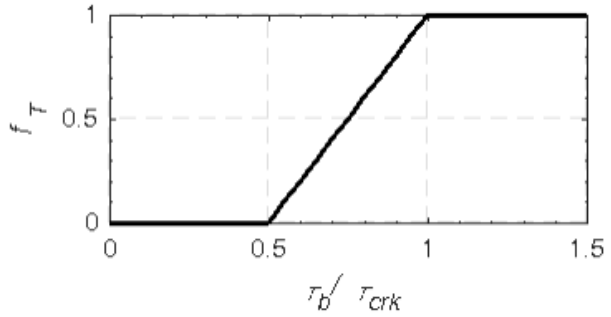

Figure 3 27. Transport stage correction.

The transport stage correction is somewhat ad-hoc but avoids unrealistc transport of sediments at low flow conditions.

In order to avoid unrealistic results such as sediment concentrations which are higher than the bed dry bulk density, the sediment transport potentials are limited. Formulas which only compute the total-load transport potential are limited as

198) $$\hat{q}^*_{tk} = q^*_{tk} \min\left(\frac{C_{t,\max}}{C_{t*}}, 1\right)$$

where

$C_{t,\ max}$ = maximum total-load sediment concentration [M/L^3]

$C_{t*} = \frac{1}{Uh}\sum_k f_{1k} q^*_{tk}$ = total-load concentration capacity [M/L^3]

U = current velocity [L/T]

h = water depth [L]

The maximum total-load concentration may be adjusted by the user but has a default value of 1590 kg/m^3.

Similarly, the bed-load transport potential is limited as

199) $$\hat{q}^*_{bk} = q^*_{bk} \min\left(\frac{c_{b,\max}}{c_{b*}}, 1\right)$$

where

$q_{bk}{}^*$ = bed-load transport rate potential [M/L/T]

$c_{b*} = \sum_k c_{bk*}$ = bed-load concentration capacity [M/L^3]

$c_{bk*} = \frac{q_{bk*}}{u_{bk}\delta_{bk}}$ = fractional bed-load concentration capacity [M/L^3]

$c_{b,max}$ = maximum bed-load concentration [M/L^3]

u_{bk} = fractional bed-load velocity [L/T]

δ_{bk} = fractional bed-load layer thickness [L]

The bed-load velocity is computed using one of the methods specified by the user. If no method is specified, the current velocity is utilized which represents an upper limit. The fractional bed-load layer thickness is computed using the van Rijn (1984) formula

200) $$\frac{\delta_{bk}}{d_k} = 0.3 d_*^{0.7} T_k^{0.5}$$

where

δ_{bk} = maximum saltation height [L]

d_k = grain size diameter [L]

d_* = non-dimensional grain size [-]

T_k = $\tau'_b/\tau_{crk} - \tau_1$ = transport stage [-]

τ_b' = bed skin shear stress [M/L/T^2]

τ_{crk} = critical shear stress [M/L/T^2]

The suspended-load transport potential is limited as

201) $$\hat{q}_{sk}^* = q_{sk}^* \min\left(\frac{C_{s,\max}}{C_{s*}}, 1\right)$$

where

q_{sk}^* = suspended-load transport rate potential [M/L/T]

$C_{s*} = \frac{1}{Uh}\sum_k f_{1k} q_{sk}^*$ = suspended-load concentration capacity [M/L^3]

3.8 Adaptation Coefficient Limiter

The suspended-load adaptation coefficient α_s may be related to the near-bed sediment concentration c_b by $c_b = \alpha_s C_s$ where C_s is the depth-averaged suspended sediment concentration. Since it is not reasonable for the near-bed concentration to be larger than the bed concentration, it follows that the adapatation coefficient should be limited as

202) $$\hat{\alpha}_{sk} = \min\left(\alpha_{sk}, \rho_{dk}/C_{sk}\right)$$

where

ρ_{dk} : user-sepcified dry bulk density [M/L^3]

C_{sk} : suspended sediment mass concentration [M/L^3]

3.9 Bed Sorting and Layering Model

The bed sorting and layering model begins with the calculation of the layer thickness of the first and second layers. This is followed by the dry bulk density of the first layer and finally the grain fractions by weight of the first and second layers.

The active layer thickness is given by

$$\delta_{1i}^{n+1} = \min\left[\max\left(f_{1,90}d_{90,i}, 0.5\Delta, \Delta z_{bi}, \delta_{1,\min}\right), \delta_{1,\max}\right] \quad 203)$$

where

$\delta_{1,min}$: user-specified minimum active layer thickness [L]

$\delta_{1,max}$: user-specified maximum active layer thickness [L]

$f_{1,90}$: user-specified active layer scaling factor corresponding to d_{90} (~ 1 to 10) [-]

$d_{90,i}$: 90th percentile diameter [L]

Δ : bed form height [L]

Δz_{bi} : bed change [L]

If beforms are not being simulated, the bedform height is set to zero. The active layer thickness has a lower limit equal to the bed change so that in the case of deposition the boundary between he first and second layers does not go above the bed elevation of the previous time step. Basically, all deposition is occurs in the active layer and not deposition occurs in the active stratum.

The bed layering is computed at each subarea. However, here the subscripts for the subarea are dropped for simplicity. The minimum and maximum active layer thicknesses are used to avoid excessively small and large active layer thicknesses. It is noted that by setting the limits to the same value, then the above equation is equivalent to specifying a constant value. The thickness of the second layer is given by

$$\delta_{2i}^{n+1} = \delta_{2i}^{n} + \Delta\delta_{2i} \quad 204)$$

where

$\Delta\delta_{2i} = \Delta z_{bi} - \Delta\delta_{1i}$: change in second layer thickness [L]

$\Delta z_{bi} = z_{bi}^{n+1} - z_{bi}^{n}$: bed change [L]

$\Delta\delta_{1i} = \delta_{1i}^{n+1} - \delta_{1i}^{n}$: change in active layer thickness [L]

In order to avoid the second layer from becoming extremely thin or thick, a layer merging and splitting algorithm is implemented between layers 2 and 3. If the second layer is too thick, it is divided into two layers; thus, the previous third layer becomes the new fourth layer, and the last two bottom layers are merged into one. If the second layer is too thin, it is merged with the previous third layer to form a new second layer; thus, the previous fourth layer becomes the new third layer. To illustrate the bed layering process, the figure below shows an example of the temporal evolution of 7 bed layers during erosional and depositional regimes. Therefore, a minimum of 3 layers are required for the model. The bed layering model requires a minimum of 3 layers but does not have a maximum number of layers. Furthermore, the number of layers can vary from cell to cell. The number of layers is specified for each cell. All of the subregions within a cell have the same number of layers.

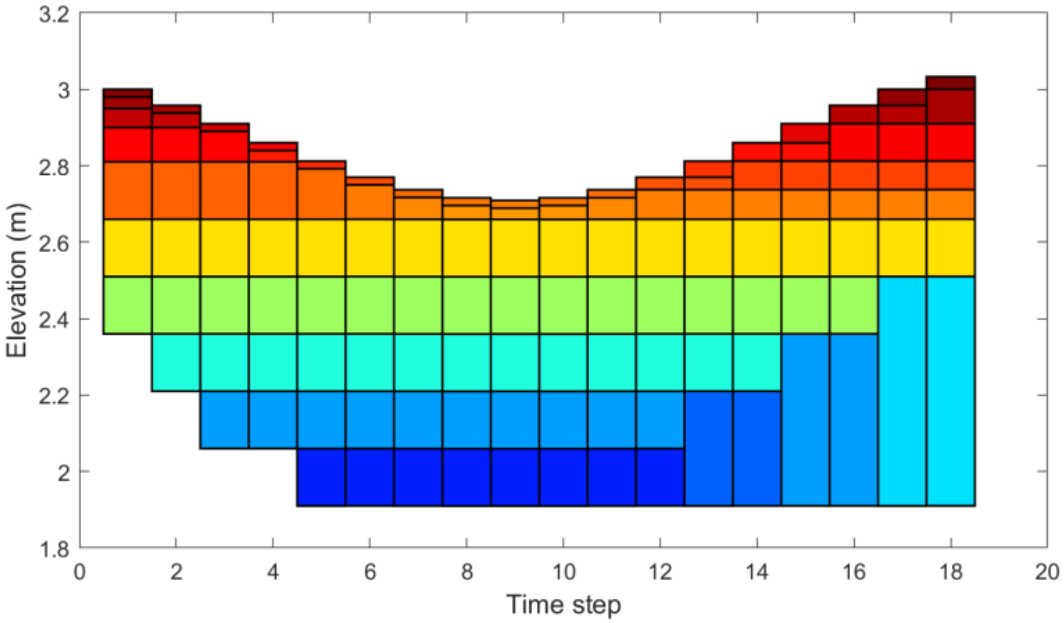

Figure 1. Schematic showing an example bed layer evolution.

The bed sorting equations for the first and second bed layers are discretized explicitly as

205) $$m_{1ki}^{n+1} = \frac{\Delta M_{bki} + m_{1ki}^{n}\delta_{1i}^{n} - m_{*ki}^{n}\Delta\delta_{2i}}{\delta_{1i}^{n+1}}$$

206) $$m_{2ki}^{n+1} = \frac{m_{2ki}^{n}\delta_{2i}^{n} + m_{*ki}^{n}\Delta\delta_{2i}}{\delta_{2i}^{n+1}}$$

where

$m_{1ki} = f_{1ki}\rho_{d1i}$: fractional mass concentration in the first (active) layer [M/L^3]

$m_{2ki} = f_{2ki}\rho_{d2i}$: fractional mass concentration in the in second layer [M/L^3]

$\rho_{d1i} = \sum_k m_{1ki}$: dry bulk density of first layer [M/L^3]

$\rho_{d2i} = \sum_k m_{2ki}$: dry bulk density of second layer [M/L^3]

ΔM_{bki} : fractional mass exchange with the bed in [M/L^2]

$\Delta\delta_{2i}$: change in second layer thickness [L]

$$m_{*ki}^{n} = \begin{cases} m_{1ki}^{n} & \text{for } \Delta\delta_{2i} \geq 0 \\ m_{2ki}^{n} & \text{for } \Delta\delta_{2i} < 0 \end{cases}$$

In the above equations, the superscripts indicate the time step level and the number subscripts indicate the bed layer. The above formulation takes into account the existing porosity of the first and second layers and

the porosity of newly deposited material. The formulation allows for the bed to be eroded more than the active layer thickness in a single time step.

In order to close the system of equations, an approximation is required to estimate the porosity of the deposited and eroded material (referred to here as the exchange material) is computed based on the net volume erosion or deposition as

207) $$\phi_b = \begin{cases} \phi_0 & \text{for } \Delta z_b > 0 \\ \phi_1 & \text{for } \Delta z_b \leq 0 \end{cases}$$

where

Δz_b : bed change [L]

ϕ_0 : porosity of (newly) deposited material [-]

ϕ_1 : porosity of layer 1 (active layer) [-]

3.10 Bed-Slope Term

The Finite-Volume discretization of the bed-slope term is

208) $$S_{bki} = \frac{w_i}{A^W} \sum_f \kappa_{bkf} \left| q_{bkf} \right| \nabla_\perp z_{bf}^W L_f^W$$

where

w_i : weights applied to each subarea [-]

A^W : cell wet area [-]

κ_{bkf} : non-dimensional bed-slope coefficient at face *f* [-]

$|q_{bkf}|$: bed-load mass transport magnitude at face [M/L/T]

$\nabla_\perp z_{bf}{}^W$: face-normal gradient of wet elevations at face *f* [L]

$L_f{}^W$: length of wet portion of face *f* [L]

The be-slope term is computed within a subcell by applying depth weighting in order to capture the effect in which deeper parts of cell are expected to experience larger bed change compared to less deep portions of the cell. The weights are computed as

209) $$w_i = \frac{h_i^b}{\sum_k h_k^b}$$

where

h_i : subarea water depth [L]

b : nondimensional empirical coefficient ($b \geq 0$)

A coefficient $b = 0$ represents applying the same slope-induced bed change to each subregion.

3.11 Subsidence and Consolidation

The bed elevation is adjusted for subsidence and consolidation as

210) $$z_{bi}^{m+1} = z_{bi}^{m} + \Delta z_{bi}^{s} + \Delta z_{bi}^{c}$$

where

Δz_{bi}^{s} = bed change due to subsidence [L]

Δz_{bi}^{c} = bed change due to consolidation [L]

The calculation of each subsidence component and the modification of bed layer thickness and dry bulk density is described below.

3.11.1 Subsidence

The subsidence for every time step is computed as

211) $$\Delta z_{bi}^{s} = -\Delta t S_R$$

where Δt is the time step and S_R is a user-specified subsidence velocity which is specified as a time series.

3.11.2 Consolidation

Consolidation is computed utilizing a user-specified curve of dry bulk density as a function of time. Below is an example of a consolidation curve.

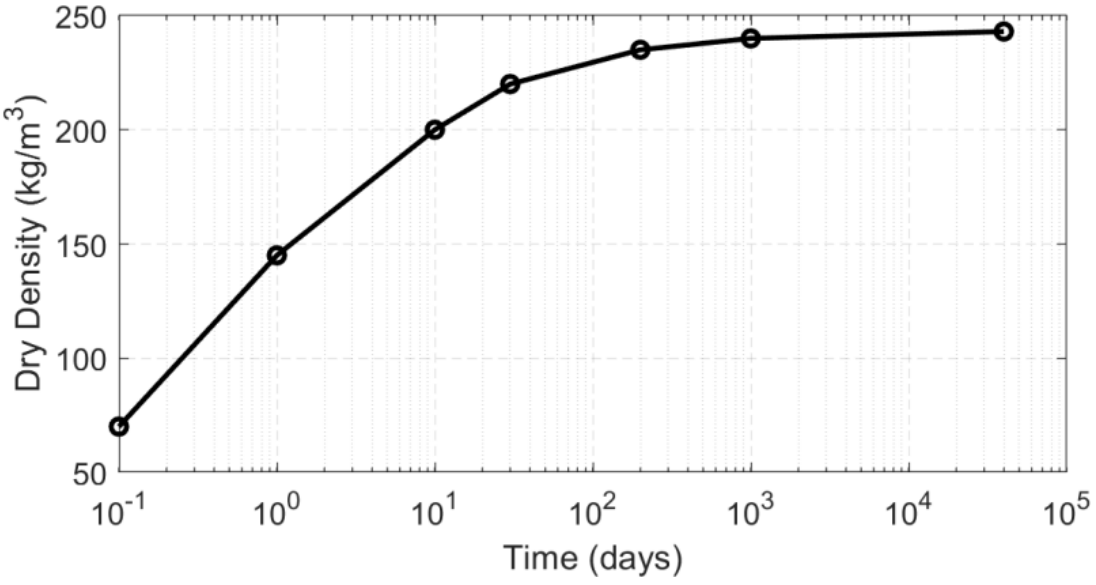

Figure 3 29. Example consolidation curve of dry bulk density as a function of time.

A schematic of the consolidation computation for a single time step is shown in the figure below.

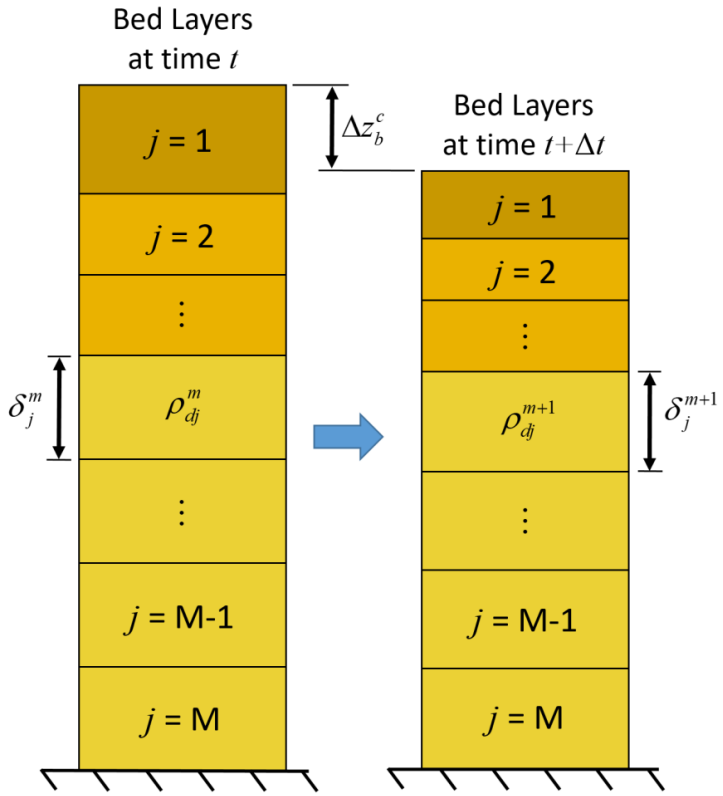

Figure 3 30. Schematic of the multiple layer bed consolidation.

The change in the bed layer dry bulk density is calculated using the following semi-analytical scheme

212) $$t_{ji}{}^m = f^{-1}(\rho_{dji}{}^m)$$

213) $$t_{ji}^{m+1} = t_{ji}^m + \Delta t$$

214) $$\rho_{dji}^{m+1} = f\left(t_{ji}{}^{m+1}\right)$$

The interpolation of the dry densities and times from the consolidation curve is done with logarithmic interpolation. The dry bulk density is computed at *m*+1, the bed layer thickness and fractional mass concentrations are updated as

215) $$\delta_{ji}^{m+1} = \frac{\rho_{dji}^m \delta_{ji}^m}{\rho_{dji}^{m+1}}$$

216) $$m_{jki}^{m+1} = \frac{m_{jki}^{m} \delta_{ji}^{m}}{\delta_{ji}^{m+1}}$$

The total shallow subsidence due to consolidation is therefore the sum of the bed layer thickness change

217) $$\Delta z_{bi}^{c} = \sum_{j=1}^{M} \left(\delta_{ji}^{m+1} - \delta_{ji}^{m} \right)$$

where *M* is the total number of shallow bed layers. Consolidation is computed at all computational cells with cohesive sediments whether they are submerged or unsubmerged.

It is important to understand that the time here does necessarily match the time at which the sediment was deposited, since the dry density of deposited sediments can be larger than the dry density in the user-defined as at time zero, especially if the deposited sediments include coarser material. Therefore, the time should be viewed as a relative time which does not necessary start at zero.

Alhtough an algorithm could be conceived in which the consolidation times are saved, which would save the the first step above, the approach would not work for the first and second layers because their dry densities are affected by erosion, deposition, and mixing. The current approach has the advantage of treated all layers the same. Noncohesive sediments increase the dry bulk density of mixture and also reduce the ability of soil to consolidation under self weight. Since the presense of noncohesive sediment fractions have a big impact on the overall dry bulk density of the material, the dry bulk density of cohesive/noncohesive sediment mixtures usually result in consolidation times which are beyond the user-specified consolidation curve and therefore resulting in zero consolidation. If the initial dry bulk density is higher than the highest value on the consolidation curve, consolidation is not computed.

3.12 Sediment Concentration Correction due to Bed Change

After the bed elevation is adjusted the sediment concentration should be corrected to preserve local sediment mass balance. This correction is done using the following simple formula

218) $$C'_{tk} = \frac{C_{tk}^{n+1} h^{n+1}}{h^{n+1} - \Delta z_b^{W}}$$

where

C_{tk}^{n+1} = uncorrected cell-averaged total-load sediment concentration [M/L^3]

$C_{tk}^{'n+1}$ = corrected cell-averaged total-load sediment concentration [M/L^3]

h^{n+1} = cell hydraulic (average) water depth [L]

Δz_b^{W} = average bed change for wetted portion of a cell [L]

It is noted that the sediment concentration is not resolved at a subgrid level which is why the water depth in the above equation corresponds to the hydraulic water depth.

3.13 Cohesive Parameters

The cohesive parameters in HEC-RAS are: (1) critical shear for erosion, (2) erosion rate coefficient, (3) critical shear for mass erosion, and (4) mass erosion rate coefficient. It is well known that these parameters can be sensitive to the bulk density. If the user specifies sediment bed layers, the parameters can be computed with power-law functions to represent these parameters as a function of the dry bulk density. Utilizing functional forms of the cohesive parameters has several benefits. Firstly, it provides a way of computing the cohesive parameters for newly deposited sediments. Secondly, since the bed dry density is continually updated during the simulation due to bed mixing and consolidation, the functional form provides a convenient and robust way of computing the cohesive parameters.

The user-specified cohesive parameters are interpreted as initial values corresponding to the initial dry bulk density of the bed. If bed layers are specified, the bed layer values are utilized to fit the coefficients to the power-law function. The power-law form fitted to each cohesive parameter is

219) $$P = a\rho_d^b$$

where *P* is one of the cohesive parameters and *a* and *b* or fitted empirical coefficients. If a single bed layer is specified, the coefficient *b* is assumed to be one. Otherwise if multiple bed layers are specified, the power-law equation is fit using a weighted least-squares in log-space as

220) $$a = \exp\left(\overline{y}_w - b\overline{x}_w\right)$$

221) $$b = \frac{\sum_i w_i \left(x_i - \overline{x}_w\right)\left(y_i - \overline{y}_w\right)}{\sum_i w_i \left(x_i - \overline{x}_w\right)^2}$$

where

$$\overline{x}_w = \frac{\sum_i w_i x_i}{\sum_i w_i}, \overline{y}_w = \frac{\sum_i w_i y_i}{\sum_i w_i}, x_i = \ln(\rho_{d,i}), y_i = \ln(P_i),$$
$$w_i = \rho_{d,i}^{-2}$$

As an example, the figure below shows a curve fit to the critical shear for erosion as a function of the dry bulk density.

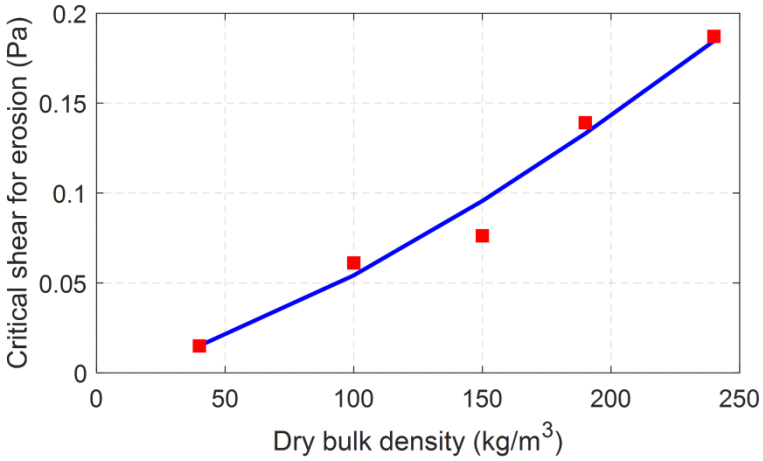

Figure 1. Example power-law fit to critical shear for erosion as a function of the dry bulk density.

If a single bed layer or no bed layers are specified, then the cohesive parameters are assumed to be constant (i.e. *b* = 0).

3.14 Avalanching Numerical Methods

When the slope of a non-cohesive bed, ϕ_b, is larger than the angle of repose, ϕ_R, the bed material will slide (avalanche) to form a new slope approximately equal to the angle of repose. The process of avalanching is simulated by enforcing $|\phi_b| \leq \phi_R$ while maintaining mass conservation between adjacent cells (Sánchez and Wu 2011a). When the angle of repose is exceeded, the bed change due to avalanching between cell *P* and its adjacent cell *N* is given by (see figure below)

222)
$$\frac{(z_{bN} + \Delta z_{bN}^a) - (z_{bP} + \Delta z_{bP}^a)}{\delta} = \text{sgn}\phi_b \tan \phi_r$$

where

Δz_b^a = avalanching bed change [m]

δ = cell center distance between cells *P* and *N*,

$\text{sgn}(X) = \begin{cases} l - 1 \text{ for } X \geq 0 \\ 1 \quad \text{for } X < 0 \end{cases}$ = sign function

$\tan \phi_b = \frac{z_{bN} - z_{bP}}{\delta}$

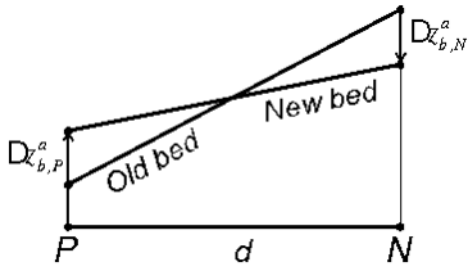

Figure 3 32. Avalanching between two cells.

The sgn(*X*) function accounts for the fact that the bed slope may have a negative or positive sign. The corresponding mass balance equation is given by

223) $$A_N \Delta z^a_{b,N} + A_p \Delta z^a_{b,P} = 0$$

where *A* is the cell area and Δz^a_b is the avalanching bed change. Combining the last two equations leads to

224) $$\Delta z^a_{b,P} = \frac{A_N \delta}{A_P + A_N} (\tan \phi_b - \mathrm{sgn}\phi_b \tan \phi_R)\, \mathrm{H}(|\phi_b| - \phi_R)$$

where H(*X*) is the Heaviside step-function equal to 1 for $X \geq 0$ and equal to 0 for $X < 0$. H(*X*) represents the activation of avalanching. The above equation is exact but limited to avalanching between two cells. Avalanching may occur over multiple cells and induce additional avalanching at neighboring cells. A relaxation approach is adopted as follows (see figure below):

225) $$\Delta z^a_{b,P} = \alpha_a \sum_N \frac{A_N \delta}{A_P + A_N} (\tan \phi_b - \mathrm{sgn}\phi_b \tan \phi_R)\, \mathrm{H}(|\phi_b| - \phi_R)$$

where α_a is the under-relaxation factor (approximately 0.25 to 0.5). α_a is used to stabilize the avalanching process and avoid overshooting.

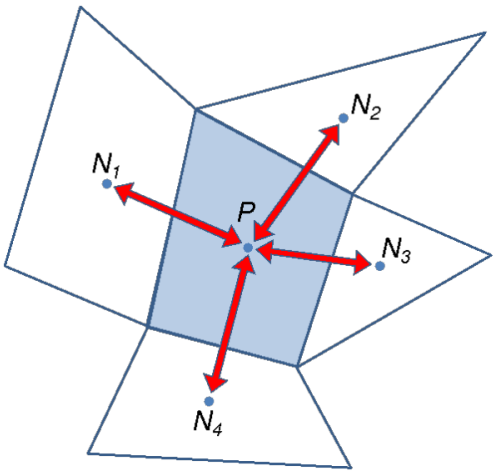

Figure 3 33. Avalanching computational stencil.

The above equation may be applied to any grid geometry type (i.e. triangle, rectangle, etc.) and for situations in which neighboring cells are joined at corners without sharing a cell face. The above equation is implemented by sweeping through all computational cells to calculate Δz_b^a and then modifying the bathymetry as

226) $$z_b^{m+1} = z_b^m + \Delta z_b^a$$

where the superscript *m* indicates the avalanching iteration. The sweeping process is repeated until avalanching no longer occurs. The above avalanching procedure is relatively simple and is very stable. The algorithm parameters are the maximum number of iterations, the relaxation factor, and the angle of repose. Because the algorithm is called every time step it is not necessary to iterative until convergence every time step and usually about 3 to 6 iterations are sufficient for good results.

3.15 Non-Erodible Surfaces

Non-erodible surfaces (also known as hard bottoms) may be simulated in HEC-RAS and are specified using a minimum bed elevation, $z_{b,\min}$, or maximum depth, $h_{\max}$ $h_{\max}$. In the 2D model the non-erodible surfaces are specified at both cells and faces independently. Non-erodible surfaces are modeled at the subarea scale by limiting the erosion rate so that the minimum bed elevation is preserved (i.e. $z_{bi} \geq z_{b,\min}$). The time stepping scheme is given by $z_{bi}^{n+1} = z_{bi}^n + \Delta z_{bi}$ in which z_{bi}^n is the previous bed elevation, z_{bi}^{n+1} is the new bed elevation, and Δz_b is the bed change. Assuming that the bed elevation at the current time is higher than the hard bottom (i.e. $z_{bi}^n \geq z_{b,\min}$). Inserting the above equation into the bed change equation leads to the hard-bottom limited erosion rate

227) $$E_{tki,hb} = D_{tki} + \Psi_{na,i} \frac{f_{1ki}\rho_{d1}}{f_M \Delta t}\left(z_{bi}^n - z_{bi,hb}\right)$$

where

$E_{tki,hb}$: hard-bottom limited fractional erosion rate [M/L^2/T]

D_{tki} : fractional deposition rate [M/L^2/T]

$\Psi_{na,i}$: non-alluvial erosion limiter [-]

ρ_{d1} : dry density of active layer [M/L^3]

f_{1ki} : grain fractions by weight [-]

f_M : morphologic acceleration factor [-]

Δt : computational time step [T]

The non-alluvial erosion limiter $\Psi_{na,i}$ is function which limits the maximum erosion rate based on the proximity of the mobile bed surface to the non-erodible surface and is computed here as

228) $$\Psi_{na,i} = \frac{\delta_{1i}^n}{\delta_{1i}^*}$$

where

δ_{1i}^{n} : active layer thickness [L]

δ_{1i}^{*} : potential or maximum active layer thickness if there was no non-erodible surface present [L]

When δ_{1i}^{n} = 0, no erosion is possible and the maximum erosion rate becomes equal to the deposition rate (i.e. $E_{tki,hb} = D_{tki}$) . Likewise when $\delta_{1i} = \delta_{1i}^{*}$, the maximum erosion rate is equal to the amount of material in the active layer available to erode in a timestep plus the deposition rate.

The hard-bottom limited erosion rate is therefore

229) $$E'_{tki} = \min\left(E_{tki,hb}, \quad E_{tki}\right)$$

The bed-slope term and avalanching algorithm are also modified so that only deposition may occur over non-erodible surfaces following an approach similar to that described above.

When simulating multiple grain classes, the bed gradation can significantly change at non-erodible surfaces during a time step. This means that the model may require at least one to two iterations to converge when simulating non-erodible surfaces with multiple grain classes.

4 References

Ackers, P., and White, W.R. 1973. Sediment transport: New approach and analysis, Proceedings. ASCE, Journal of the Hydraulic Division, 99, HY11, pp. 2041-2060.

Ackers, P. 1993. Sediment transport in open channels: Ackers and White update. Proceedings of the Institution of Civil Engineers - Water and Maritime Engineering. 101(4), 247249.

Ariathurai, C.R. 1974. A finite element model for sediment transport in estuaries, PhD Thesis, University of California, Berkley, USA.

Ariathurai, C.R., and Arulanandan, K. 1978. Erosion rates of cohesive soils, Journal of Hydraulics Division, American Society of Civil Engineering, 104(2), 279282.

Armanini, A., di Silvio, G. 1988. A one-dimensional mode for the transport of a sediment mixture in non-equilibrium conditions. Journal of Hydraulic Research. 26(3), 275292.

Baas, J. H. 1993. Dimensional analysis of current ripples in recent and ancient depositional environments, PhD Thesis, University of Utrecht, The Netherlands, 199 p.

Brown, G.L. 2012. Modification of the bed sediment equations of Spasojevic and Holly (1993) to account for variable Porosity, variable grain specific gravity, and nonerodable boundaries, IIHR Third International Symposium on Shallow Flows, Iowa City, IA, June 46 2012.

Brownlie, W.R. 1981. 'Prediction of flow depth and sediment discharge in open channels' and 'Compilation of fluvial channel data: laboratory and field', Rep. No. KH-R-43A&B, W.M. Keck Lab. of Hydr. and Water Resources, California Institute of Technology, Pasadena, California, USA.

Brownlie, W. R. 1983. Flow depth in sand-bed channels. Journal of Hy-draulic Engineering, ASCE 109(7), 959990.

Camenen, B., and Larson, M. 2007. A unified sediment transport formulation for coastal inlet application. ERDC/CHL CR-07-1. Vicksburg, MS: US Army Engineer Research and Development Center.

Cheng, N.-S. 1997. Simplified settling velocity formula for sediment particle. Journal of Hydraulic Engineering, 123(2), 149152.

Colby, B.R. 1963. Discussion of "Sediment transportation mechanics: Introduction and properties of sediment", Progress report by the Task Committee on Preparation of Sediment Manual of the Committee on Sedimentation of the Hydraulics Division, V. A. Vanoni, Chmn., Journal of Hydraulics Division., ASCE, 89(1): 266268.

Coleman, N.L. 1981. Velocity profiles with suspended sediment. Journal of Hydraulic Research 19(3):211-229.

Copeland, R.R., and Thomas, W.A. 1989. Corte Madera Creek sedimentation study. Numerical Model Investigation. TR-HL-89-6. US Army Waterways Experiment Station, Vicksburg, MS. USA.

Corey, A.T., 1949. Influence of shape on the fall velocity of sand grains, MS Thesis, Colo. A & M College, Fort Collins, CO.

Cowan, W.L. 1956. Estimating Hydraulic Roughness Coefficients. Agricultural Engineering, 37(7), 473475.

Christoffersen, J.B., and Jonsson, I.G. 1985. Bed friction and dissipitation in a combined current and wave motion, Ocean Engineering, 12(5), 387423.

Dahl, T.A, Heath, R.E., Gibson, S.A., and Nygaard, C.J. 2018. HEC-RAS unsteady flow and sediment model of the Mississippi River: Tarbet Landing to the Gulf, Mississippi River Geomorphology & Potomology Program, Report No. 25, Engineer Research and Development Center, Vicksburg, MS, USA.

Day, T.J. 1980. A study of the transport of graded sediments. Report N. IT 190, HR Wallingford, U.K.

Dietrich, W.E. 1982. Settling velocity of natural particles, Water Resources Research, 18(6), 16151626.

Engelund, F., and Hansen, E. 1967. A monograph on sediment transport in alluvial streams, Teknisk Forlag, Copenhagen, 65.

Fernandez Luque, R. 1974. Erosion and transport of bed-load sediment. Dissertation, Krips Repro B.V., Meppel, The Netherlands.

Fernandez Luque, R., and Beek, R. van. 1974. Erosion and transport of bed-load sediment. Journal of Hydraulic Research, 14(2): 127144.

Folk, R.L. 1955. Student operator error in determination of roundness, sphericity and grain size, Journal of Sedimentary Petrology, 25, 297-301.

Frings, R. M., Schüttrumpf, H. and Vollmer, S. 2011. Verification of porosity predictors for fluvial sand-gravel deposits. Water Resources Research, 47, 15 p. W07525.

Han, Q.W., Wang, Y.C. and Xiang, X.L. 1981. Initial specific weight of deposits. Journal of Sediment Research. No. 1, pp. 113 (in Chinese).

Hayashi, T.S., Ozaki and Ichibashi, T. 1980. Study on bed load transport of sediment mixture, Proc. 24th Japanese Conf. on Hydraulics, Japan.

Harrison, A.J.M., and Owen, M.W. (1971), Siltation of fine sediments in estuaries, paper presented at XIV Congress, Int. Assoc. for HydroEnviron. Eng. and Res., Paris

HEC 2010. HEC-RAS River Analysis System: Hydraulic Reference Manual, Version 4.1. CPD-69

Hwang, K.-N. 1989. Erodibility of fine sediment in wave dominated environments. MS Thesis, University of Florida, Gainesville, FL.

Jones, C., and Lick, W., 2001. Sediment erosion rates: Their measurement and use in modeling 6th International Conference on Estuarine and Coastal Modeling. ASCE, College Station, Texas, 280293.

Julien, P.Y., and Bounvilay, B. 2013. Velocity of rolling bed load particles. Journal of Hydraulic Engineering, ASCE, 139(2), 177186.

Kilinc, M., and Richardson, E.V. 1973. Mechanics of soil erosion from overland flow generated by simulated rainfall. Hydrology Paper No. 63, Colorado State Univ., Fort Collins, CO.

Karim, F. 1995. Bed configuration and hydraulic resistance in alluvial-channel flows, J. Hydraulic Eng., ASCE, 121(1), 1525.

Koch, F.G. and Flokstra, C. 1981. Bed level computations for curved alluvial channels. 19th IAHR congress, Vol. 2, New Delhi, India.

Kovacs, A. and Parker, G. 1994. A new vectorial bedload formulation and its application to the time evolution of straight river channels, Journal of Fluid Mechanics , 267, 153183.

Krone, R. 1962. Flume studies of the transport of sediment in estuarial shoaling process, Hydraulic Engineering Laboratory and Sanitary Engineering Research Laboratory, University of California, Berkeley, CA.

Krumbein, W.C. 1934. Size frequency distributions of sediments. Journal of Sedimentary Petrology, 4(2): 6577.

Lai, Y.G. 2020. A two-dimensional depth-averaged sediment transport mobile-bed model with polygonal meshes, Water, 1032: 121.

Laursen, E.M. 1958. The total sediment load of streams, J. Hydr. Div., ASCE, 84(1), 1 36.

Lin, Q., and Wu, W. 2013. A one-dimensional model of mixed cohesive and non-cohesive sediment transport in open channels. Journal of Hydraulic Research. 112.

Mehta, A.J., and Partheniades, E. 1975. An investigation of the depositional properties of flocculated fine sediment. Journal of Hydraulic Research. 13(4), 361381.

Mehta, A.J. 1981. Review of erosion function for cohesive sediment beds, paper presented at First Indian Conference on Ocean Engineering, Indian Inst. Technol. on Ocean Eng., Indian Inst. of Technol., Madras, India.

Meyer-Peter, E., and Müller, R. 1948. Formulas for bed-load transport, Proceedings of the 2nd Congress IAHR, Stockholm, Sweden.

Neumeier, U., Ferrarin, C., Amos, C.L., Umgiesser, G., and Li, M.Z. 2008. Sedtrans05: An improved sediment-transport model for continental shelves and coastal waters with a algorithm for cohesive sediments. Computers & Geosciences, 34, 12231242.

Owen, P.R. 1964. Saltation of uniform grains in air, Journal of Fluid Mechanics, 20(2), 225242.

Owen, M.W. 1975. Erosion of avonmouth mud. Report No. INT 150. Hydraulics Research Station, Wallingford, England.

Parker, G., P. C., Kilingeman, and McLean, D.G. 1982. Bed load and size distribution in paved gravel-bed streams. Journal of the Hydraulics Division, ASCE 108(4): 544571.

Parker, G., Seminara, G., and Solari L. 2003. Bedload at low shields stress on arbitrarily sloping beds: Alternative entrainment formulation, Water Resour. Res., 39(7), 1249.

Partheniades, E. 1962. A study of erosion and deposition of cohesive soils in salt water. Ph.D thesis, University of California, Berkeley, 182 p

Partheniades, E. 1965. Erosion and deposition of cohesive soils. Journal of Hydraulics Division. 91(1), 105139.

Perera, C., and Wu, W. 2016. Erosion coefficients of cohesive sediments. World Environmental & Water Resources Congress, Pittsburg, PA. 10 p.

Powers, M.C. 1953. A new roundness scale for sedimentary particles, Journal of Sedimentary Petrology, 32, 117119.

Proffitt, G.T. and Sutherland., A.J. 1983. Transport of nonuniform sediment, Journal of Hydraulic Research, IAHR, 21(1), 3343.

Raudkivi, A.J. 1990. Loose Boundary Hydraulics, 3rd Ed., Pergamon Press, Inc., Tarrytown, N.Y.

Richardson, J.F. and Zaki, W.N. 1954. Sedimentation and fluidisation, Part I. Transaction of the Institute of Chemical Engineers., 32(1), 3553.

Riley, J.P., and Skirrow, G., 1965. Chemical Oceanography, Vol 3. Academic Press, London, 564 pp.

Rogers, J.W., and Head, W.B. 1961. Relationships between porosity, median size, and sorting coefficients of synthetic sands. Journal of Sedimentary Petrology, 31(3): 467470.

Rubey, W.W. 1933. Settling velocities of gravel, sand, and silt particles, American Journal of Science, 5th Series, 25(148), 325338.

Sánchez, A., and W. Wu. 2011. A non-equilibrium sediment transport model for coastal inlets and navigation channels. Journal of Coastal Research, Special Issue (59): 3948.

Sanford, L.P., and Halka, J.P. 1993. Assessing the paradigm of mutually exlusive erosion and deposition of mud, with examples from upper Chesapeake Bay. Marine Geology, 114: 3757.

Soulsby, R.L. 1997. Dynamics of marine sands. London, England: Thomas Telford Publications.

Soulsby, R.L., and R. J.S. W Whitehouse. 1997. Threshold of sediment motion in coastal environments. In, Proceedings Pacific Coasts and Ports ’97 Conference, 1, 149154. New Zealand: Christchurch, University of Canterbury.

Spasojevic, M. and Holly, F.M. Jr., 1993, Three-dimensional numerical simulation of mobile-bed hydrodynamics, Technical Report No. 367, Iowa Institute of Hydraulic Research, The University of Iowa, USA.

Toffaleti, F.B. 1968. A procedure for computation of total river sand discharge and detailed distribution, bed to surface, Technical Report No. 5, Committee on Channel Stabilitzation, U.S. Army Corps of Engineers, November.

Toro-Escobar, C. M., G. Parker, and C. Paola. 1996. Transfer function for the deposition of poorly sorted gravel in response to streambed aggradation, J. Hydraul. Res., IAHR, 34, 3553.

UNESCO, 1981. The Practical Salinity Scale 1978 and the International Equation of State of Seawater 1980. UNESCO technical papers in marine science 36, 25 p.

U.S. Interagency Committee 1957. Some fundamentals of particle size analysis, A study of methods used in measurement and analysis of sediment loads in streams, Report No. 12, Subcommittee on Sedimentation, Interagency Committee on Water Resources, St. Anthony Falls Hydraulic Laboratory, Minneapolis, Minnesota, USA.

van Rijn, L.C. 1984a. Sediment transport, Part I: Bed load transport. Journal of Hydraulic Engineering, ASCE 110(10): 14311456.

van Rijn, L.C. 1984b. Sediment transport, Part II: Suspended load transport. Journal of Hydraulic Engineering, ASCE 110(11): 16131641.

van Rijn, L.C. 1984c. Sediment transport: Part III: Bed form sand alluvial roughness. Journal of Hydraulic Engineering 110(12), 1,733-1,754.

van Rijn, L.C. 1993. Principles of sediment transport in river, estuaries, coastal seas, and oceans. International Institute for Infrastructural, Hydraulic, and Environmental Engineering, Delft, The Netherlands.

van Rijn, L.C. 2007a. Unified view of sediment transport by currents and waves. Part I: Initiation of motion, bed roughness, and bed-load transport. Journal of Hydraulic Engineering 133(6): 649-667.

van Rijn, L.C. 2007b. Unified view of sediment transport by currents and waves. Part II: Suspended Transport. Journal of Hydraulic Engineering 133(6): 668-689.

Wei, H., Nearing M.A., Stone J.J., Guertin D.P., Spaeth K.E., Pierson F.B., Nichols M.H., and Moffett C.A.. 2009. A new splash and sheet erosion equation for rangelands. Soil Science Society of America Journal 73(4), 13861392.

Wilcock, P.R., and Crowe, J.C. 2003. Surface-based transport model for mixed-size sediment. Journal of Hydraulic Engineering, 129(2), 120128.

Winterwerp, J.C. 2003. On the deposition flux of cohesive sediment. In J.P.Y. Maa (Ed.), Book of abstracts 7^{th} International Conference on Nearshore and Estuarine Cohesive Sediment Transport Processes, Virginia, US.

Winterwerp. J.C., and van Kesteren, W.G.M. 2004. Introduction to the physics of cohesive sediment in the marine environment. Series Editor: T. van Loon. Developments in Sedimentology, 56, 466 p.

Wong, M. and Parker, G., 2006. Reanalysis and Correction of Bed-Load Relation of Meyer-Peter and Müller Using Their Own Database. Journal of Hydraulic Engineering, 132(11), 1159-1168.

Wooster, J.K., Dusterhoff, S.R., Cui, Y., Sklar, L.S., Dietrich, W.E., and Malko, M. 2008. Sediment supply and relative size distribution effects on fine sediment infiltration into immobile gravels, Water Resources Research, 44, W03424.

Wu, W. 1991. The study and application of 1-D, horizontal 2-D and their nesting mathematical models for sediment transport, Ph.D. Dissertation, Wuhan University of Hydraulic and Electric Eng., Wuhan, China (in Chinese).

Wu, W. 2004. Depth-averaged two-dimensional numerical modeling of unsteady flow and nonuniform sediment transport in open channels. Journal of Hydraulic Engineering, 130(1), 10131024.

Wu, W., Altinakar, M., and Wang, S.Y. 2006. Depth-average analysis of hysteresis between flow and sediment transport under unsteady conditions. International Journal of Sediment Research, 21(2), 101112.

Wu, W. 2007. Computational river dynamics. United Kingdom: Taylor & Francis. London.

Wu, W., S. S. Y. Wang, and Y. Jia. 2000. Non-uniform sediment transport in alluvial rivers. Journal of Hydraulic Research, IAHR 38(6): 427434.

Wu, W., and Li, W. 2017. Porosity of bimodal sediment mixture with particle filling. International Journal of Sediment Research. 32(2): 253259.

Wu, W. and Wang, S.S.Y. 2006. Formulas for sediment porosity and settling velocity, Journal of Hydraulic Engineering, ASCE, 132(8), 858862.

Wu, W., Perera, C., Smith, J., and Sánchez, A. 2017. Critical shear stress for erosion of sand and mud mixtures. Journal of Hydraulic Research, 56(1): 96110.

Wu, W. and Li, W. Porosity of bimodal sediment mixture with particle filling. International Journal of Sediment Research. 32(2): 253259.

Yang, C.T. 1973. Incipient motion and sediment transport. Journal of the Hydraulics Division, 99(HY10), 10067.

Yang, C.T. 1979. Unit stream power equations for total load, Journal of Hydrology, 40, 123-128.

Yang, C.T. 1984. Unit stream power equation for gravel, Journal of Hydraulic Division, ASCE, 110(12)17831797.

Zheng, F.-d., and An, J.-f. 2017. Study on the critical shear stress of cohesive sediments, 1st International Global on Renewable Energy and Development, Earth and Environmental Science, 100, 15.